Max-Planck-Institut
für Meteorologie

MAX-PLANCK-GESELLSCHAFT

International Max Planck Research School
on Earth System Modelling

Impact of Climate Change on the Coastal Climate of South-Western Africa

Andreas Hänsler

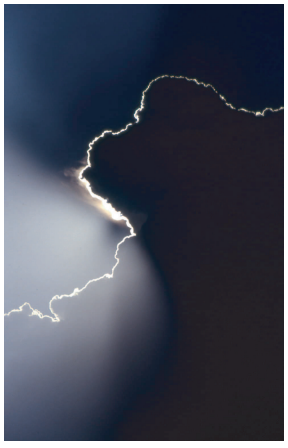

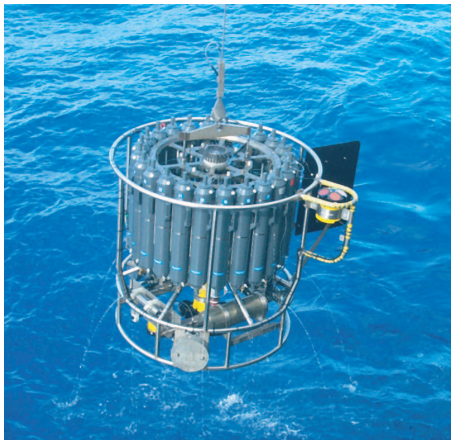

Berichte zur Erdsystemforschung 93
2011

Reports on Earth System Science

Hinweis

Die Berichte zur Erdsystemforschung werden vom Max-Planck-Institut für Meteorologie in Hamburg in unregelmäßiger Abfolge herausgegeben.

Sie enthalten wissenschaftliche und technische Beiträge, inklusive Dissertationen.

Die Beiträge geben nicht notwendigerweise die Auffassung des Instituts wieder.

Die "Berichte zur Erdsystemforschung" führen die vorherigen Reihen "Reports" und "Examensarbeiten" weiter.

Notice

The Reports on Earth System Science are published by the Max Planck Institute for Meteorology in Hamburg. They appear in irregular intervals.

They contain scientific and technical contributions, including Ph. D. theses.

The Reports do not necessarily reflect the opinion of the Institute.

The "Reports on Earth System Science" continue the former "Reports" and "Examensarbeiten" of the Max Planck Institute.

Anschrift / Address

Max-Planck-Institut für Meteorologie
Bundesstrasse 53
20146 Hamburg
Deutschland

Tel.: +49-(0)40-4 11 73-0
Fax: +49-(0)40-4 11 73-298
Web: www.mpimet.mpg.de

Layout:

Bettina Diallo, PR & Grafik

Titelfotos:
vorne:
Christian Klepp - Jochem Marotzke - Christian Klepp
hinten:
Clotilde Dubois - Christian Klepp - Katsumasa Tanaka

Berichte zur Erdsystemforschung 93/2011

Impact of Climate Change on the Coastal Climate of South-Western Africa

Andreas Hänsler

aus Wangen im Allgäu

Hamburg 2011

Reports on Earth System Science 93/2011

ISSN 1614-1199

Andreas Hänsler
Max-Planck-Institut für Meteorologie
Bundesstrasse 53
20146 Hamburg
Germany

Als Dissertation angenommen
vom Department Geowissenschaften der Universität Hamburg

auf Grund der Gutachten von
Prof. Dr. Martin Claussen
und
Dr. Stefan Hagemann

Hamburg, den 28. Juni 2011
Prof. Dr. Jürgen Oßenbrügge
Leiter des Departments für Geowissenschaften

ISSN 1614-1199

Impact of Climate Change on the Coastal Climate of South-Western Africa

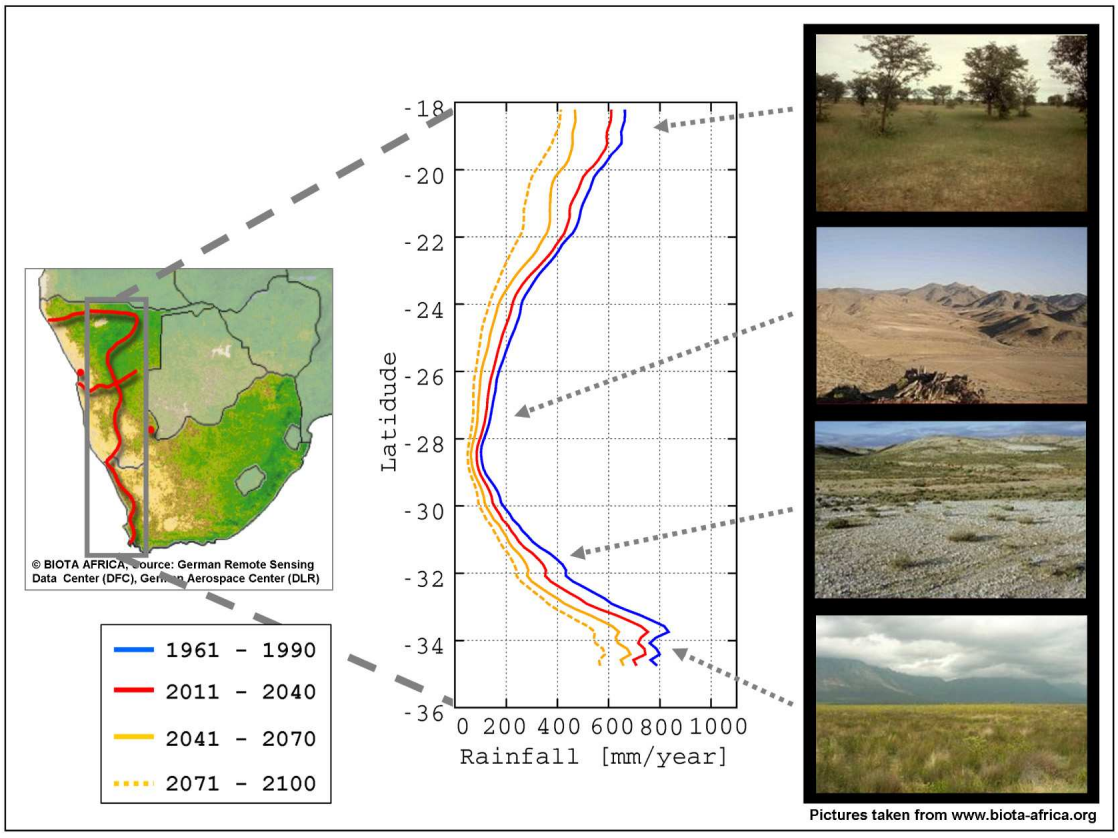

Andreas Hänsler

Hamburg 2011

Contents

Abstract

High-resolution regional climate simulations have recently been in the spotlight as they may offer an added value when compared to global climate model simulations. Regional models benefit from a better representation of topographic and land surface features. Unfortunately, over many regions of the globe, and especially over the southern African region, the availability of long-term high-resolution climate simulations is so far rather limited. In this thesis I present a suite of high-resolution regional climate simulations for the southern African region, conducted with the regional climate model (RCM) REMO at roughly 50 and 18 km grid spacing. The simulations considered comprise 50 year hindcast simulations (1958-2007) and transient climate change simulations for the period from 1960-2100. The 18 km transient climate change simulation is the longest available climate change projection at such a high resolution for the region. Additionally, a set of sensitivity simulations have been performed to account for deficits in the SST simulation of coupled general circulation models as well as time slice experiments to simulate the frequency of the southern African west coast fog. On the one hand, this unique set of high-resolution regional climate model simulations allowed to study large scale climate features and their potential future changes. On the other, it also enables to focus on regionally important mesoscale and local circulation patterns.

To ensure basic consistency with the local climatological features, in a first step the ability of the regional model to simulate the predominant climate characteristics over the region had to be assessed. Generally, it was found that the model is capable to adequately simulate the mesoscale circulation and related precipitation patterns of the southern African region. Especially along the focus region in south-west Africa, the application of REMO leads to an added value in the description of topographically induced precipitation events. With respect to the transient regional climate projection, a severe warming and drying is simulated for the southern African region towards the end of the 21st century. While the average magnitude of projected changes by REMO are in

the same order as those of the general circulation model (GCM) used to force the simulation, the RCM projections provide more spatial details. However, the forcing coupled GCM suffered from poor resolution of the mesoscale upwelling regions offshore the southern African west coast. To remedy this deficit a method had to be established and applied to correct for the too warm sea surface temperatures in the forcing data before the transient climate projection was started. As this shortcoming is a common feature of all available coupled global climate models the established method was proposed to be used as the standard setup for regional downscaling studies over the region.

The high horizontal resolution of the RCM simulations further allowed to study, whether the model is able to capture regional and local scale processes such as the occurrence of west-coast fog and the local scale thermally induced wind systems over the Central Namib. It was in fact found that the major characteristics of both systems are adequately represented in REMO. For the future the model projected a reverse change in the fog characteristics with an increase at the coast and a decrease in fog frequency further inland. With respect to the local wind systems, rather constant behavior was projected by the model throughout the 21st century. At a first glance this seemed contradictory to the simulated strong thermal changes projected for the region. However, the lack in the climate change response could on the one hand be related to the nature of the small scale forcing for the wind systems, on the other also be a consequence of the identified missing feedback processes in the model between the ocean and the atmosphere.

In general the thesis clearly highlights the benefit of high-resolution regional climate simulations over southern Africa. The RCM offers improved representation of rainfall patterns, which increases the credibility of the regional projections in this region. Furthermore, the present study identifies important model deficits that were not pointed out previously. Thereby, it presents possibilities of compensating these shortcomings and puts forward questions for future research activities in the field of regional climate modelling.

Chapter 1

Introduction

Concerning projected future climate change, the southern African region has been reported to be one of the regions most dramatically impacted upon. In the 4th Assessment Report (AR4) of the Intergovernmental Panel on Climate Change (IPCC) a general warming accompanied by a decrease of precipitation is predicted for the region. The global climate models used in the AR4 have projected a temperature rise for the region of about 3.5 K until the end of the 21st century (compared to the reference period 1980 to 1999), a decrease of annual mean precipitation of 4% and especially a strong decrease in winter rainfall by more than 20% (Christensen et al., 2007). These severe changes will have significant environmental consequences for the region, which is known to be a biodiversity hotspot (e.g. Cowling et al., 2003, Midgley et al., 2003).

The climate change projections discussed above were solely based on coarse scale general circulation models (GCMs). These can not resolve regionally specific peculiarities such as the Benguela upwelling system. However, spatially explicit climate change information is required to assess the impacts of climate change on a regional or even local scale. This information was so far not available with sufficient detail for the southern African region. Embedded in the framework of the BIOTA southern Africa project (**BIO**diversity Monitoring **T**ransect **A**nalysis in Africa: more details can be found at Jürgens et al., 2010 or at www.biota-africa.de) this dissertation focuses on high-resolution regional climate modeling over the southern African region with a regional focus on the coastal climate of south-western Africa. Within this thesis the strengths and weaknesses of the regional climate model REMO (Jacob and Podzun,

1997) in simulating the region's climatic characteristics are assessed. Furthermore, the first transient long-term climate change projection with a horizontal resolution higher than 50 x 50 km is conducted for the southern African region.

As it is located in the subtropical high-pressure zone, the climate of the southern African region is mainly determined by semi-arid to arid conditions. Especially the coastal zone of south-western Africa – where the Namib desert is located – is characterized by a large precipitation deficit (Schulze, 1965). Therefore other moisture sources like the frequent fog occurrence are of significant importance (e.g. Henschel and Seely, 2008). The central Namib region is further characterized by a local wind system, which is completely decoupled from the regional scale circulation. However the impact of future climate change on these region-specific climate characteristics could so far not be analyzed, due to the lack of sufficiently resolved climate model data.

Driven by the existing lack and scientific demand for high-resolution climate modeling studies over the southern African region several research questions emerge:

i.) Can the regional climate model REMO be transferred to the southern African region and applied for high-resolution 18x18km climate simulations?

ii.) Is there an added value of high-resolution climate simulations in comparison to coarse scale global model simulations over the southern African region?

iii.) How do existing deficits of the coupled atmosphere ocean GCMs over the region influence the high-resolution regional climate simulations and how can these weaknesses be circumvented?

iv.) Does the climate change signal of a regional climate projection differ from GCM projections for the southern African region?

v.) Can predominant regional scale climate characteristics – such as the occurrence of Namibian west coast fog – satisfactorily be simulated by the model and how does the fog occurrence behave under future climate change?

vi.) Can thermo-topographically induced local wind systems be reasonably simulated with a regional climate model?

The objective of this thesis is to contribute to the research questions identified above. Along the lines of these research questions a comprehensive analysis of the simulation of processes, occurring on different spatial as well as temporal scales, will be given in the subsequent chapters.

This thesis consists of five independent scientific chapters (2 - 6), each of it designed to be a full paper itself. Therefore some repetitions may inevitably occur in the model description and the simulation setup. However, apart from the study of local wind fields, each study required unique model specifications; hence, repeated note of model specifics could not be avoided. Note that the references of all chapters are gathered together into a single reference list at the end of the thesis.

The structure of the thesis is as follows: In the following chapter, a description of the climate characteristics of the study region as well as the past changes in the mean climate state as observed and documented in the literature is provided. This chapter has recently been published as part of a book series (Haensler et al., 2010a).

The third chapter aims at providing the answers to the first and second of the above proposed scientific questions. The validation of the high-resolution climate model REMO over the southern African region is presented. Furthermore, the added value of this simulation in comparison to the forcing ERA40 reanalysis data is discussed. This chapter has been published in the International Journal of Climatology (Haensler et al., 2010b).

The question whether deficits in the GCM forcing have an influence on the high-resolution regional climate simulations is tackled in Chapter 4. A methodology of how to cope with deficits of the forcing GCM is established. Additionally, some results of the high resolution climate change projection are presented and compared to the forcing GCM data. This chapter has recently been accepted for publication in Theoretical and Applied Climatology (Haensler et al., 2011a), but in this thesis a slightly modified

version is presented. More results from the climate change projection are discussed in Haensler et al. (2010c) and Haensler et al. (2010d).

Chapter 5 analyses how mesoscale features such as the occurrence of fog along the southern African west coast can be simulated using the regional climate model REMO. This chapter consists of both a section on model validation and on future climate projection. Large parts of this chapter have recently been accepted for publication in the international journal ERDKUNDE (Haensler et al., 2011b).

The final research question is tackled in Chapter 6, which focuses on the ability of REMO to capture the local thermo-topographically induced wind systems of the central Namib Desert region. Further, the simulation of the regional scale circulation patterns is included in this chapter as well as a study of how these circulation characteristics are affected by future climate change.

Chapter 7 summarizes the findings of the thesis with respect to the research questions identified above. Furthermore, it presents an outlook for future research in the field of regional climate modeling over the southern African region.

Chapter 2

Climate history of Namibia and western South Africa

2.1 Climate characteristics of Namibia and western South Africa

The climate of Namibia and western South Africa is characterized by semi-arid to arid conditions with strong rainfall seasonality and a pronounced north-south rainfall gradient (e.g. Schulze, 1965). During the summer season (October to March) the western part of southern Africa is generally influenced by a weak heat low (low pressure system induced by regional heating of land surface) located in the north-east, which tends to produce convective rainfall systems over these areas (e.g. Mason and Jury, 1997). In winter the situation changes to a predominant anticyclonic circulation system caused by a large single high pressure cell centred further east. In the more humid regions towards the north-eastern part of Namibia, tropical systems sometimes carry a substantial amount of rain during the summer season. The central region around the Namibian – South African border and a large part of the western coastal areas, where the Namib Desert is located, are characterized by arid conditions throughout the year. The lack of rainfall in these regions can mainly be attributed to the cold Benguela upwelling system which occurs off the western coast and which suppresses rain formation (e.g. Muller et al., 2008). In the arid regions of the western part of southern Africa, coastal fog and dew are important moisture sources. Further south, the climate becomes more humid again but still shows strong rainfall seasonality. Around the Cape Region a Mediterranean climate with a rather dry summer and a wet winter (April to September) season is predominant. This region is characterised by prevailing westerly

flows and frontal systems. Only a limited part of the South African south coast receives rainfall throughout the year (e.g. Schulze, 1965).

In Figure 2.1 mean temperature and rainfall patterns derived from globally available datasets are displayed. Temperature patterns in the region are affected by the relatively cold sea surface temperatures of the South Atlantic. They show a distinct annual temperature cycle in the range of about 8 °C in Namibia and about 12 °C around the Cape region. Mean annual temperature on the adjacent land, however, ranges from about 15 °C in the south up to about 23 °C in the north-east of Namibia (Figure 2.1a). Seasonal rainfall amounts (Figure 2.1b & c) vary from about 100 mm/month in the north and around the Cape during the respective rainy seasons to almost no rain in the desert regions. Furthermore, the region is affected by a strong variability in rainfall, often connected to anomalies in the sea surface conditions of the South Atlantic and the adjoining Southern Ocean (e.g. Reason et al., 2002; Rouault et al., 2003; Muller et al., 2008). Rainfall variability is largest in the arid regions along the coast and declines towards the more humid regions. Large scale circulation patterns are frequently superimposed on by local circulation features, induced by the land sea contrast and the complex orography, often leading to locally very different climate states. As a consequence of the unique and extreme climate conditions a specialized flora and fauna has evolved in the region.

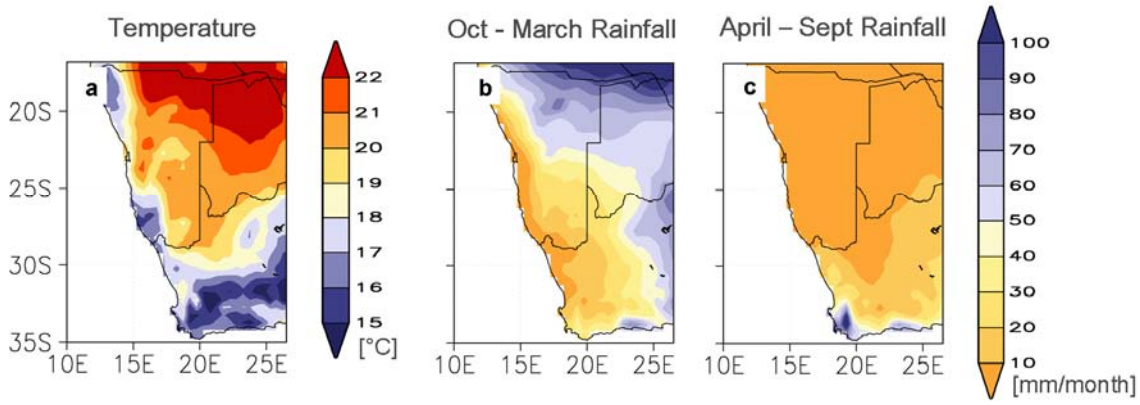

Figure 2.1: Observed (Climate Research Unit (CRU) dataset, Vs. 2.1; New et al., 2002) mean annual temperature (a) and mean seasonal precipitation (Global Precipitation Climatology Centre dataset (GPCC); Schneider et al., 2008) for the summer (b) and winter (c) season for the period from 1951 to 2000.

2.2 Observed changes in the past

This section focuses on the observed changes of the climate characteristics of Namibia and western South Africa over the last century. However, one has to keep in mind that there are only a limited number of long-term climate observations available for the southern African region. The analysis of long-term trends is therefore based on the most recent version of the globally available dataset of the Climate Research Unit (CRU3), which has a horizontal resolution of 0.5 degree. In the 4th Assessment Report (AR4) of the Intergovernmental Panel on Climate Change (IPCC) a synthesis of observed changes of surface and atmospheric climate characteristics at a global scale was given (Trenberth et al., 2007). They found that the global mean temperature increased in the period from 1906 to 2005 by 0.74 °C. In AR4 increasing temperature trends were also reported for the southern African region. Kruger and Shongwe (2004) analysed South African temperature station data for the period 1960 to 2003. For the western part of South Africa, they found a statistically significant temperature increase of about 0.1 – 0.2 °C per decade. In Figure 2.2 (upper panels) the observed temperature trend for Namibia and western South Africa for three different time periods (1901 to 2006, 1951 to 2006, 1981 to 2006) are shown for the CRU3 dataset. According to this dataset a warming occurred over the majority of the region for all investigated periods. Furthermore, an increasing warming trend is visible in the second half of the observed period. Maximum warming trends occur in the north-east of the region and with about 0.35 °C/decade for the period from 1951-2006 and about 0.5 °C/decade for 1981-2006. However, during the last period most of the changes observed in Namibia and western South Africa are not statistically significant.

For precipitation, AR4 indicated that a drying trend is evident over the greater southern Africa region since 1901. The observed decrease in annual rainfall is mainly caused by a decrease in dry season rainfall, as a long-term analysis of mean summer rainfall (December to April) did not show a significant downward trend (Fauchereau et al., 2003). Connected to the decrease in annual rainfall is an increase in drought conditions over the region (Trenberth et al., 2007).

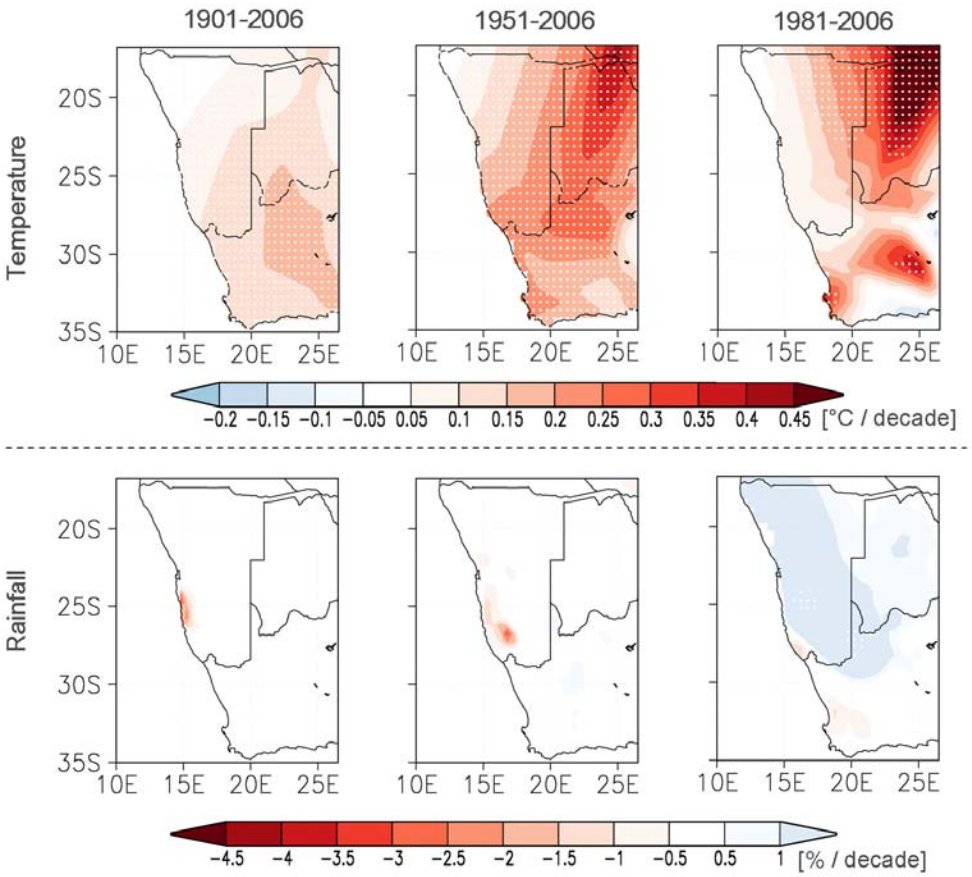

Figure 2.2: Observed (CRU3) temperature (upper panels) and precipitation trends per decade for three different periods (1901 to 2006; 1951 to 2006; 1981 to 2006). Statistically significant trends on a 95th level are stippled.

For the Namaqualand region MacKellar et al. (2007) investigated rainfall changes that occurred during the 1950 to 1999 period. They found a rather heterogenic behaviour that somehow seems to be related to topographical patterns. In general, a trend towards more rainfall was observed for the low-lying costal regions, whereas further inland over the higher elevated regions a drying trend was noted. This patchy structure of observed rainfall trends during the second half of the 20th century can also be extended to the whole western part of South Africa (Warburton and Schulze, 2005). In both studies no measure for the statistical significance of the observed trends over the Namaqualand region as well as for the greater western South Africa was provided. An analysis of observed annual precipitation trends for western South Africa and Namibia based on the CRU3 data is presented in Figure 2.2 (lower panels). This analysis shows that for the whole region only very small, but statistically insignificant changes occurred during the 20th century.

Analyses of long-term trends on a higher temporal resolution than discussed above are rather sparse for the southern African region. New et al. (2006) analysed daily temperature and precipitation station data for the southern African region for the 1961 to 2000 period. They found a consistent pattern for daily temperature trends, with a statistically significant increase of both, daily maximum and minimum temperatures. For rainfall, the trends found at the stations are less consistent and significant. Averaged for the whole southern African region statistically significant increases of average rainfall intensity, one day maximum rainfall, and extend of the dry spell length were found, but no clear signal for the western part of the southern African region could be identified.

Instead of showing a clear significant trend towards a drier climate, the western part of southern Africa is characterised by strong interannual rainfall variability (Figure 2.3; lower panels) which is, as already mentioned, mainly connected to anomalies in the South Atlantic surface characteristics. The interannual rainfall variability shows a cyclic behaviour, which varies for different areas of the southern African region. Around the south-western part of South Africa, Tyson et al. (1975) assigned an oscillation interval of more than 20 years. The oscillation of South African rainfall is related to interdecadal anomalies of the Ocean surface and atmospheric waves (Mason and Jury, 1997). The time series of annual rainfall anomalies also confirms that not only does annual rainfall amount show no significant trend, but also the interannual variability remains relatively constant throughout the period covered by the observations (Figure 2.3; lower panels). For the central Namibian region, represented by the North area, evidence suggests that the last 25 years of the observation period have been remarkably dry. However, a significant change towards a drier climate can not be seen yet. For temperature (Figure 2.3, upper panels), the general warming trend is also visible in the time series of both regions. Generally a gradual warming occurred in the first half of the 20th century, followed by an extended period of cooling. It is only since the mid seventies that a continuous warming trend is observed.

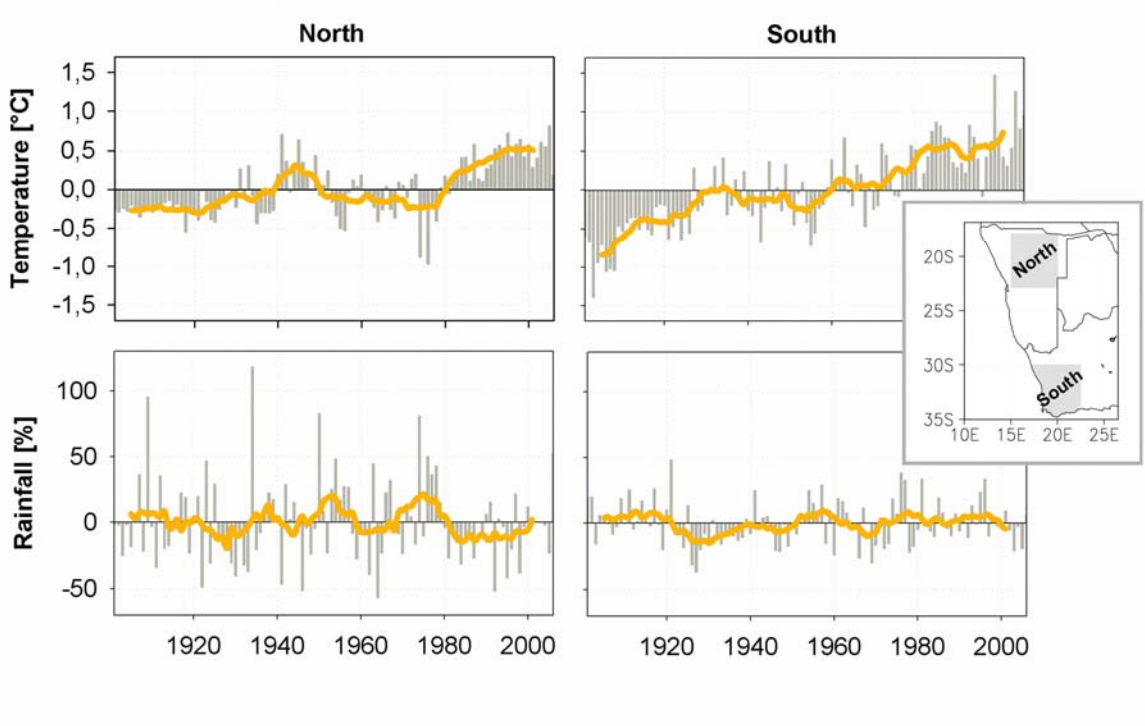

Figure 2.3: Observed (CRU Vs. 3) yearly anomalies of the long-term mean (1901-2006) of temperature (in °C, upper panels) and rainfall (in %, lower panels). The orange line depicts a 10-year running mean. Data is an area average over all land points for the region from 15E to 20 E and 18S to 23S in the case of the North region and from 17E to 22 E and 30S to 35S for the South region (indicated in the inlet figure).

2.3 Summary and Conclusions

The climate of Namibia and western South Africa is characterised by semi-arid to arid conditions with strong rainfall seasonality. During the 20th century a statistically significant temperature increase was observed for the region. However, the temperature increase was not linear but showed an extended period of cooling in the middle of the 20th century. Since the 1970s temperature has again risen gradually. For annual precipitation no significant trend is visible in the observation record, but a strong interannual variability can be noted throughout the observed period. However in Namibia, the data might indicate a tendency to a drier climate during the last 25 years. To investigate if the observed tendencies are likely to continue in the future, high-resolution climate projections are required. A regional climate projection for the western part of the southern African region is discussed in Chapter 4 and in Haensler et al. (2010c) and Haensler et al. (2010d).

Chapter 3

Dynamical downscaling of ERA40 reanalysis data over southern Africa: added value in the simulation of the seasonal rainfall characteristics

3.1 Introduction

In the present chapter a high-resolution regional climate model simulation is evaluated over the southern African region. To assess the impacts of climate change on the environmental conditions, detailed climate change information is needed for the region. Due to the amount of computer power required, climate estimates from global climate models are so far only available on a coarse resolution of about 200 to 300 km and therefore less suitable to be used for process studies on the local or regional scale. Qualified tools to receive the needed detailed information are statistical (e.g. von Storch et al., 1993; Hewitson and Crane, 2006) or dynamical (Giorgi, 1990, Laprise, 2008) downscaling methods. Dynamical downscaling is based on the application of regional climate models (RCMs) to derive high-resolution regional climate information on a selected region that covers the area of interest. With the application of RCMs climate information can be downscaled to a kilometer scale. So far, most of the RCM-downscaling studies were conducted at horizontal grid spacings between 50 and 15 km (Giorgi, 2006). However, in some regions of the world even more detailed simulations are available (e.g. Jacob et al., 2008).

Due to the surplus of gained information RCMs have been applied several times over southern Africa in the past. To assess the diurnal precipitation cycle over the region the

MM5 RCM was used (Tadross et al., 2006). The same model was applied to investigate the role of vegetation on the regional climate (MacKellar et al., 2009). The RegCM3 RCM was used to study the rainfall variability over southern Africa (Kgatuke et al., 2008). Nevertheless, even a significant amount of RCM studies already exists over the region most of them are restricted to very short time periods of a couple of seasons.

Additionally to the above mentioned process studies, several RCMs also have been applied over the region to downscale future climate projections (e.g. Arnell et al., 2003; Tadross et al., 2005). Furthermore, the variable-resolution global model CCAM was applied for regional climate change scenario simulations over subequatorial Africa (Engelbrecht et al., 2009). Nevertheless, none of these simulations have been conducted on a horizontal resolution higher than about 50 km. For the use in impact models climate information on this scale might not be appropriate.

Within the framework of the BIOTA South project (e.g. Jürgens et al., 2010; Krug et al., 2006), the Max Planck Institute for Meteorology (MPI-M) regional climate model REMO is applied over the southern African region at a horizontal resolution of about 18 km for transient climate change projection from 1960 to 2100 (see Chapter 4). This will be the first long-term climate projection that has ever been performed over the region at such a high horizontal resolution. The REMO model has already been successfully applied over several other regions of the world (e.g. Europe: Jacob et al., 2007; South America: Silvestri et al., 2009; South Asia: Roy et al., 2008; Saeed et al., 2009). Over tropical and northern Africa REMO has been applied to assess the future climate and also to estimate the effects of land use changes on the climate (Paeth and Thamm, 2007; Paeth et al., 2009).

In the present study the capability of REMO to reproduce the predominant climate characteristics of the southern African region is evaluated, as shown in Figure 3.1, with a focus on South-West Africa (SWA) and the main BIOTA North-South Transect (BNST). For this hindcast simulation almost 50 years of ERA40 reanalysis and operational analysis data of the European Centre for Medium-Range Weather Forecasts (ECMWF) have been downscaled to 18 km horizontal resolution. So far, no long-term dynamical downscaling study has been conducted at a comparable resolution for the southern African region. The main challenge the model has to face in this region is to simulate its unique rainfall characteristics, with a strong seasonality on the one hand and the change between semiarid climates and desert climates on the other hand. Due to the fact that REMO so far has not been applied over the southern African region this

evaluation of the hindcast simulation will indicate the quality of the model results and is seen as an essential first step before the start of the transient climate change projection. Furthermore, due to its high resolution, the data is also used in the framework of the BIOTA South project as a supplement to existing climate station data.

The chapter is organized as follows: In Section 3.2, a short description of the model and the simulation setup as well as the observation data, used in this study, is given. In Section 3.3, the results of the REMO simulations for the full domain and especially for SWA and BNST are presented. In the discussion section the remaining model deficits and the added value of the application of a RCM over the southern African region are discussed. Finally, a short summary and conclusion section is presented.

3.2 Model description, simulation setup and observation data

3.2.1 Model description

The simulations are conducted with the three-dimensional hydrostatic limited-area atmospheric model REMO (Jacob and Podzun, 1997; Jacob, 2001a) in the version 5.7. The model is based on the “Europamodell”, the former numerical weather prediction model of the German Weather Service (Majewski, 1991). In its original version the physical parameterizations of REMO were based on those of the global climate model ECHAM4 (Roeckner et al., 1996). The prognostic variables of REMO are surface pressure, horizontal wind components, temperature, specific humidity and cloud water.

Lateral boundary conditions can be taken from analysis/reanalysis data as well as from global climate models. A relaxation scheme following Davies (1976) is used to adjust the prognostic variables towards the boundary forcing in a zone of 8 lateral grid boxes. The parameters representing the vegetation and land surface characteristics in the model are taken from the LSP2 dataset (Hagemann, 2002). Thermal properties of the soil are parameterized according to ECHAM 4 (Roeckner et al., 1996). Soil temperatures are calculated for 5 discrete soil layers with zero heat flux at the bottom (10m). The heat diffusion in the soil solely depends on the heat capacity and the heat conductivity of the soil and therefore is independent of the soil water content. Water infiltration into the soil is calculated by the improved Arno scheme (Hagemann and Dümenil Gates, 2003) that

separates rainfall and snowmelt into surface runoff and infiltration. The soil hydrology is represented by a bucket scheme, which lower boundary is constraint by the mean rooting depth of the grid box.

3.2.2 Simulation setup

The simulation is conducted at a horizontal resolution of approximately 18 km. The model domain for this simulation is presented in Figure 3.1. To achieve this high resolution, the double nesting procedure was applied, in which the boundary forcing for the high-resolution simulation is generated by an intermediate resolution simulation. The lateral boundary forcing for the current high-resolution simulation was obtained from a Sub-Saharan REMO-simulation (south of 10N) at a resolution of about 50 km, which was forced with ERA40 reanalysis data (Uppala et al., 2005) and ECMWF operational analyses data. The update frequency of the lateral boundaries of the model was set to 6 hours. The simulation period covers the years from 1958 to 2007.

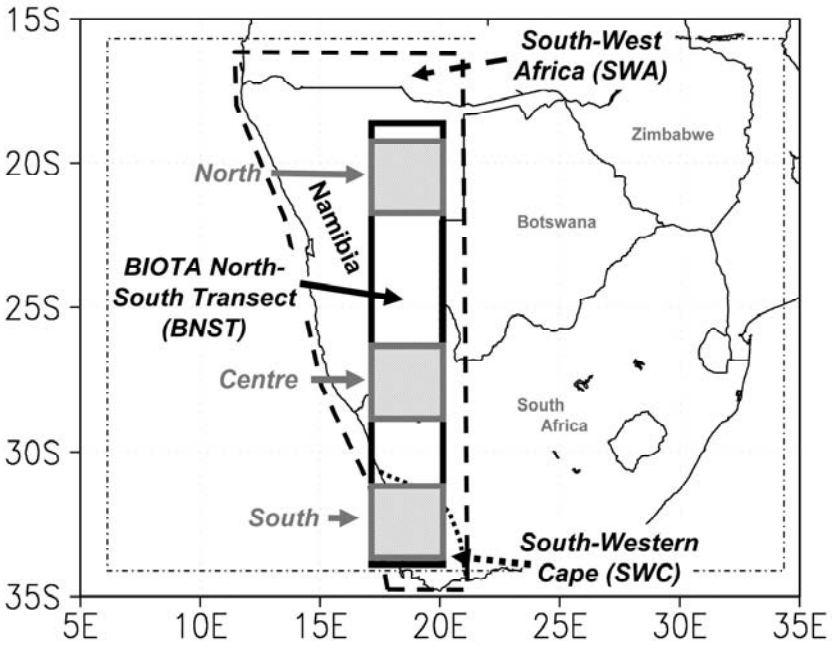

Figure 3.1: REMO model domain for the 18 km simulation and the focus regions of the study. The BIOTA North-South Transect (BNST, solid black box) is defined for the region between 17 to 20 E and 18 to 34 S. The North region coves the area between 17 to 20 E and 19 to 22 S, the Centre region between 17 to 20 E and 26.5 to 29.5 S and the South region between 17 to 20 E and 31 to 34 S. The dashed frame defines the border of the boundary relaxation zone, which was excluded from the analysis.

3.2.3 Observational data

To evaluate the performance of REMO over the region, detailed observational data are required. For South Africa, a gridded daily precipitation dataset at a horizontal resolution of 10 km was compiled (hereafter referred to as HCPD; Hewitson and Crane, 2005). Daily temperature data based on about 900 stations are also available for the region (Schulze and Maharai, 2003). Additionally the globally available monthly dataset of the Climate Research Unit (CRU VS.2.1) for precipitation and temperature was used (New et al., 2002) as well as a gridded global precipitation climatology available at a horizontal resolution of 0.25 degree from the Global Precipitation Climatology Centre (GPCC; Schneider et al., 2008). The regional circulation climatology is taken from ERA40 reanalysis data (Uppala et al., 2005). In general, the analysis of the model data is performed for the period from 1960 to 2000. However, the South African gridded station dataset for precipitation was only available for the period 1960 to 1999 and the GPCC dataset was only available as a climatological mean for the period from 1951 to 2000. Even though both datasets deviate from the standard analysis period; it was decided to still use them, as their high horizontal resolution implies more regional details than the 0.5 degree CRU dataset.

3.3 Evaluation of the model results

3.3.1 South African domain

The southern African region is a mainly semiarid region with rainfall ranging from almost no rain in the arid zone along the west coast to more than 1000 mm/year in the humid mountainous region in the south east (Figure 3.2b). Rainfall shows a strong seasonality with the majority of the region receiving its rainfall in the summer season (Oct-Mar). Exceptions to this are the South-Western Cape (SWC) having its rainfall maximum in the winter season and a part of the South African south coast that receives rainfall throughout the year. Rainfall patterns are influenced by both, tropical systems (mainly in the northern, central and south-eastern parts of the domain) as well as frontal systems with prevailing westerly flows (mainly in the SWC region). During the summer season the central region is generally influenced by a weak heat low, which tends to produce convective rainfall systems over the moister eastern parts of the domain. In

winter the situation mainly changes to a predominant anticyclonic circulation caused by a large single high pressure cell.

Figure 3.2 shows that REMO is able to reproduce the spatial rainfall patterns but tends to have too much rainfall towards the more humid regions mostly in the south east and north east. Mean wet bias in these parts of the domain range between 40 to 80%. However, over the dryer regions in the western areas REMO is in good agreement with the observations (in the range of ±30%), only along the coast line a strong overestimation is visible. However, this costal wet bias should not be overstated as it is partly an artifact of the interpolation. One possible explanation for the wet bias over the humid parts of the domain can be found in the simulation of the atmospheric circulation patterns over the region, which could lead to an increased moisture input into the domain.

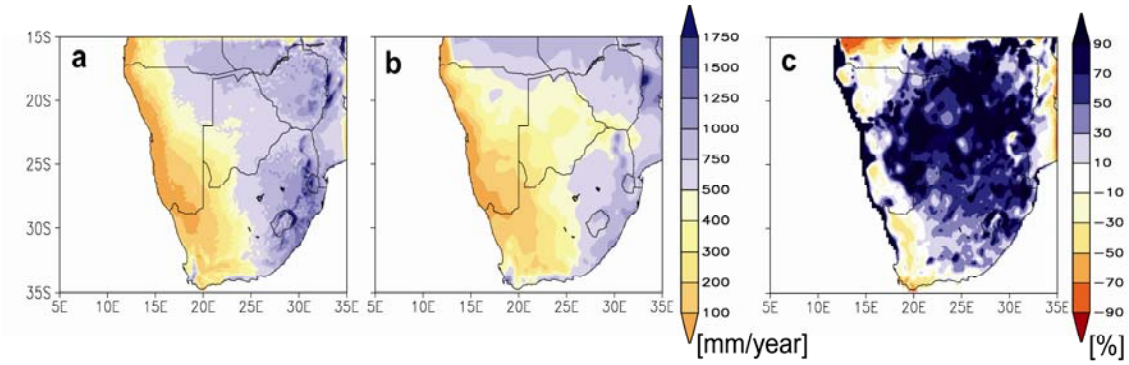

Figure 3.2: Mean annual precipitation (in mm/year) as simulated with REMO (a) for the period 1960 to 2000) and observed by GPCC (b) – for the period 1951 to 2000). Figure 3.2c shows the relative precipitation bias of the model compared to the GPCC dataset, at 0.25 degree horizontal resolution.

Figure 3.3 shows the mean sea level pressure (MSLP) and near surface winds of REMO (for the 18 km and 50 km simulation) and ERA40 as climatological mean over the 1960 to 2000 period for the summer and winter seasons. The 50 km simulation, which is used as forcing for the 18 km simulation, is included in the analysis to assure, that the large-scale features are preserved in the REMO simulations. Compared to ERA40 data the predominant circulation patterns are captured by the model for both seasons and both resolutions in a satisfactory manner. Nevertheless REMO tends to simulate a slightly

lower MSLP in the summer heat low region as well as a slightly higher MSLP in winter high pressure cell in both cases. Additionally, the centre of the winter high pressure zone is slightly shifted towards the north-east in the 50 km simulation. The overestimation of the heat low and the winter high is slightly larger in the 18 km simulation, showing about 1.5 hPa (~1 hPa in case of the 50 km simulation) difference to ERA40 in the winter season and about 1 hPa (~0.25 hPa) difference in the summer in the respective core pressure regions. With respect to the overestimation of summer precipitation of the 18 km simulation especially the former is important. The overestimation of the summer heat low, connected with an enhanced inflow of moist air originating from the warm Indian Ocean could explain the overestimated summer precipitation over the south-eastern parts of the domain. This tendency of REMO to simulate a too high moisture transport into the domain is should be considered when applying the model for climate change simulations over the region.

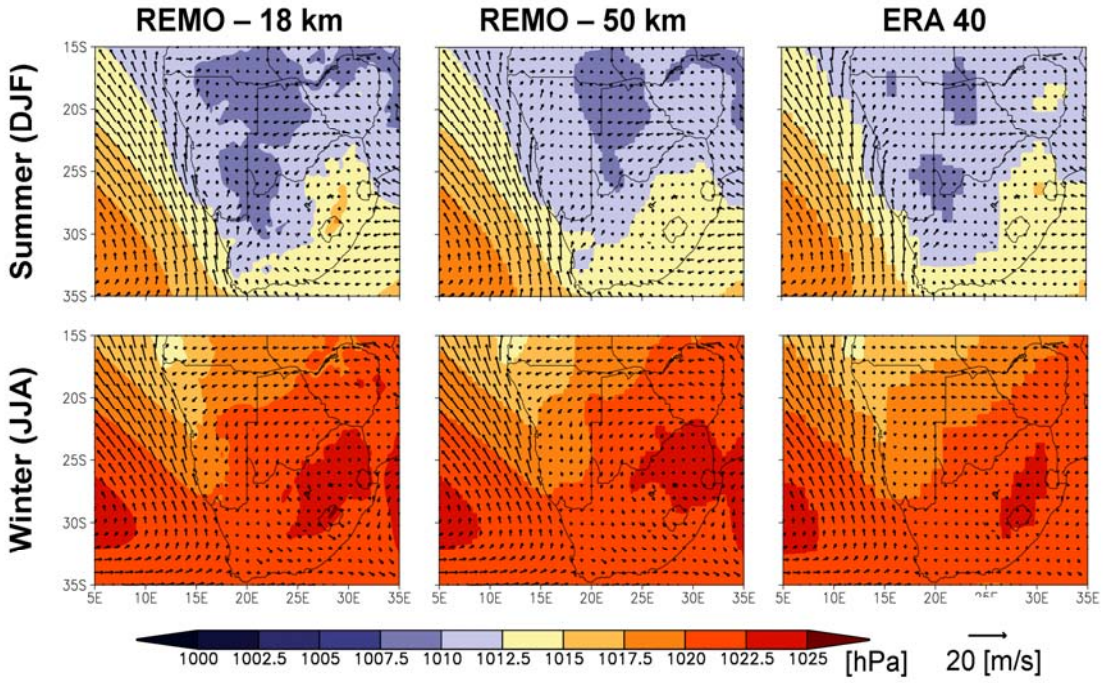

Figure 3.3: Summer (DJF) and Winter (JJA) mean sea level pressure overlain by the predominant circulation patterns simulated by REMO at 18 km horizontal resolution (left), REMO at 50 km horizontal resolution (centre) and ERA40 (right) for the period 1960 to 2000.

3.3.2 SWA and BNST

The regional focus of this study lies on the performance of REMO over the SWA region and along the BNST. SWA is characterized by the cold upwelling regions of the Benguela ocean current and the Namib coastal desert system. Rainfall in the region shows a strong north-south gradient. In the rather humid regions in the north, tropical systems during the summertime sometimes carry a substantial amount of rain. The southern tip of SWA is characterized by winterly westerly flows and winter rainfall. The centre is generally rather dry, with arid conditions along the Namib coastal desert system. Especially in the arid regions in the centre, coastal fog and dew is one of the most important moisture sources. Furthermore, the SWA region is affected by a strong variability in rainfall, often connected to anomalies in the sea surface conditions (e.g. Reason et al., 2002; Rouault et al., 2003; Muller et al., 2008). Large scale circulation features are often superimposed by local circulation features, induced by the land-sea contrast and the complex orography, often leading to locally very different climate states.

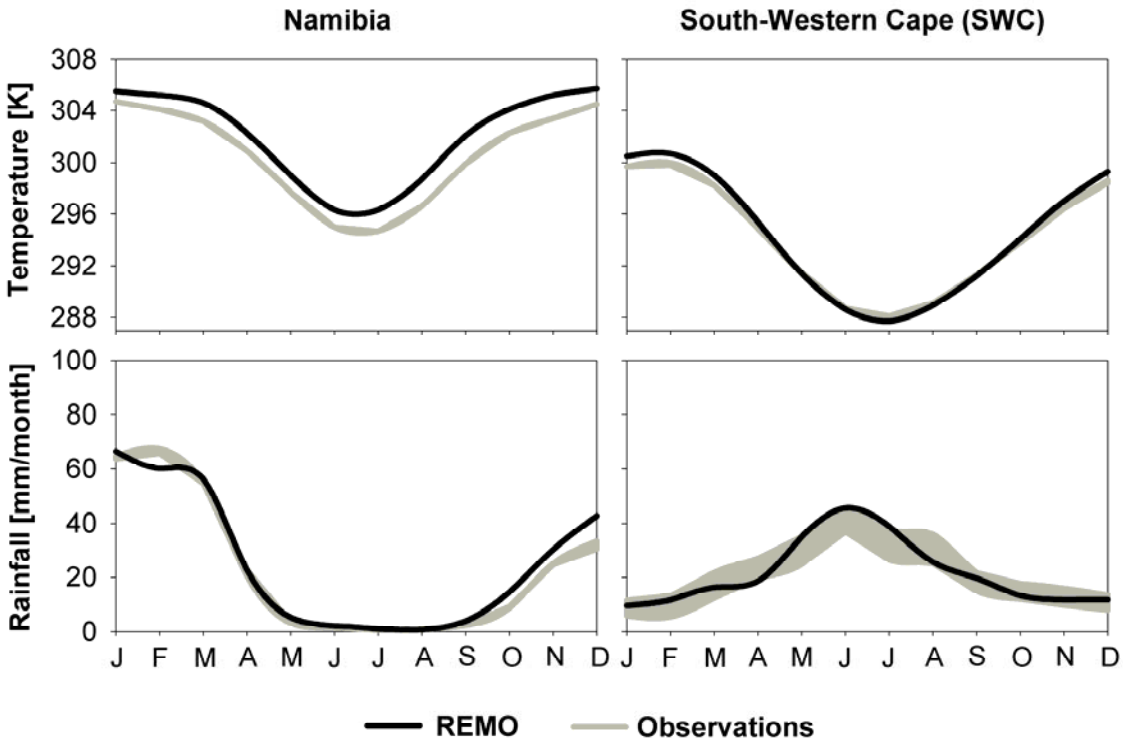

Figure 3.4: Temperature and precipitation climatology (1960 to 2000) as a weighted mean over all land points for Namibia and the SWC region as simulated and observed. The observational spread comprises for Namibia of CRU and GPCC (precipitation) and CRU (temperature); and for SWC of CRU, GPCC HCPD (precipitation) and CRU and station data (temperature).

Figure 3.4 shows the climatological annual cycle of weighted area mean temperature and precipitation for Namibia and SWC. A weighted mean was used to account for differences in the gridbox area, which is related to the distance to the equator and therefore slightly changes over the domain. The mean temperature cycle is represented very well in REMO. However in terms of absolute values REMO tends to overestimate the 2m air temperature compared to the observations. The warm bias in the simulation is generally increased in the dryer regions of Namibia, with an annual mean bias of about 1.5 K. The seasonal variations of precipitation with predominantly summer rain conditions in the north and winter rain in SWA are captured very well by the model. In addition, the mean precipitation amount for both regions is almost perfectly represented in REMO. Table 3.1 summarizes the simulated mean values and the respective bias of the model for both regions and both variables.

Table 3.1: Summary of simulated annual mean values and respective annual mean bias compared to observations for Namibia and SWC. The range of the bias is due to several observational datasets – see Figure 3.4.

Regions	Temperature			Rainfall		
	Annual Mean [K]	absolute Bias [K]		Annual Mean [mm/month]	relative Bias [%]	
		Min	Max		Min	Max
Namibia	302.08	-	1.50	25.52	13.88	21.46
SWC	294.48	0.26	0.34	21.43	-20.27	22.85

To evaluate REMO along BNST, a zonal mean over all land points was calculated for the BNST region as indicated in Figure 3.1. For BNST the performance of REMO in comparison to observations is very similar as described above (Figure 3.5). On one hand, the simulated 2m air temperatures are generally too warm, with a maximum bias of about 3.5 K around 28 S (Figure 3.5a). On the other hand, precipitation is simulated for both, summer (Figure 3.5b) and winter (Figure 3.5c) seasons in good agreement with observations. Only the summer rain in the north is slightly overestimated by the model, resulting in a relative wet bias of about 20% at this part of BNST. This bias can be attributed to the previous mentioned overestimation of the summer heat low. Nevertheless, the seasonal distribution of rainfall is simulated in almost complete

agreement to the one observed. Figure 3.5d shows the percentage of rainfall occurring in the DJF season, with almost no discrepancy of the simulated to the observed rainfall distribution. Furthermore the climate type classification after Köppen & Trewartha (see de Castro et al., 2007 for details on the allocation of the climate types) was used as an integrated measure to investigate the performance of REMO along BNST. Based on this it can be shown that in the southern part of BNST the observed climate types are well reproduced by the model (Figure 3.5e). In the northern part, REMO indicates a more humid climate type than is observed. This finding is inline with the wet bias depicted in Figure 3.5b.

Furthermore it was investigated if the climate along BNST changed during the investigated period, by calculating the trends (Figure 3.5f & g). For the 2m air temperature, a general warming is indicated in the observations as already shown in Chapter 2. REMO also simulates the temperature increase along the whole BNST but especially in the northern part the simulated warming is about 0.7K less than the observed one. For rainfall, the model and observations deviate in the direction of the trend in some parts of the transect. Whereas REMO indicates a moistening along the whole BNST, the available station observations agree with the model in the southern part of BNST. In the northern part of BNST the observations (only CRU Vs2.1 available) indicate a slight drying, which is not simulated by the model.

However, above discussed trends in precipitation and temperature are rather small compared to the strong interannual variability and can not act as a proof for a clear trend towards a dryer climate. Applying a student t-test to the data, it was found that along the transect the majority of the observed rainfall trends over the investigation period are not significant on a 95% confidence interval. Only the general increase in precipitation in the southern part of BNST (where the model and station observations agree) is supported by the statistical analysis (Figure 3.5g). However the contrary behavior of REMO and CRU in the north of BNST does not seem to be a reliable feature and could also be caused by a slight difference in the interannual variability between model and data.

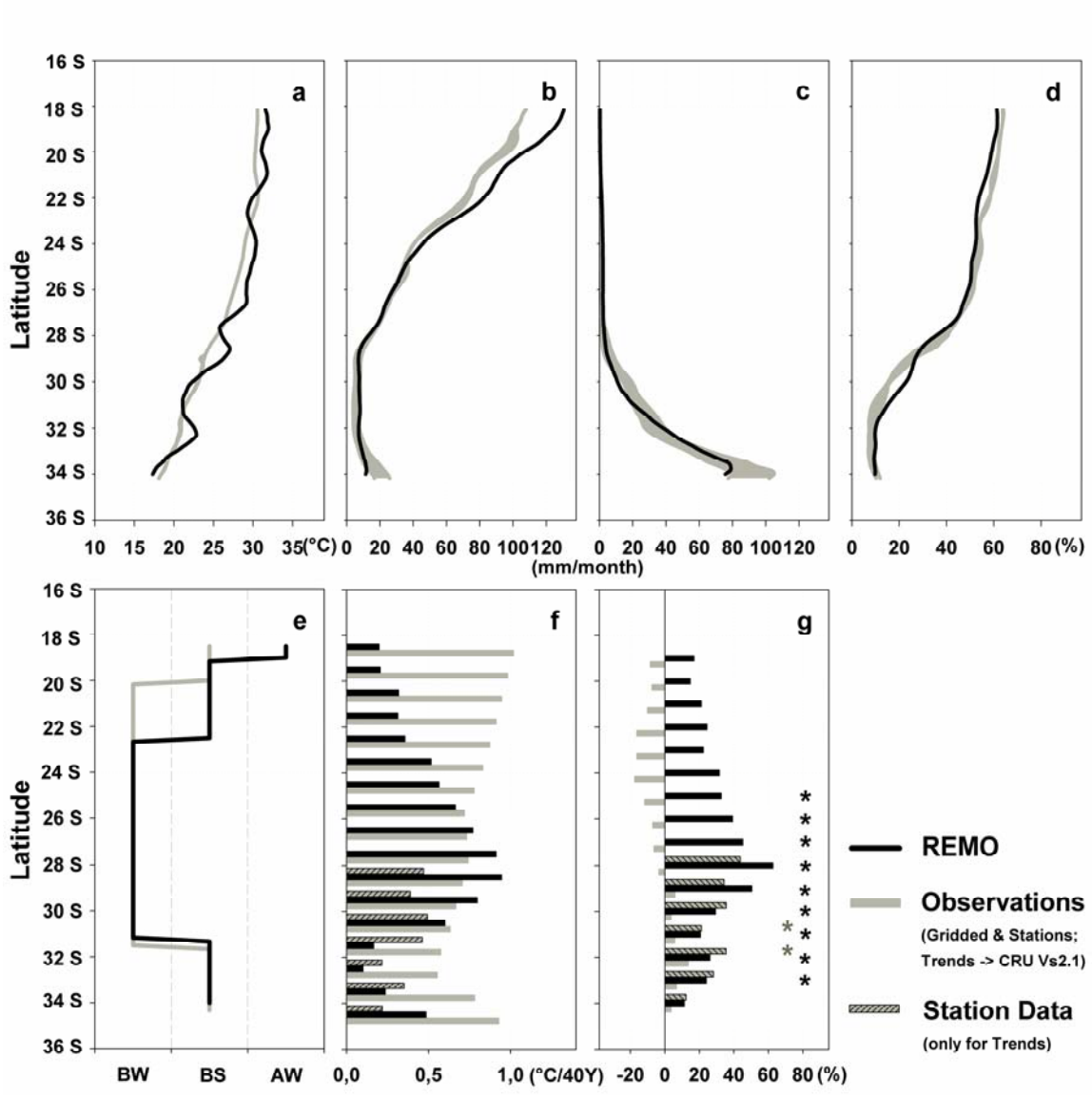

Figure 3.5: Comparison of climatological mean (1960 to 2000) REMO simulations and observations along the BNST for a) annual mean temperature, b) summer (DJF) precipitation, c) winter (JJA) precipitation, d) percentage of rainfall falling in the summer (DJF) months, and (e) Köppen & Trewartha climate types [BW: dry arid; BS – dry semiarid and AW – tropical wet-dry]. 5 f & g show the trends for this period for temperature (f) and precipitation (g). Stars indicate statistically significant rainfall trends on a 95% confidence interval (black: REMO; grey: HCPD).

In Figure 3.6 and Figure 3.7, the anomalies for precipitation and temperature for three regions along BNST are displayed (see Figure 3.1 for location; Note that the North and South region discussed here are not identical to the ones discussed in Chapter 2). The time series show a noticeable variation in temperature and precipitation. Especially the extreme wet years in the mid-seventies are pronounced at all three locations. Moreover,

these extreme wet years seems to be a turning point in the southern part of BNST, with rather dry years before and rather wet condition afterwards. Observed annual mean temperatures for those wet years are generally lower than the long-term average. This colder period is especially prominent in CRU dataset for the north and central part of BNST. REMO is generally able to simulate the strong variability in the rainfall. The highest correlation between REMO and observations is in the South, having an anomaly correlation coefficient of 0.65 for the CRU dataset and 0.73 for the stations (HCPD dataset). In the north, the anomalies are less well captured. Focusing on the last third of the anomaly time series of the northern part of BNST, REMO shows for 8 out of 17 years wetter than average conditions, whereas the CRU data for the same period consists of only four wet years. This discrepancy can lead to the previous indicated contrary trend behavior of REMO and CRU in that part of BNST.

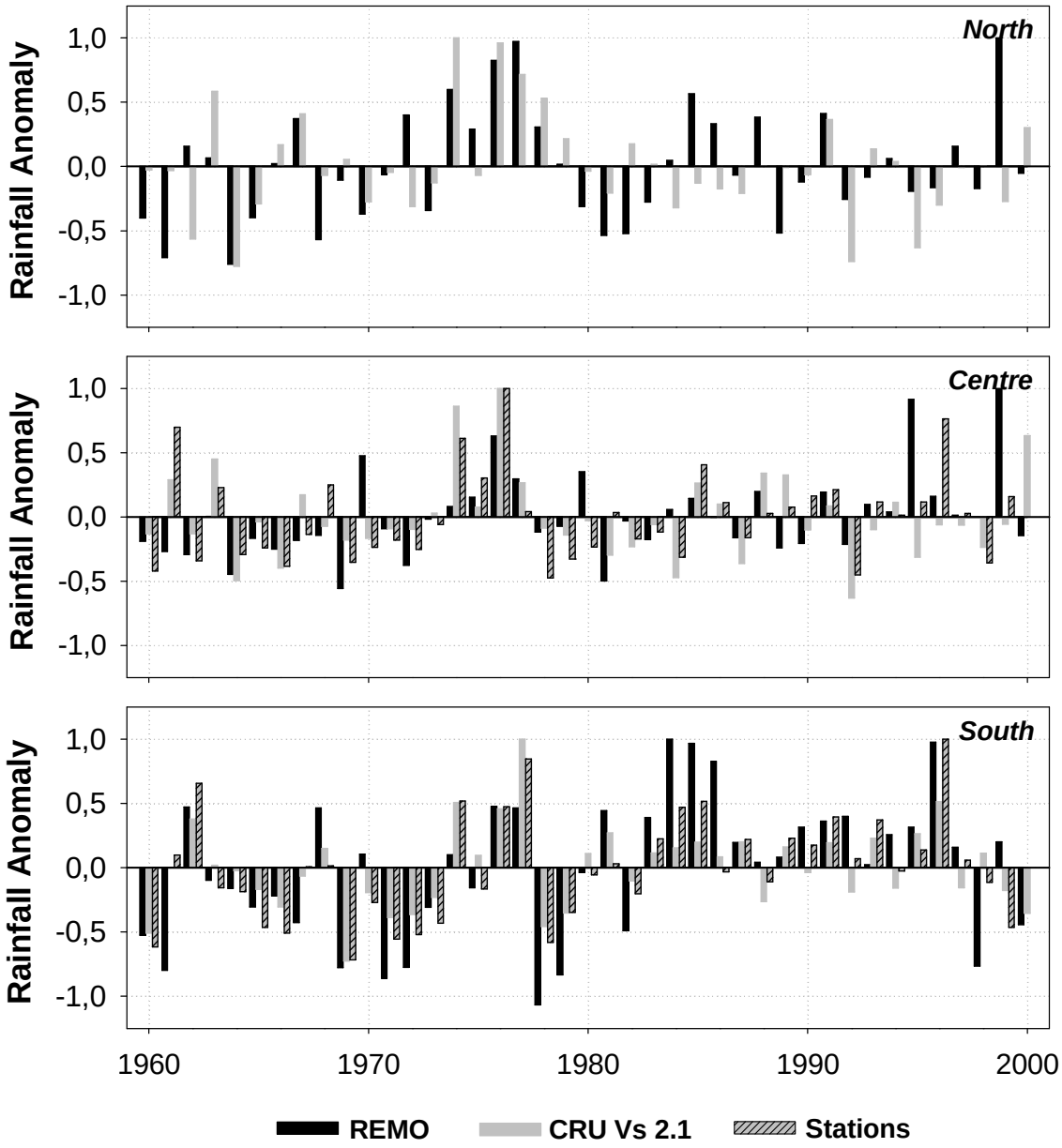

Figure 3.6: Standardized rainfall anomaly over the period 1960 to 2000 as a weighted mean over all land points for the three subregions of BNST (see Figure 3.1 for details) as simulated with REMO and observed. Data represent the deviation of annual precipitation sum from the long-term mean annual precipitation in relation to the maximum precipitation anomaly.

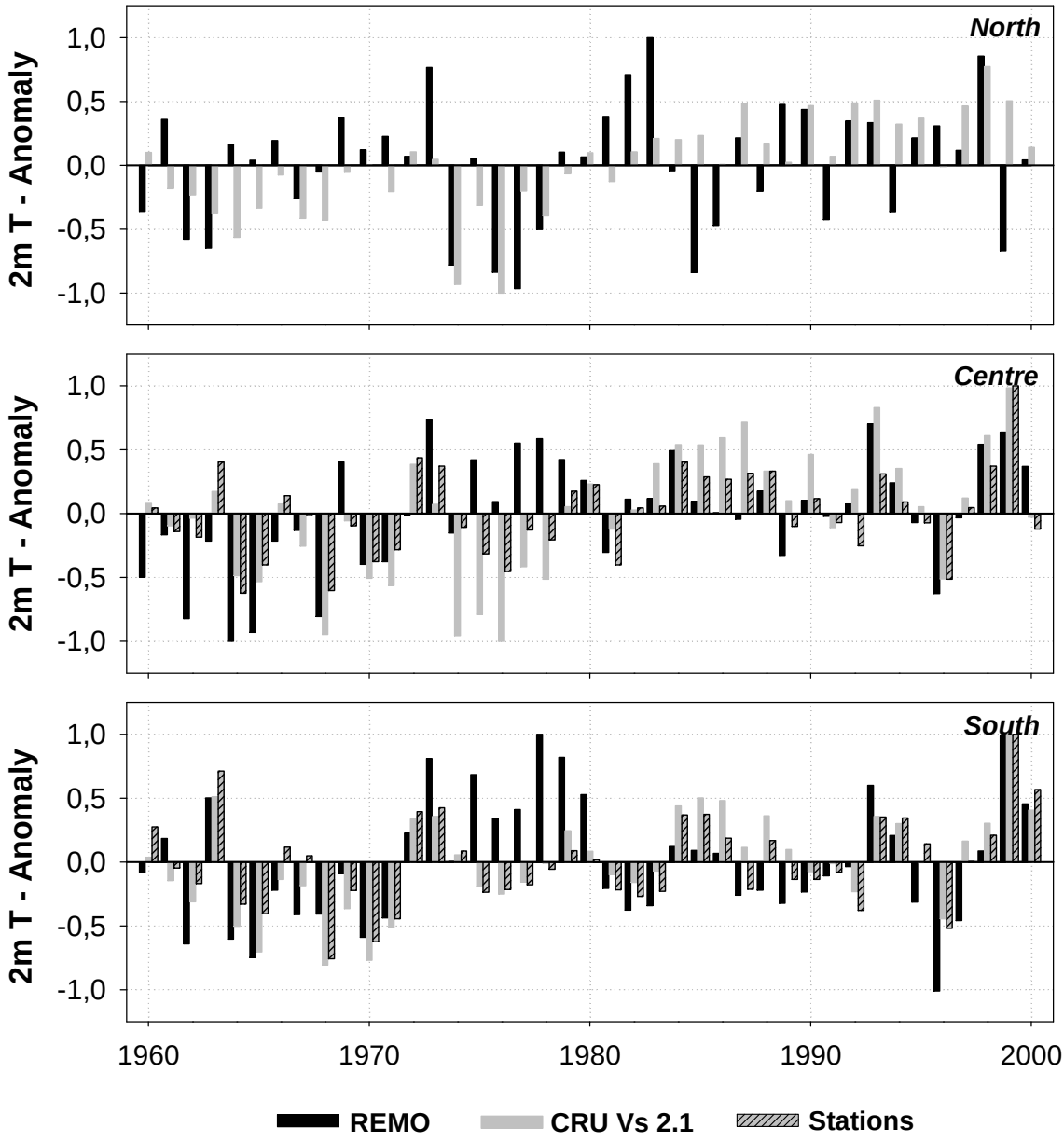

Figure 3.7: Same as Figure 3.6 but for 2m air temperature

The extreme wet years in the mid seventies, which are connected to anomalies of the Indian Ocean sea surface temperatures and ENSO (Washington and Preston, 2006) as well as the switch in rainfall in the southern parts of the transect are well captured by the model. In the case of temperature, REMO simulates a pronounced interannual variability for all three cases as it is also observed. The anomaly correlation coefficients for temperature range between 0.43 for the northern and central parts and 0.62 in the

south when compared to the CRU dataset, and are slightly higher for the stations. Furthermore, the link between the extreme wet years and a lower than average temperature is very well represented in the northern part. For the central and southern part, where the colder period is less pronounced, the model however simulates warmer than average years.

Even there is an agreement between the simulated and observed anomalies as described above, the consensus of the time series could partly also be random. To test the significance of the simulated interannual variability, the rainfall and temperature anomaly produced by REMO was compared for each region to a set of 10000 randomly compiled time series, each following a normal distribution. The random time series were generated with FORTRAN by using the inbuilt random number generator. Due to the fact, that the output of the random number generator in FORTRAN is equally distributed a transfer function based on the central limit theorem was applied to receive normally distributed random values. To assure the same range of variability in the resulting normal distribution, the standard deviation of the equally and normally distributed time series were kept in the same range. Each of the resulting random time series was normalized to its maximum anomaly. For each timestep the difference between the normalized observed (CRU) and the randomly compiled anomaly was calculated. To not only consider the differences in the anomalies, but also the direction (positive vs. negative anomalies) a further constraint for the case that the direction of the anomalies did not agree was introduced. For these cases the estimated anomaly difference was doubled. Finally, the deviation of each random time series was summarized and the resulting cumulative deviations were scaled according to the maximum cumulative deviation. The same procedure already described for the 10000 randomly compiled time series was applied to the REMO time series. In Figure 3.8 the scaled distribution of the cumulative deviations between the anomalies and random time series as well as the cumulative deviation of REMO are depicted. For rainfall the difference between REMO and the observations is significantly smaller than the one of the random time series. This finding indicates that the interannual rainfall variability simulated by REMO is a consequence of the fact that the regional rainfall dynamics are well captured by the model and that the match between REMO and observations is not based on a coincidence. For temperature, the anomalies in the southern and central part are significantly better captured by the model, compared to the random time series. In the northern part, the temperature anomalies in REMO are not closer to the observed

anomalies than the random anomalies. This result is inline with the general finding that there are still some deficits in REMO in simulating the 2m air temperature. As the observed anomalies do not directly follow a normal distribution, the experiment was repeated with a set of 10000 time series each equally distributed. In the case of equally distributed time series REMO results are even better (not shown). Especially in the northern part, REMO temperature anomalies then scale very close to the 5th percentile of the random experiments.

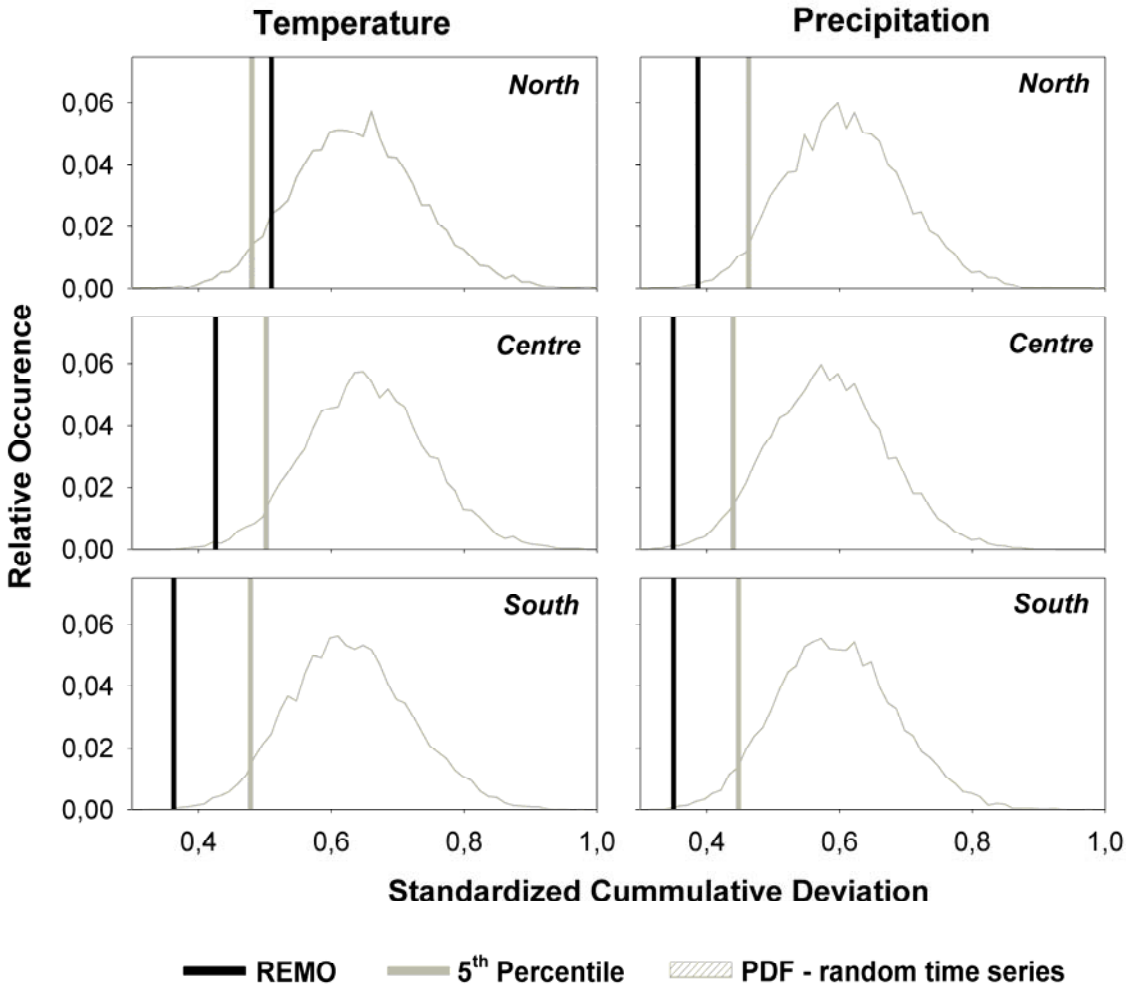

Figure 3.8: Probability density function (PDF) for the cumulative anomaly deviation of 10000 randomly compiled time series (which each time series following a normal distribution of the anomalies) compared to the CRU anomaly for temperature and precipitation for the three subregions of BNST (see Figure 3.1 for details). Grey bar: 5th percentile of PDF; black bar: Cumulative anomaly deviation of REMO.

3.4 Discussion

In the previous section the simulation results of REMO were compared to a set of several observations. It could be shown that REMO adequately simulates the predominant patterns of precipitation. Especially in the focus region of this study, in SWA and along BNST, the REMO results are very close to the observations; particularly the simulation of the mean rainfall conditions is almost in perfect agreement. One of the deficits of the model seems to be the warm bias in the temperature. Whereas the seasonal temperature cycle is well reproduced by the model, an absolute warm bias compared to observations is persistent. An analysis of the spatial patterns revealed, that there is a linkage between warm bias and the model's soil moisture content. To identify the link between the soil moisture and temperature bias the analysis of a monthly time series covering the period 1960 to 2000 of gridded REMO soil moisture and temperature bias (with respect to CRU data) was included. The soil moisture data was separated into several bins and for each gridbox and month the corresponding warm bias was identified. Afterwards, for each soil moisture bin, the mean warm bias and the standard deviation was calculated and plotted. The result of this analysis is generally, that the model seems to stronger overestimate the temperature in regions with lower soil moisture, than in wetter regions (Figure 3.9a). Based on these findings, it can be speculated that the resulting warm bias might be caused by two factors. First, the warming could be a consequence of the parameterization of the heat transfer in the soil. In the current model version, soil wetness is not affecting the thermal properties of the soil, so that they solely depend on the soil types. This could theoretically lead to a too large heat transfer into the soil, which would result in too warm surface temperatures and therefore also influence the 2m air temperature.

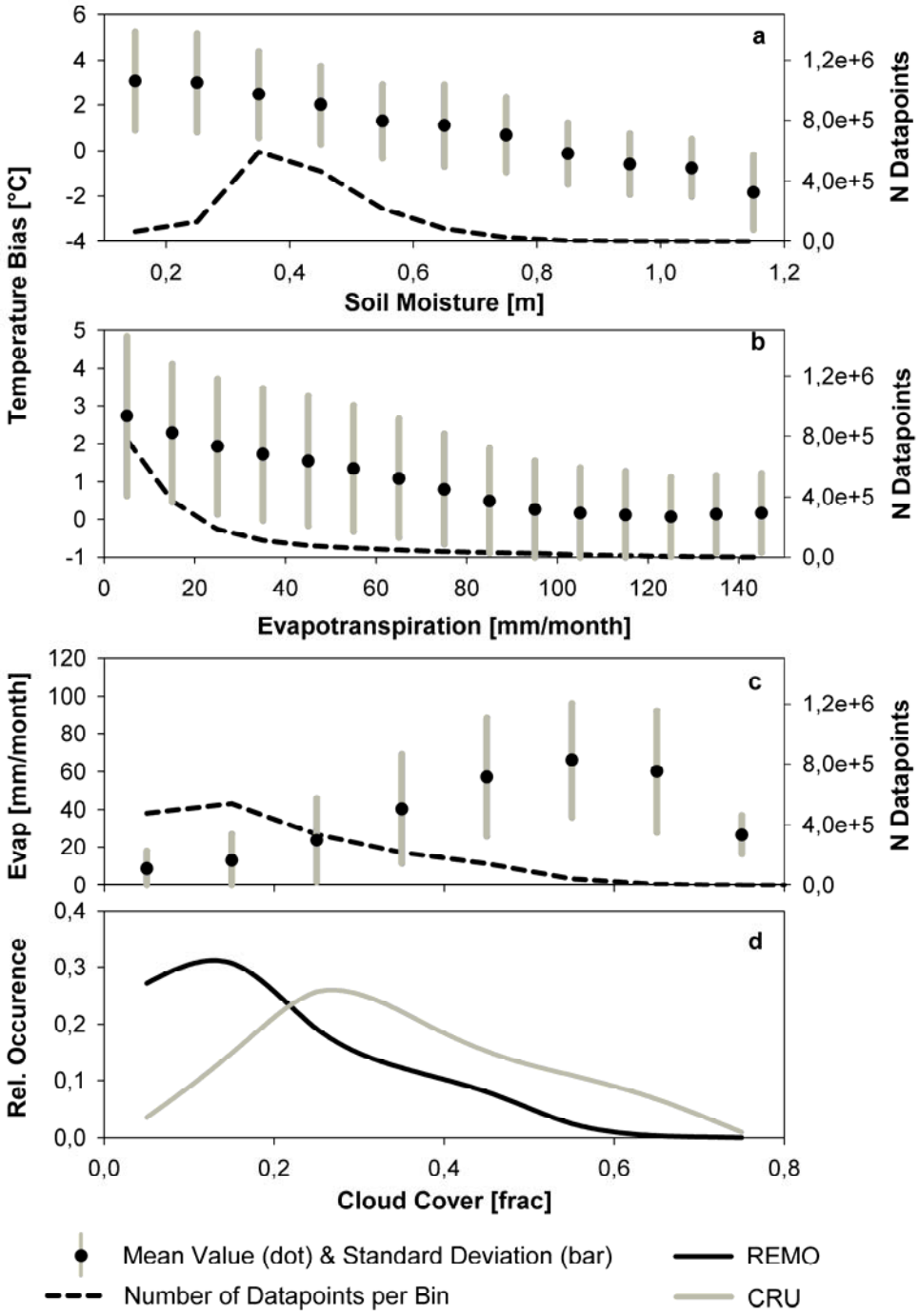

Figure 3.9: Correlation analysis between REMO temperature bias and a) REMO soil moisture, b) REMO evaporation. Analysis is based on a monthly time series (1960 to 2000) of gridded observation and model data for the South-West African region (SWA). Figure 3.9c shows the result of a correlation analysis of REMO evaporation and REMO cloud cover for the same time period and region. Figure 3.9d presents a probability density function of REMO and CRU fractional cloud cover for SWA.

Second, the warm bias of the REMO results over rather dry regions could also be a consequence of a too low soil water content in REMO, which would have an effect on the latent heat transport. A correlation analysis applying the above described method to a time series of REMO evaporation data revealed a significant (at the 99th confidence level) linkage between the observed warm bias and the evaporation fluxes, with a correlation coefficient of the respective bin means of 0.96 (Figure 3.9b). Generally it is obvious that the warm bias in the REMO simulation is strongest in regions with low soil water availability and therefore related to this with a rather low evaporation rate. These findings support the theory of the availability of soil moisture as a control element for the energy budget. Unfortunately neither soil moisture observations nor evaporation measurements are available for the region that are comparable to REMO output. Therefore it only can be speculated that the available soil moisture is too low in REMO. Nevertheless some support for the previous argumentation can be gained by comparing the REMO cloud cover to the CRU cloud cover dataset, which finds the simulated cloud cover in REMO significantly lower than the one of the CRU dataset (Figure 3.9d). Even though it is not supposed that local water recycling is the only reason for cloud formation in the region, clear a linkage between evaporation rates and cloud cover in the REMO results that encourages the argumentation (Figure 3.9c) can be identified. Furthermore, it is concluded that a too low cloud cover itself could lead to a warm bias in the simulation, as the incoming radiation and therefore the potential available energy is increased. The close connection in the model between soil moisture, evaporation and cloud cover on the one hand, and a bias in the 2m air temperature on the other can also be seen in the above discussed temperature anomalies for the three regions. Whereas in the north, the temperature decrease connected to the extreme wet years is captured in REMO, the model fails to simulate this link for the central and especially for the southern region (Figure 3.7). When analyzing the anomaly of simulated soil moisture, evaporation and cloud cover it can be shown that in the north (cold period captured by REMO) these parameters are maximum for the wet period, whereas for the south, none of these three parameters are significantly higher than in other years (Figure 3.10). To improve the simulation of the 2m air temperature the parameterization of both, the thermal as well as the hydrological properties of the REMO soil are currently improved. Some further simulations with a changed parameterization of the soil properties will be done in the near future.

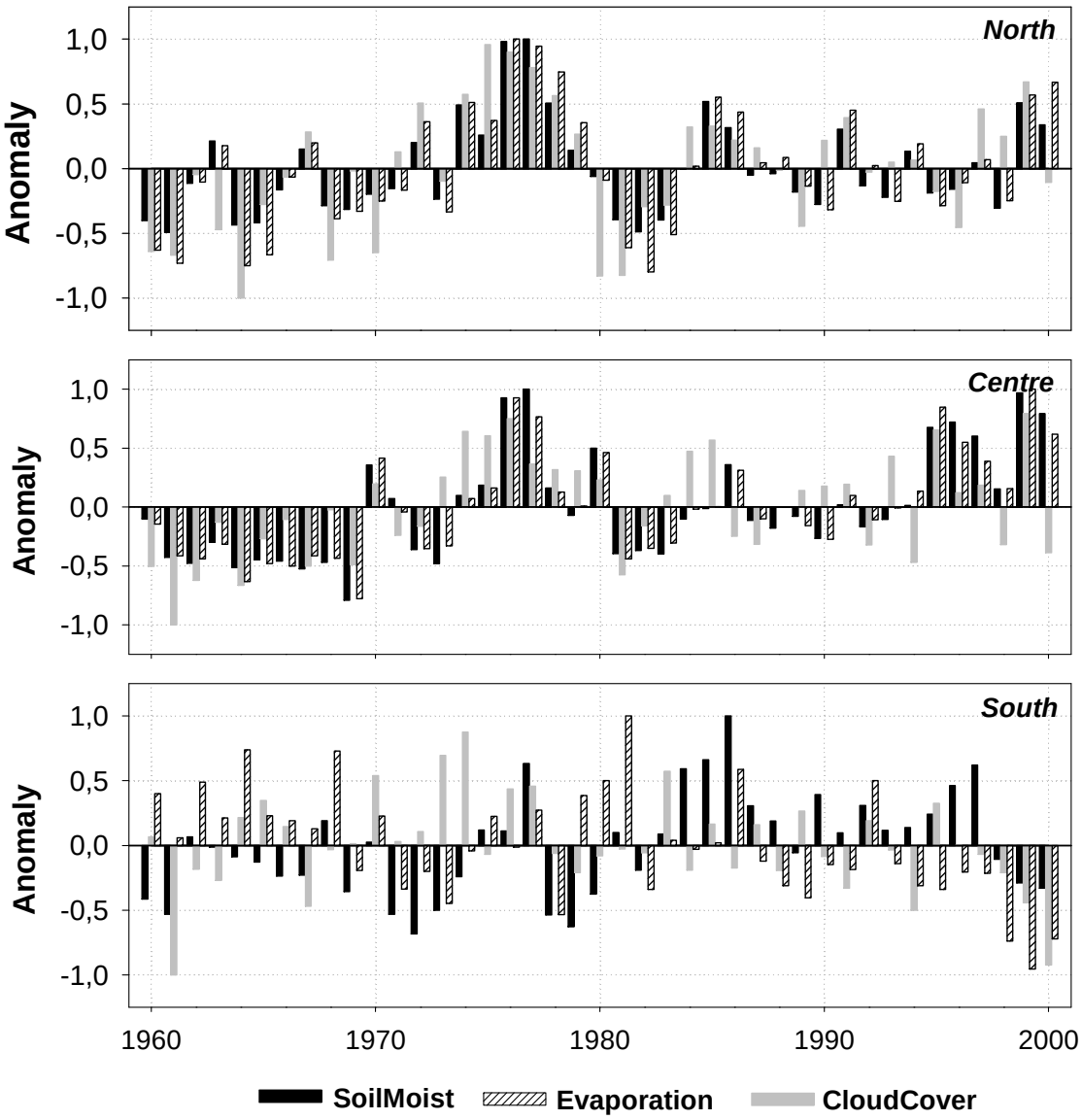

Figure 3.10: Simulated standardized anomalies of soil moisture, evapotranspiration and cloud cover over the period 1960 to 2000 as a weighted mean over all land points for the three subregions of BNST (see Figure 3.1 for details). Data represent the deviation of annual mean from the long-term mean in relation to the maximum anomaly.

3.4.1 Added value by the application of a RCM

Generally the purpose of applying a RCM is to improve the representation of the regional to local climate compared to the more coarsely resolved global climate models. The enhanced resolution of a RCM with its better representation of the topography and vegetation patterns allows for a better description of mesoscale atmospheric dynamics, especially along mountains or coastal regions (Laprise, 2008). Still it sometimes

remains difficult to proof the added value of a RCM. In the present study an added value can clearly be identified when downscaling globally available reanalysis data. As already mentioned in Section 3.3 REMO reproduces the observed rainfall along BNST in both seasons very well with only a slight overestimation of the summer rainfall in the northern parts (Figure 3.5b). One of the challenges along BNST is the correct simulation of the seasonal distributed rainfall, with winter rainfall occurring around SWC. When focusing on SWC, the REMO simulation clearly shows an added value compared to the ERA40 forcing data. While in the ERA40 reanalysis data rainfall is underestimated by about 60 to 70 % REMO rainfall is well in the rainfall range defined by the observations (Figure 3.11). This clearly identifies the benefit of using a regional climate model especially in regions with complex topography and climate characteristics.

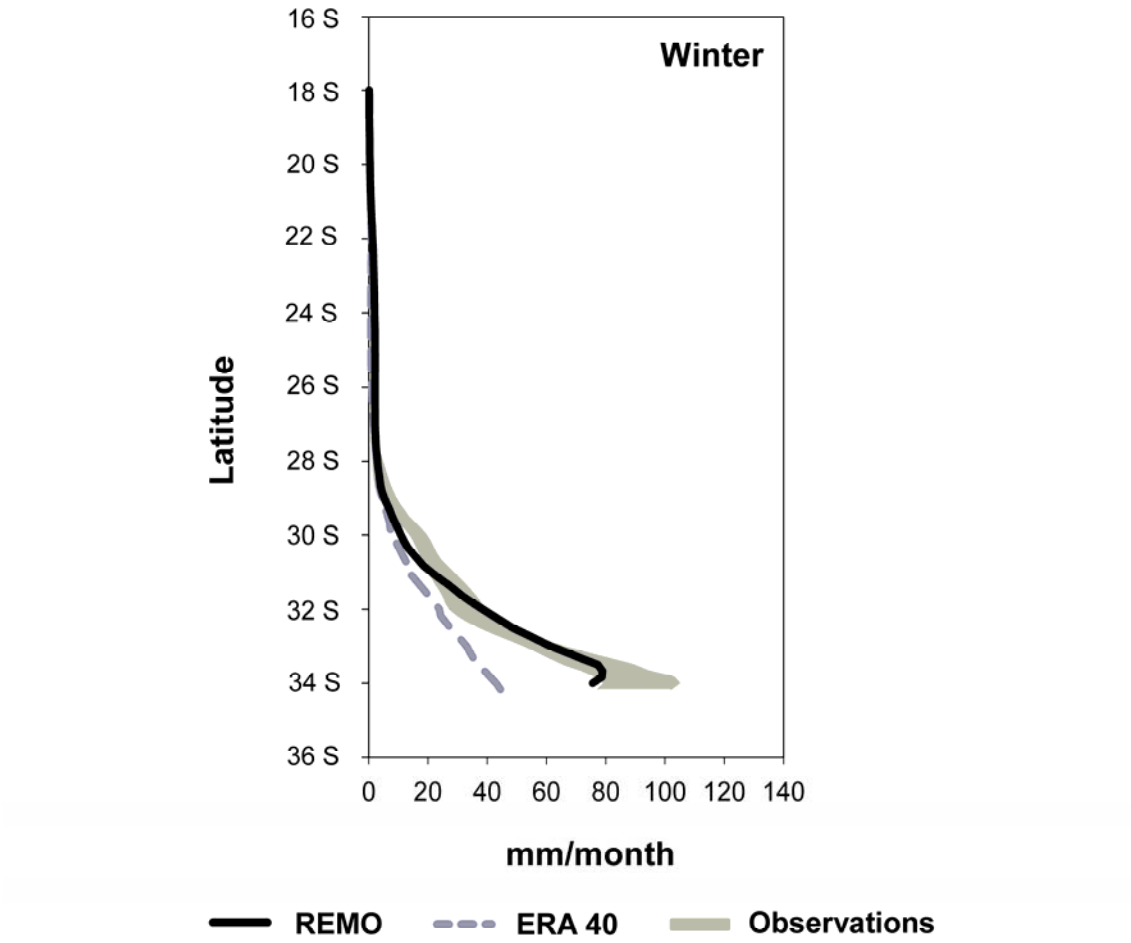

Figure 3.11: Simulated (REMO; ERA40) and observed (CRU; GPCC; HCPD) seasonal mean winter (JJA) rainfall along BNST for the period from 1960 to 2000.

3.5 Summary and Conclusions

In this chapter the performance of the regional climate model REMO was evaluated over the southern African region with a focus on South-West Africa (SWA) and the main BIOTA North-South Transect (BNST). The model ably reproduces the observed patterns of temperature and precipitation. Especially the precipitation characteristics in SWA and along BNST are captured in a very satisfactory manner by the model. Both, the seasonal rainfall distribution as well as the inter-annual rainfall variability are represented by the REMO results. Further, compared to the forcing ERA40 reanalysis data, a distinct added value in the form of a significantly better representation of the seasonal rainfall amounts around the southern African cape region could be achieved. This finding highlights the need for high-resolution regional climate simulations, especially with regard to the application of the model results as input for impact models in follow up studies. Based on the promising results of this study, it can be concluded that REMO is capable to reproduce the major climate characteristics of the southern African region and therefore can be applied to generate the first transient long-term (1960 to 2100) high-resolution climate change projection over the region.

Chapter 4

The role of the simulation setup in a long-term high-resolution climate change projection for the southern African region

4.1 Introduction

In the 4th Assessment report (AR4) of the Intergovernmental Panel on Climate Change (IPCC) a severe drying was projected for the southern African region, with a majority of the models accounted for in the report agreeing on this tendency (Christensen et al., 2007). However, this projection was solely based on coarse scale general circulation models (GCMs). For impact studies on a regional to local scale it is essential to have projections of the future climate on a higher horizontal resolution. Therefore the rather coarse transient climate change projections from GCMs, which typically are available at a horizontal resolution between 200 and 300 km, have to be downscaled to a higher resolution. This can be achieved by either applying statistical downscaling methods (e.g. von Storch et al., 1993; Hewitson and Crane, 2006) or dynamical downscaling using regional climate models (RCMs) (Giorgi, 1990; Laprise, 2008). The typical horizontal resolution for dynamical downscaling studies lies in the range between 50 and 15 km (Giorgi, 2006) and therefore chances are much higher that region specific climate patterns are resolved in RCMs than in GCMs.

The current chapter describes the application of the MPI-M regional climate model REMO (Jacob, 2001a) at a horizontal resolution of about 18 km over the southern African region for a ~140 year transient climate change projection for the period from

1960 to 2100. The work is conducted within the interdisciplinary BIOTA South project (e.g. Krug et al., 2006), which focuses on biodiversity dynamics in response to climate change. As biodiversity implies a high horizontal variety, high-resolution climate information is required for impact assessment studies. The current simulation is the first long-term transient climate change projection at such a high horizontal resolution, that has ever been conducted for the southern African region. However, the RCM REMO has already been successfully applied for long-term high-resolution climate change projections in various regions of the world e.g. over Europe (Christensen and Christensen, 2007; Jacob et al., 2008) or over West Africa (Paeth and Thamm, 2007; Paeth et al., 2009)

The added value of applying a high-resolution RCM over the southern African region was shown in Chapter 3, in which a comparison to observations yielded that the REMO RCM satisfactorily represents the specific temporal and spatial mesoscale climate characteristics of the region. Furthermore, compared to the driving ERA40 reanalysis data (Uppala et al., 2005), a significant improvement of the simulation of the seasonal rainfall characteristics along the major BIOTA North-South research transect (BNST) has been shown. This was mainly attributed to an improved representation of orographically induced rainfall events over the southwestern part of the southern African region.

Based on the results of the validation study it was concluded that the model with its current parameterization is well suited for long-term, high-resolution transient climate change simulations. However when using data from the global ECHAM5/MPIOM (Roeckner et al., 2003; Jungclaus et al., 2006) IPCC-A1B simulation instead of the ERA40 reanalysis data to force REMO, unrealistic high rainfall amounts were simulated. In order to remove this wet bias, several sensitivity studies with several adaptations in the simulation setup were conducted, which are described in more detail in this chapter. Based on the results of these sensitivity studies an improved model setup could be determined that was used for the transient climate change projections.

So far, long-term high-resolution transient climate change projections are still rather sparse for the southern African region. The existing studies to achieve horizontally detailed climate change information for the region consist of both, statistical and

dynamical downscaling methods. Statistical downscaling methods have been used to downscale time slices of GCM climate projections (e.g. MacKellar et al., 2007; Hewitson and Crane, 2006; Zhao et al., 2005) in the order of about 30 years. RCMs also have been applied for time slice experiments over the southern African region, ranging from 10-year simulations of current and future climates (Tadross et al., 2005) up to 30-year simulation in the case of Hudson and Jones (2002). Engelbrecht et al. (2009) applied a variable resolution GCM at a horizontal resolution in the range of about 50 x 50 km for a 30-year time slice experiment to project future climate change. Data of the downscaling activities have been used for various studies over the region, e.g. to investigate changes in runoff over southern Africa (Arnell et al., 2003). However, none of the existing studies generated a comparably long climate change information on such a high horizontal resolution.

The chapter is structured as follows. In Section 4.2 the REMO RCM is introduced and the model domain and setup are described. Section 4.3 describes the impact of the warm SST bias and the sensitivity studies that were carried out to improve the model setup. The findings of the long-term high-resolution climate change projection are shown in Section 4.4. Section 4.5 delivers a discussion of the sensitivity experiments and the projected climate change signals. Finally, the chapter ends with a summary and conclusion section.

4.2 Model description and simulation setup

4.2.1 Model description

The simulations are conducted with the three-dimensional hydrostatic atmospheric circulation model REMO (REgional MOdel) (Jacob and Podzun, 1997; Jacob, 2001a) in its 2008 version. The model is based on the “Europamodell”, the former numerical weather prediction model of the German Weather Service (Majewski, 1991). Furthermore, the physical parameterizations of REMO are based on those of the global climate model ECHAM4 (Roeckner et al., 1996). The prognostic variables of REMO are surface pressure, horizontal wind components, temperature, specific humidity and cloud water.

The lateral boundaries of the model are updated every six hours. These boundary conditions can be taken from analysis/reanalysis data as well as from global climate models. A relaxation scheme is used to adjust the prognostic variables prescribed by the boundary forcing in a zone of eight lateral grid rows (Davies, 1976). The parameters representing the vegetation and land surface characteristics in the model are mainly taken from the LSP2 dataset (Hagemann, 2002). Surface albedo follows a prescribed seasonal cycle according to Rechid et al. (2009). The surface in REMO is represented by a fractional distribution of land, water and sea ice within one gridbox. The vertical fluxes at the atmosphere-surface interface are calculated separately for each of three components. Thermal properties of the soil fraction are parameterized according to ECHAM 4 (Roeckner et al., 1996). Water infiltration into the soil is calculated by the improved Arno scheme (Hagemann and Dümenil Gates, 2003) that separates rainfall and snowmelt into surface runoff and infiltration. The soil hydrology is represented by a standard bucket scheme.

4.2.2 Simulation setup

For the current study the focus region are the western and central parts of southern Africa as indicated in Figure 4.1. This includes Namibia and the Cape Region in the South (SWC). Also the main BIOTA research transect (BNST), which spans from the north of Namibia to the Cape region in the south, is represented. Further, the Orange River catchment, located in the centre of the southern African domain, is included in the analysis. Since the Orange River is the main watershed in the region, it is of major economic importance for the region as its water is used for drinking water purposes, irrigation and electricity production. Therefore spatially high resolved future climate change projections are of particular interest for several economic sectors.

For the transient climate change projection, the model has been integrated at a horizontal resolution of approximately 18x18 km for the years 1960 to 2100. The model domain, excluding the boundary relaxation zone for the 18 km REMO simulation is also presented in Figure 4.1 as well as different sub regions over which the analysis discussed in this chapter is performed. Transient global input fields are provided by the ECHAM5/MPIOM IPCC-A1B scenario simulation, but some adaptations to the forcing have become necessary. Detailed descriptions of the adaptations and the model setup are given in the following section.

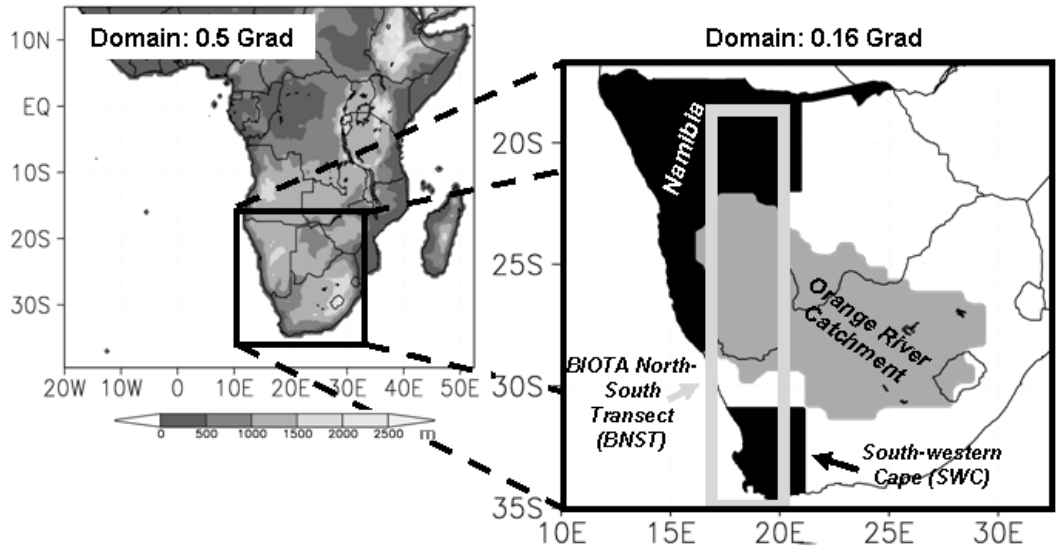

Figure 4.1: REMO orography of the driving 0.5 degree simulation (left) as well as the domain for the 18 x 18 km REMO simulation (right; without relaxation zone). The focus regions Namibia, South-Western Cape (SWC), the Orange River Catchment and the BIOTA North-South Transect (BNST) over which the analyses of this study are conducted, are indicated in the right panel.

4.2.3 Setup of sensitivity simulations and of the transient climate change projection

An initial simulation at ~18 km horizontal resolution was conducted with REMO directly nested into the global ECHAM5/MPIOM forcing fields. However this simulation showed a strong wet bias over the domain. To investigate the mechanisms leading to the increase in simulated rainfall and to find a way to reduce the unrealistic rainfall amounts two sensitivity simulations with a changed setup were conducted, each of them lasting five years.

In the first sensitivity experiment, the simulation setup was changed from a direct-nesting to a double-nesting setup, which is the setup applied for the original ERA40 forced validation simulation (see Chapter 3). For this setup, the forcing data for the high resolution REMO simulation is provided by an intermediate REMO simulation at 0.5° (about 50 km) horizontal resolution spanning an area between 10N to 40S and 20W to 40 E (Figure 4.1, left). The forcing for this intermediate simulation is provided by the global ECHAM5/MPIOM fields.

For the second sensitivity simulation, the double-nesting setup was kept. Additionally the sea surface temperature (SST) field of the ECHAM5/MPIOM forcing was corrected

by applying an anomaly approach to the data. This implies that for each time step (six hourly boundary forcing) the climatological annual mean SST anomaly for the period 1961 to 1990 of the ECHAM5/MPIOM forcing compared to the ERA40 SST is subtracted from the forcing. The main advantage in using the anomaly approach in comparison to constant bias correction methods is that changes only apply for regions, where a bias occurs. Further, using only a climatological but not a monthly or seasonal anomaly leads to the fact, that the seasonal dynamics of the GCM forcing data are still conserved after the correction. However, it has to be kept in mind that the applicability of any bias correction method implies a constant bias throughout the application period.

Based on the findings described in the subsequent section, the anomaly approach was also applied to the full ECHAM5/MPIOM SST time series (from 1960 to 2100) when conducting the transient climate change projection (see Section 4.4).

4.3 Sensitivity experiments to define simulation setup

Figure 4.2 depicts the five year (1960 to 1964) rainfall climatology for the winter (April to September) and the summer (October to March) season as simulated by REMO when directly forced by ECHAM5/MPIOM as well as rainfall observations from the Climate Research Unit (CRU, New et al., 2002). Rainfall is overestimated over the entire southern African region with an average wet bias of more than 100%. This strong wet bias further influences the energy budget in the model and therefore strongly impacts on the credibility of the model simulations over the southern African region.

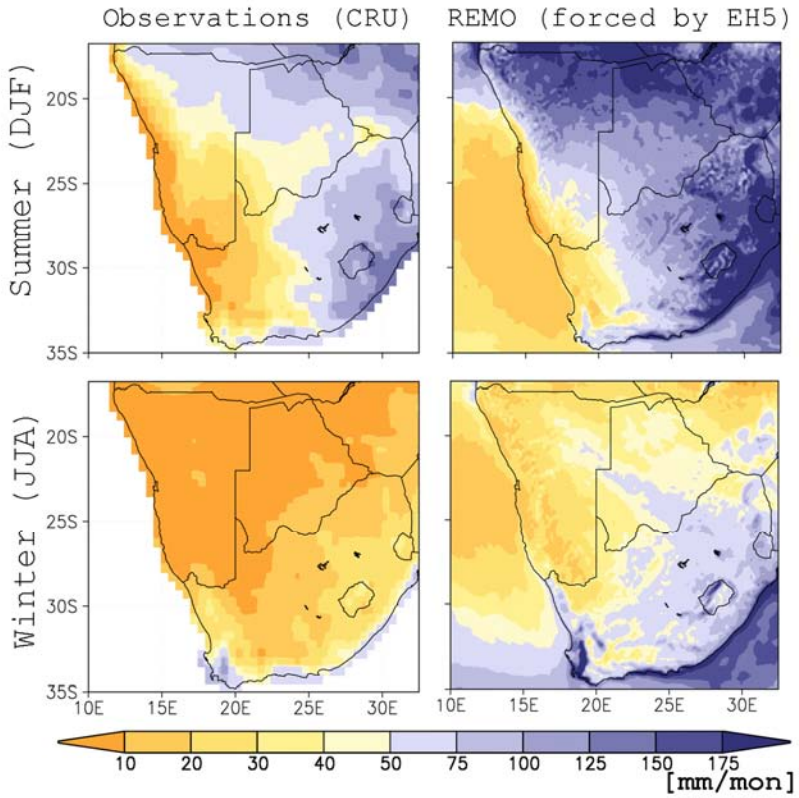

Figure 4.2: Observed (CRU; left panels) and simulated (REMO directly forced by ECHAM5/MPIOM; right panels) seasonal mean rainfall amount for the period 1960-64.

However, as the spatial patterns and also the seasonal rainfall characteristic still match the observed, it can be concluded that the wet bias is not a result of a general model deficiency. This is also supported by the fact that the previously conducted validation simulation with REMO led to satisfactory simulation results for the same domain (see Chapter 3). As the model parameterization of the validation simulation and of the current simulation are similar, the major changes between the current simulation and the validation simulation are on the one hand the change in the forcing data, and on the other the switch to a direct-nesting setup. Therefore, the conclusion has to be, that the increase in the precipitation is a consequence of an increased moisture advection from the boundary fields into the simulation domain. The analysis of the forcing fields is described in the following section (Section 4.3.1). The results of the sensitivity experiments conducted to improve the simulated rainfall are presented in Section 4.3.2. In Section 4.3.3 the rainfall simulation for a 30-year control simulation along BNST, using the adapted simulation setup, is discussed.

4.3.1 Analysis of the forcing fields

Figure 4.3a depicts the mean SST of ECHAM5/MPIOM for the period from 1961 to 1990. A comparison of this SST data to the one of the ERA40 forcing – used in the double-nested validation simulation – revealed a strong warm bias (~2.5K to more than 6.5K) of the ECHAM5/MPIOM SST over the entire sub-equatorial Atlantic Ocean (Figure 4.3b). Connected to this large scale warm bias in the SST is a higher amount of atmospheric moisture over the ocean in the GCM data (Figure 4.3d).

The bias in the simulation of Atlantic SST by ECHAM5/MPIOM is not a model specific feature, but a common shortcoming of most coupled models assessed in the IPCC AR4. Figure 4.3e and Figure 4.3f show the number of IPCC models having a SST bias over the major Benguela upwelling region when compared to ERA40 reanalysis data. Focusing on the mean bias over the region, all 25 models show a warm bias, which is for more than 50% of the models at least 2K (Figure 4.3e). With respect to the maximum bias within the defined region, all models have a maximum warm bias of more than 2K and about 66% of all models show a maximum SST bias of more than 6K (Figure 4.3f). This common shortcoming of the coupled GCMs to simulate the large scale Atlantic SST has already shown before by Ashfaq et al. (2010). At least for some models this deficiency seems to be induced by a weakness of the GCMs to simulate the right amount of stratiform clouds over large parts of the Atlantic Ocean (e.g. Large and Danabasoglu, 2006). However the extremely large warm bias around the Benguela upwelling region has not yet been discussed explicitly.

To remove the warm bias in the ECHAM5/MPIOM SST and also to reduce the evaporation over ocean a correction based on the anomaly approach (see Section 4.2.3 for details) was applied to the SST forcing. The spatial pattern of the applied correction is similar to the SST bias shown in Figure 4.3b. Over most of the Atlantic Ocean the correction leads to a cooler ECHAM5/MPIOM SST with a maximum reduction along the Namibian shoreline, where the cold upwelling regions of the Benguela current are located. In this region, for some grid boxes the annual mean SST is reduced by almost 9 K, but for many other regions the changes were negligible. South of the Agulhas current, the correction leads to an increase of the ECHAM5/MPIOM SST. The corrected mean SST for the period from 1961 to 1990 is depicted in Figure 4.3c.

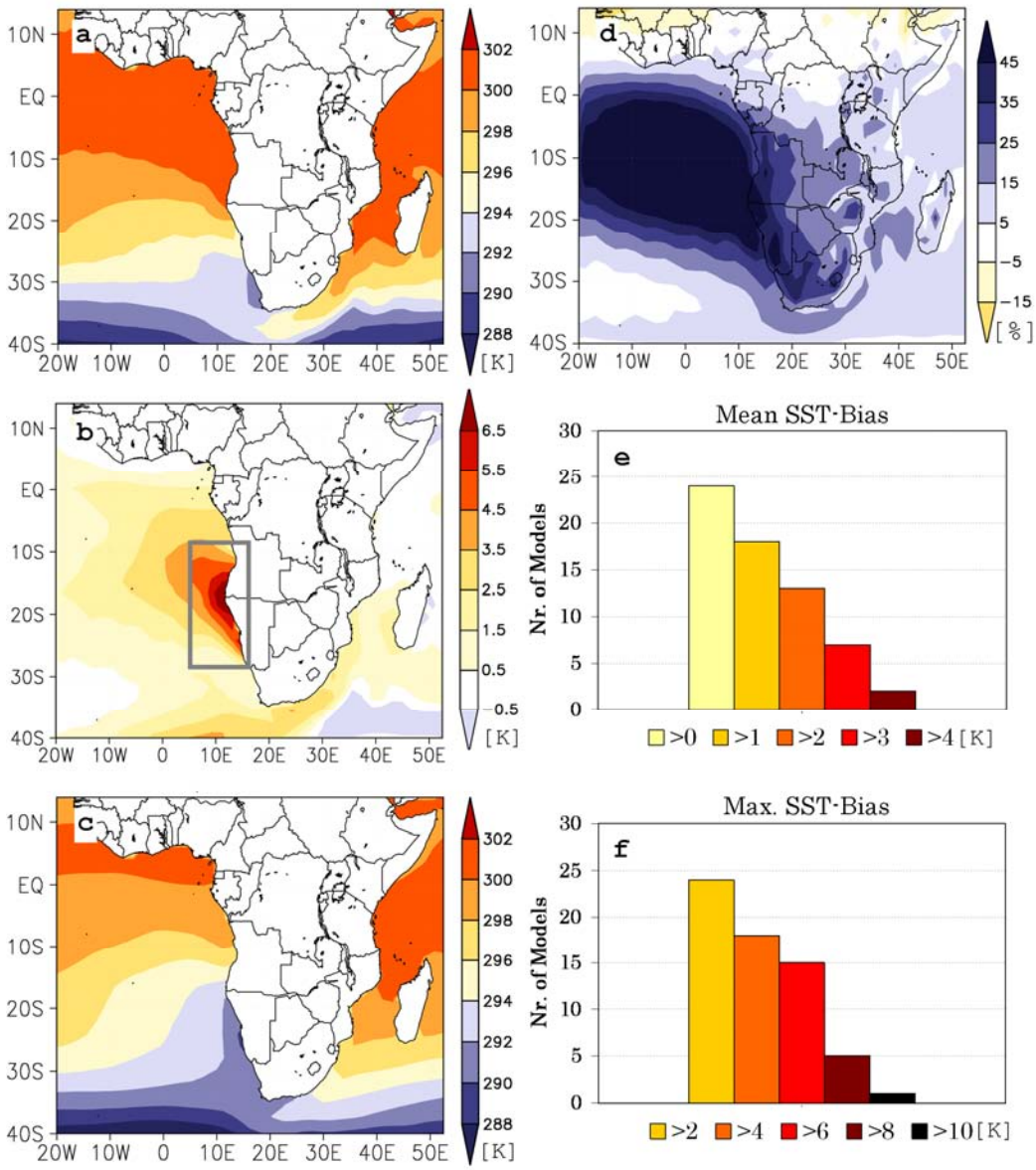

Figure 4.3: (a) Mean SST of the ECHAM5/MPIOM forcing for the period from 1961 to 1990 period. (b) Mean differences in the SST between the ECHAM5/MPIOM and the REMO/ERA40 forcing for the 1961 to 1990 period. (c) Mean SST of the ECHAM5/MPIOM forcing for the period from 1961 to 1990 period, after applying the SST correction based on the anomaly approach to the data. This SST is identical to the ERA40 SST. (d) Mean differences in the vertically integrated water vapor between the ECHAM5/MPIOM and the REMO/ERA40 forcing for the 1961 to 1990 period in %. (e & f) Number of coupled GCMs used in the IPCC AR4 having – compared to ERA40 – a SST bias above a certain threshold over the major upwelling region identified by the grey box in (b). Panel (e) depicts the mean bias over the region and panel (f) the maximum bias.

As discussed in Section 4.2.3 not only the SST was corrected in the sensitivity simulations, but also the simulation setup was changed. In the following section, the results of these sensitivity experiments are presented.

4.3.2 Results of sensitivity experiments

Figure 4.4 summarizes the impacts of the adaptations of the simulation setup on the rainfall simulation over the focus regions identified in Figure 4.1. Compared to the initial simulation with REMO directly nested into ECHAM5/MPIOM forcing (R_Ctrl) both sensitivity simulations show a remarkably decreased rainfall over all three regions. The change to the double-nesting setup (R_DN) already reduces the simulated rainfall amount substantially. Especially over the Orange River catchment and during the dry season over Namibia, rainfall is already almost reduced to observed values. In particular the representation of the dry season in Namibia – during which almost no rain is generated – is a major improvement of R_DN compared to the initial R_Ctrl simulation. However over the SWC region and also during the rainy season over Namibia a considerable wet bias remains in the R_DN simulation. A further improvement of the rainfall simulation can be reached when additionally applying the SST correction approach to the forcing data (R_DN&AA). But compared to the earlier conducted REMO validation simulation (R_Val) a noticeable wet bias still persists in the SWC region and in Namibia during the respective rain seasons.

Additionally it has to be noted that the R_Val simulation shows a contrary rainfall pattern to the other simulations in the SWC region during the winter season (Figure 4.4). This pattern seems to be related to the size of the single anticyclone present over land areas during that time of the year (see also below), which varies from month to month and is influenced by the large scale forcing. Even though the mean winter circulation is simulated to be almost identical in the different sensitivity simulations (see Figure 4.5), the month to month variations differ between the ECHAM5/MPIOM forced simulations (R_Ctrl; R_DN; R_DN&AA) and the validation simulation.

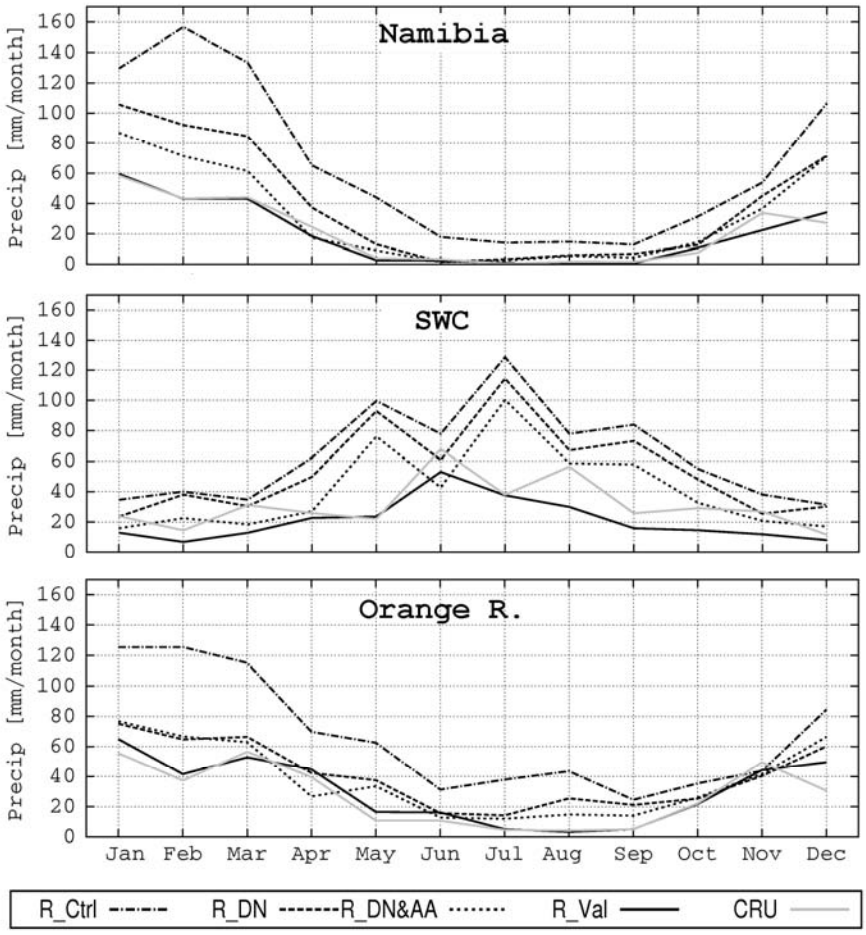

Figure 4.4: Mean climatological rainfall (1960-64) for the validation (R_Val), direct-nesting (R_Ctrl), double-nesting (R_DN) and combined double-nesting – SST reduction (R_DN&AA) simulation as well as the CRU observations as areal mean over Namibia, the South-Western Cape (SWC) and the Orange River catchment.

In order to explore if the reduction of rainfall is caused by a mismatch in the circulation patterns the REMO circulation of the lower atmosphere (850 hPa) is shown for the R_Ctrl, for the two sensitivity simulations (R_DN; R_DN&AA) and the R_Val simulation for the summer and winter seasons (Figure 4.5). The main circulation, which is characterized by the influence of the Atlantic and the Indian Ocean anticyclone during the summer season and the single anticyclone during the winter season, is simulated in all four simulations almost identically. Only above the mountainous parts of the domain in the southeastern part of South Africa and along the escarpment in Namibia a slight, but rather sporadic change in the 850 hPa circulation is notable.

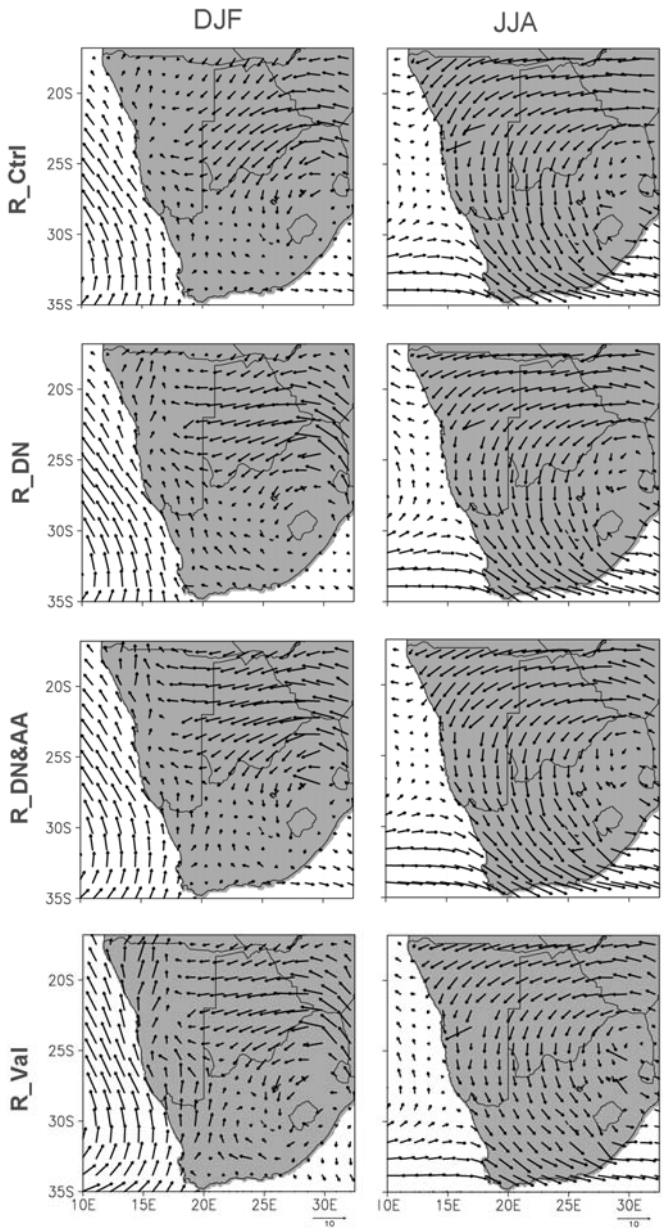

Figure 4.5: Mean seasonal (1960-64) 850 hPa circulation for the direct-nesting (R_Ctrl), double-nesting (R_DN), combined double-nesting – SST reduction (R_DN&AA) and validation (R_Val) simulation for the summer (left panels) and winter (right panels) season.

Additionally to the lower atmospheric circulation, the vertical characteristics of the zonal wind components were investigated for all simulations and both seasons (Figure 4.6). During both seasons a slightly southerly shifted jet core can be observed in the R_Ctrl, R_DN and R_DN&AA simulations when compared to the R_Val simulation. The vertical extend of the jet, however, differs only slightly in the depicted simulations.

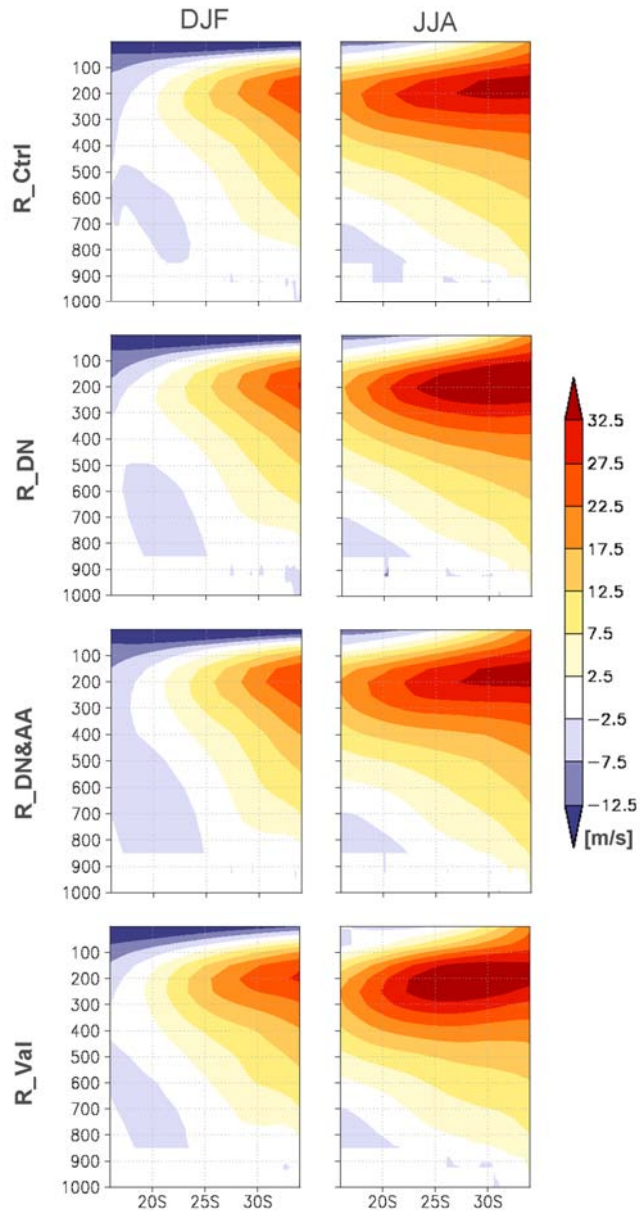

Figure 4.6: Mean seasonal (1960-64) zonal wind component for the direct-nesting (R_Ctrl), double-nesting (R_DN), combined double-nesting – SST reduction (R_DN&AA) and validation (R_Val) simulation for the summer (left panels) and winter (right panels) season over the southern African region.

Due to the fact that the atmospheric circulation is only slightly affected by the SST correction the simulated reduction of precipitation has to be linked to other processes. To further investigate the mechanism behind the decrease of precipitation in the sensitivity simulations the atmospheric moisture input into the regions of interest was calculated. This analysis is based on the general balance equation for atmospheric water vapor defined by Peixoto and Oort (1992). Using this approach, the moisture convergence C into a specific region can be expressed as:

$$C = (E - P) - \frac{\delta S}{\delta t} \qquad (1)$$

where P is the precipitation rate, E is the evaporation rate and $\delta S / \delta t$ defines the change of atmospheric water vapor storage S with time t. The calculations are done at a six hourly time step for the complete five year simulation period. The spatially and temporarily integrated moisture convergence is depicted for the different regions in Figure 4.7. For both sensitivity simulations the moisture convergence into the selected regions is considerable lower than those of the too moist R_Ctrl simulation. This supports the previous statement that the wet bias in the direct-nested simulation is due to a larger moisture input from the forcing fields. For a qualitative measure to identify the origin of the moisture transported into the western and central part of the southern African region, the mean vertically integrated moisture fluxes was calculated for the 5-year simulation period. This includes the mean vertically integrated atmospheric water vapor influx into the region of interest $Q_{M\text{-}in}$, which is defined as

$$\vec{Q}_{M-in} = \frac{\sum_{t=0} \int_{P_{TOP}}^{P_{SURF}} \vec{v}_{in}(p) q(p) \frac{\delta p}{g}}{t} \qquad (2)$$

where g is the gravitation constant, q is the specific humidity, p is pressure, v_{in} is the two-dimensional wind velocity vector directed into the region of interest, t is the time period and the integration boundaries P_{SURF} and P_{TOP} are the pressure at the surface and the top of the atmosphere, respectively. Furthermore, the mean integrated atmospheric water vapor outflux from the region of interest $Q_{M\text{-}out}$ was calculated. This flux is defined in the same way as stated in (2), but having a two-dimensional wind velocity vector v_{out}, which is directed out of the region of interest. Finally, $Q_{M\text{-}in}$ and $Q_{M\text{-}out}$ can be summed up to receive the net integrated atmospheric water vapor flux $Q_{M\text{-}net}$. The calculations for $Q_{M\text{-}in}$, $Q_{M\text{-}out}$ and $Q_{M\text{-}net}$ have been conducted for each time step of 6-hourly model output for the western part of the southern African region and along the whole coastline. Because the major interest of this study lies in the western part of the southern African region (including the focus regions BMST, Namibia and SWC) the

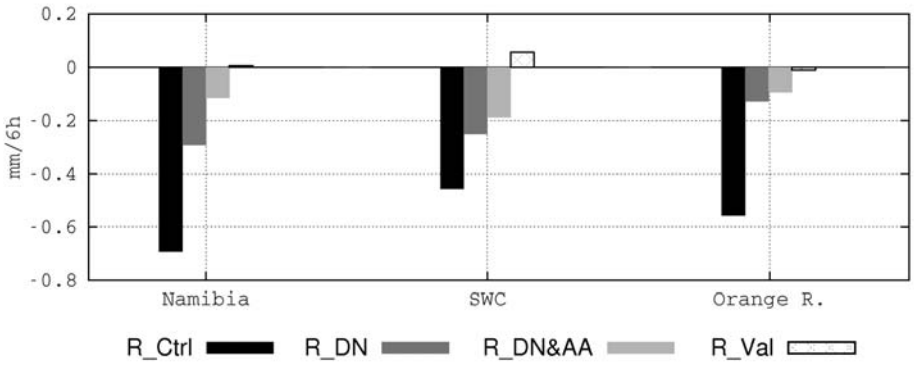

Figure 4.7: Mean moisture convergence (1960-64) into the region of interest for the validation (R_Val), direct-nesting (R_Ctrl), double-nesting (R_DN) and combined double-nesting – SST reduction (R_DN&AA) simulation as areal mean over Namibia, the South-Western Cape (SWC) and the Orange River catchment.

moisture influx into the western part of the domain is of special importance. However, as the Orange catchment is not completely covered by this, also the mean fluxes along the whole coast line were calculated (Figure 4.8; upper two rows). The major part of the integrated atmospheric water vapor is transported from west to east, meaning that the influx is larger on the western boundary of the investigated region and the mean outflow is increased on the eastern part. This flux pattern indicates that the transported moisture mainly originates from the central South Atlantic Ocean from where it is advected over the southern part of the African continent. This seems to be contradictory to the near surface wind fields, which do not show the prevailing westerly flows (see Figure 4.5 and 4.8; lower left panel). However the circulation above the planetary boundary layer at 700 hPa and also the midlevel circulation at 500 hPa clearly show the predominant westerly flows, that transport the moisture load from the South Atlantic Ocean towards the land (Figure 4.8; lower panels) Therefore, the reduction of the moisture convergence in the two sensitivity experiments also indicates a decreased atmospheric moisture content over this part of the Atlantic Ocean (Figure 4.9a). This assumption is strengthened when considering the fact that the atmospheric circulation patterns in the two sensitivity experiments only show minor changes compared to the R_Ctrl simulation. In the case of the R_DN simulation, the lower atmospheric moisture content over ocean can be explained by a reduced moisture inflow at the domain boundaries (Figure 4.9b) as the forcing 50 km simulation is already compensating the higher atmospheric moisture amounts of ECHAM5/MPIOM by an increased precipitation

formation over the ocean. However, a part of the moisture reduction of this simulation is again compensated by an increased evaporation over ocean. With the combination of the double nesting and the correction of the too warm SST forcing (see Figure 4.3) using the anomaly approach, this compensating process can be minimized by reducing the evaporation to the level of the R_Val simulation (Figure 4.9c), which leads to a further reduction of the atmospheric moisture content.

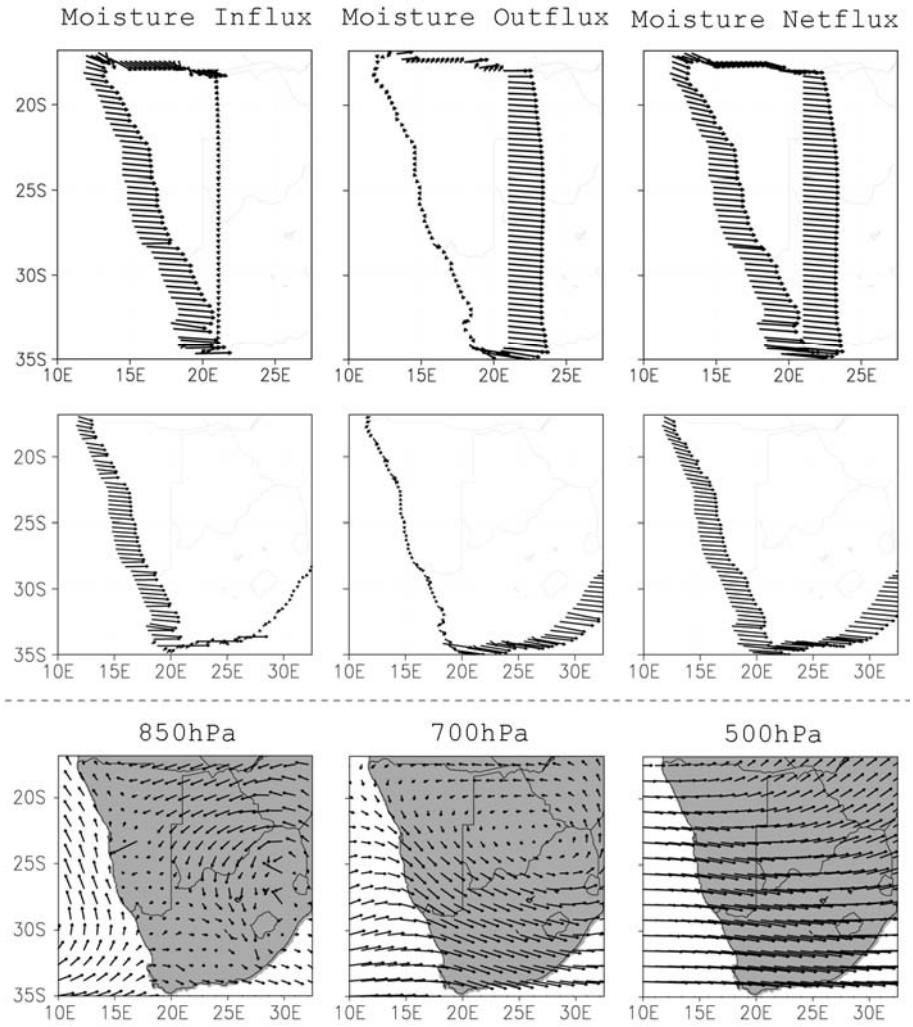

Figure 4.8: Mean vertically integrated moisture fluxes (1960-64) along the south-west African region (upper panels) and along the coast line (center panels) indicating the moisture transport into and out of the focus regions of this study, which are mainly located in the western part of the domain. The length of the vectors depicts the moisture load; the angle depicts the main flow direction. The lower panels show the mean circulation (1960-64) for different vertical levels in the lower and middle atmosphere.

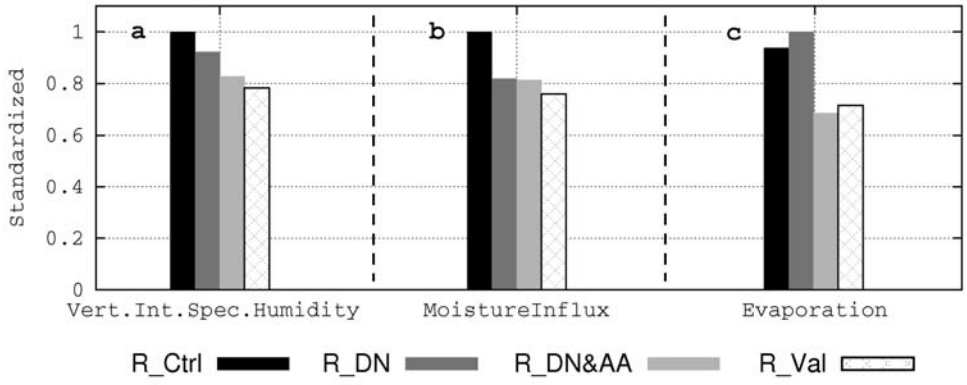

Figure 4.9: (a) Mean vertically integrated specific humidity for the period 1960-64 for the validation (R_Val), direct-nesting (R_Ctrl), double-nesting (R_DN) and combined double-nesting – SST reduction (R_DN&AA) simulation as areal mean over all Ocean points only. (b) Same as Figure 4.9a, but for vertically integrated moisture inflow over Ocean from the boundary forcing. (c) Same as Figure 4.9a, but for Evaporation.

Nevertheless, as shown in Figure 4.4 a noticeable wet bias is still persistent in the R_DN&AA simulation. Further tests however revealed, that a stronger reduction of the rainfall could only be achieved by either completely removing the moisture inflow from the boundary field of the 50 km REMO simulation or by a drastic change of the model parameterization. In the first case a general moisture deficit would be generated at the lateral boundary which could only be partially compensated by increased evaporation over the Atlantic Ocean. In the latter case, the cloud parameterization of the model could be directly influenced. As both actions, however, would be based on the pure subjective goal to somehow tune the model to observations and are not justifiable by any scientific explanation, they were not considered to be an option to solve the precipitation problem.

The simulation setup that therefore was used for the long term transient climate change projection is the combination of the double-nesting setup and the SST correction of the forcing data as it was used in the R_DN&AA sensitivity experiment. As the subtracted SST-anomaly is kept constant throughout the transient climate change projection it is assumed, that the correction will not alter the projected climate change signal. In the subsequent section simulated rainfall amounts of REMO (using the previously defined setup) and of ECHAM5/MPIOM are compared along BNST to available rainfall observations for a 30-year control experiment.

4.3.3 Simulation of rainfall along BNST

As indicated in Section 4.2 the Biota North-South Transect (BNST) located in the western part of the southern African region (Figure 4.1) is one of the focus regions of this study. Figure 4.10 depicts the simulated rainfall of REMO along BNST for the summer and winter season for the three sensitivity simulations for the 1960 to 1964 period. Furthermore, a comparison with observations and the forcing GCM is given for the 1961 to 1990 control period. The spatial rainfall patterns along BNST are generally the same in the R_Ctrl, R_DN and R_DN&AA sensitivity simulations, but a different rainfall magnitude is obvious. As already shown above for the other regions, the introduction of the SST reduction in combination with the double-nesting setup clearly reduces the simulated rainfall amount along BNST in the sensitivity simulations for the summer (DJF) and winter (JJA) seasons (Figure 4.10, left two panels). Furthermore, when comparing the simulations to the CRU observations (available globally at 0.5°; New et al., 2002) over the control period, simulated rainfall of REMO still shows a wet bias for the northern and southern part of BNST, but the rainfall peak during winter is captured rather closely by the model (Figure 4.10, right two panels). The magnitude of the winter rainfall peak seems to be rather reliable in the CRU dataset, as there are a couple of stations available around this region. Additionally to the observations also the simulated rainfall of the forcing GCM along BNST is depicted in the figure. To exclude differences in decadal variations between GCM and RCM from the analysis the seasonal mean rainfall was compared for a 30-year period from 1961 to 1990. Due to their higher horizontal resolution, RCMs often have a higher accuracy in describing regional or even local climate features compared to coarse resolution GCM or reanalysis data (see Chapter 3). Compared to the ECHAM5/MPIOM simulation the rainfall seasonality in the southern, winter-rainfall dominated part of BNST is remarkably improved in the RCM (R_DN_AA) simulation in which the high rainfall amounts visible in the observations during the winter season are reflected (Figure 4.10, right). The correct representation of the rainfall distribution along BNST can also already be observed in the R_Ctrl and R_DN simulation, however a larger wet bias persists in those simulations. Even though this wet bias exists in the sensitivity simulations it still can be concluded that all high-resolution REMO simulations better represent the rainfall characteristics along BNST than the GCM does. This can mainly be attributed to a better representation of mesoscale orographic features in the RCM compared to the coarse resolved GCM.

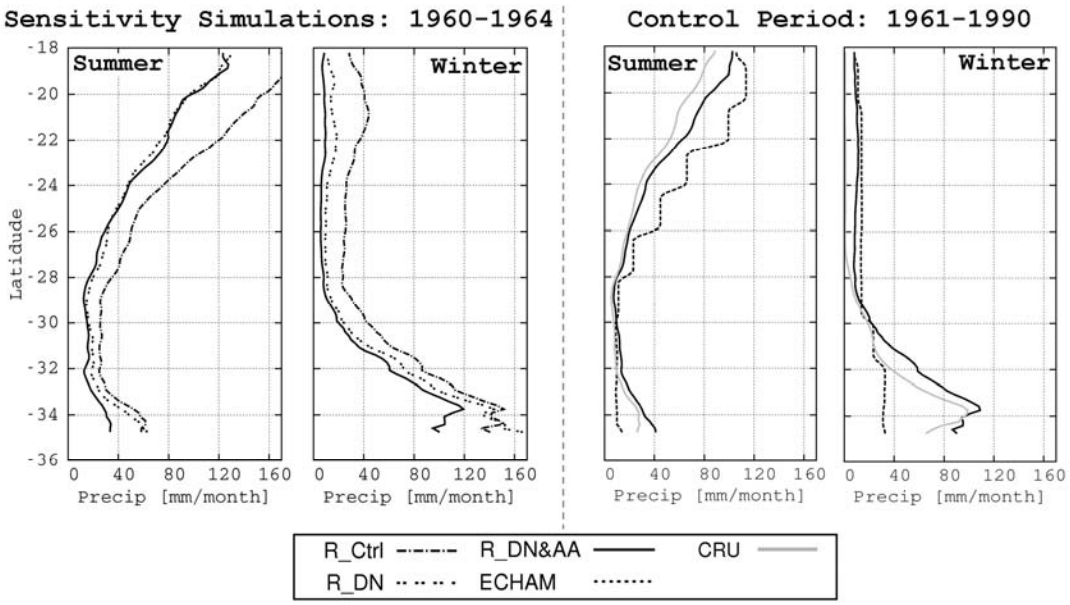

Figure 4.10: Simulated mean seasonal rainfall distribution in the sensitivity simulations (left two panels) and for the control period (right two panels) as zonal mean over the BNST region.

4.4 Future climate projections for the southern African region

In the current section the projected changes of the high-resolution 18x18 km REMO simulation (REMO_016) are presented for the southern African region. To identify the impact of the higher horizontal resolution also projections of the forcing ECHAM5/MPIOM and the intermediate, 0.5° REMO simulation (REMO_05) are included in the analysis. The GCMs accounted for in the IPCC AR4 projected a strong warming and a severe drying over the southern African region. This tendency is also represented in the projections analysed in this study. On average a general warming in all parts of the domain is projected, with a stronger temperature increase in the interior, reaching a maximum warming of about 6 K at the end of the 21st century – when compared to the control period – in all simulations (Figure 4.11). Even though the warming tendency is the same in all three models, the high resolution REMO simulation provides more spatially detailed information than the others. This resolution effect can also be noted in the simulation of the annual mean rainfall (Figure 4.12). While the global ECHAM5/MPIOM model fails to simulate the maximum rainfall amounts over the high-elevated region around the Drakensberg Mountains in the south-east of the domain and also the ones around the Cape region (see also Figure 3.2 for the

observations), the horizontally higher resolved REMO simulations clearly improve these patterns.

For the future, all models project a precipitation decrease for the western and central parts of the southern African region, whereas around the Drakensberg Mountains in the south-east (REMO) and adjacent coastal areas (ECHAM5/MPIOM) a slight increase in the projected precipitation is visible. In the IPCC AR4 it was stated that the drying in the central parts is mainly due to a positive feedback of reduced soil moisture, whereas the drying in the west results from a southerly shift of the westerly winds during the winter season. (Christensen et al., 2007). The same features can also be identified in the REMO simulations. A more detailed discussion of the changes in the regional circulation patterns is provided in Chapter 6 (Section 6.4.1; Figure 6.7).

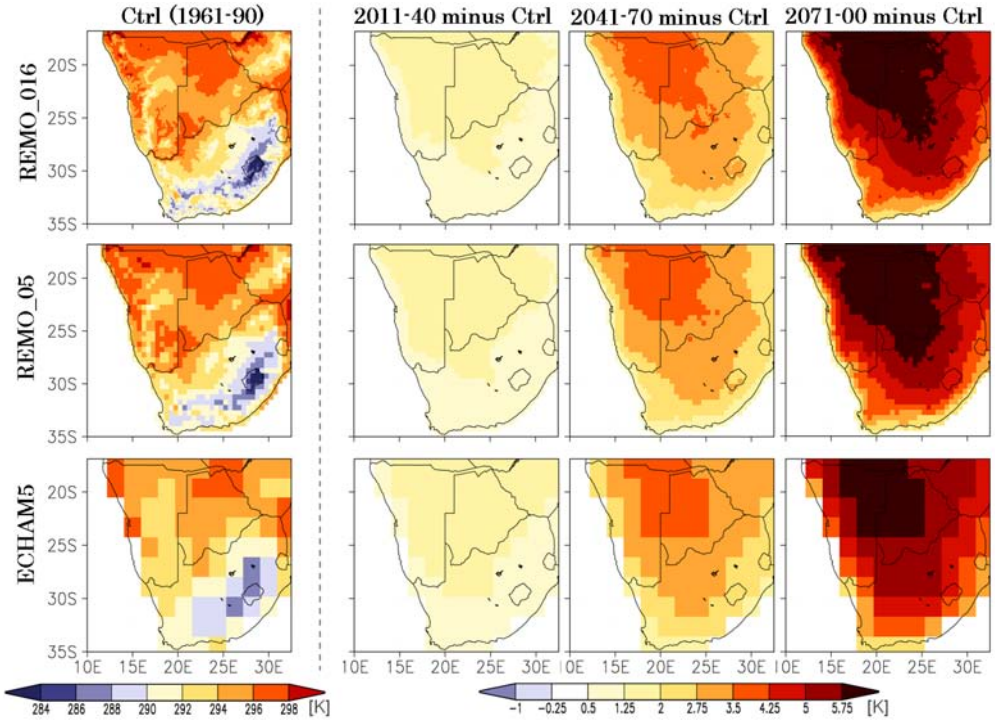

Figure 4.11: Climatological mean temperature for the control period (1961 - 1990) and the respective changes for three future 30 year periods (2011 - 2040, 2041 - 2070, and 2071 - 2100) as simulated with REMO on two different horizontal resolutions (18x18 km; upper panels and 50x50 km, central panels) and ECHAM5/MPIOM (lower panels).

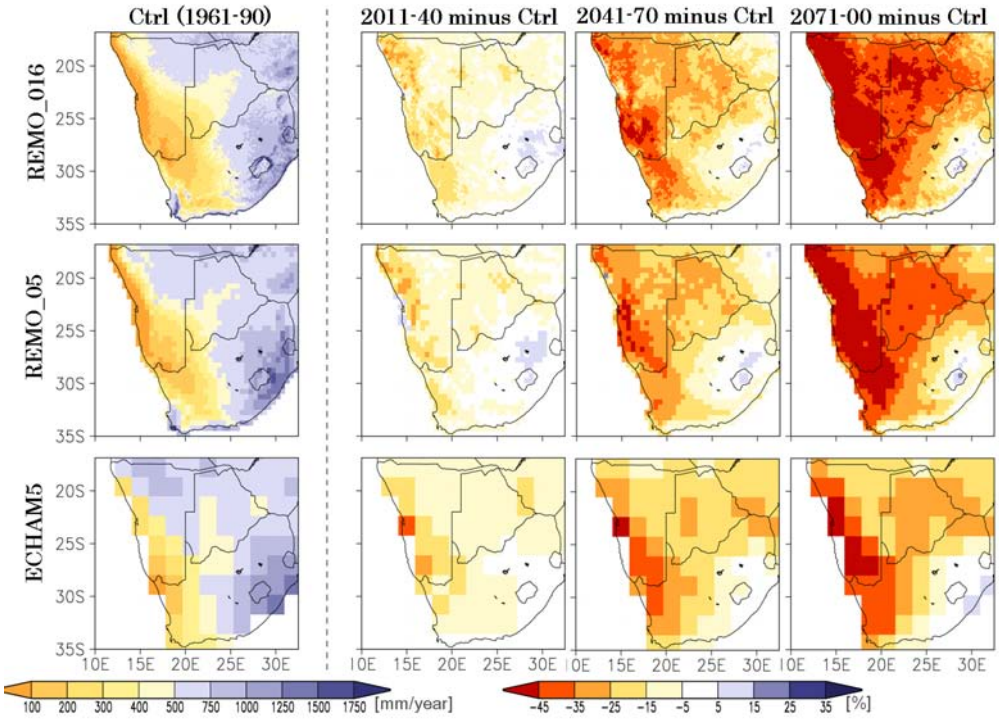

Figure 4.12: Same as Figure 4.11, but for precipitation.

In order to not only consider changes in annual mean rainfall also changes of some rainfall characteristics were investigated. As an example, the projected changes in heavy rainfall events were evaluated, which are defined as the 95th percentile of daily rainfall (Figure 4.13). Connected to a projected warming of the atmosphere is often an increase in atmospheric moisture content, as warmer air can hold more water. In the models, this frequently leads to an increased intensity of torrential rain events. For most of the southern African region however, all three simulations show a decrease in high-intensity daily rainfall events, although the atmosphere is projected to heat up. Only around the Drakensberg Mountains in the south-eastern parts of the domain (REMO) and the adjacent coastal regions (ECHAM5/MPIOM), a slight increase in heavy rain intensities is projected. Additionally, changes in the extent of the dry season were investigated. In terms of the maximum number of consecutive days without rainfall, the models project that future rainy seasons will be shorter than at present for most parts of the domain (Figure 4.14). While the two REMO simulations show the largest changes in the extend of the dry season around the arid areas along the west coast, the patterns in ECHAM are more diverse. Also during the control period the dry period is generally shorter in the GCM. These differences between REMO and ECHAM throughout the simulation period can be partly connected to the threshold value of 0.1 mm/h, which

was set to define a day without rainfall. Hence a model with a larger content of low intensity rainfall would produce a shorter dry period. Connected to the extent of the dry season is an increase in rainfall variability (see Haensler et al., 2010c), which is defined as the ratio between the standard deviation of monthly rainfall compared to the long term mean rainfall. Considering the above, it seems likely that droughts over the southern African region will occur more frequently in the future than over the control period.

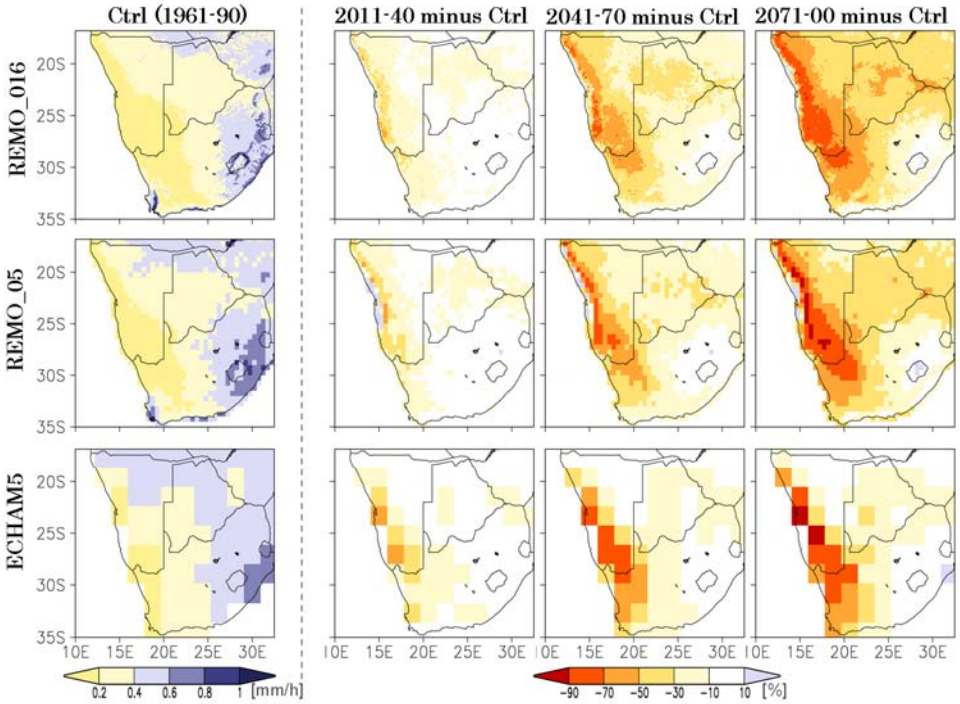

Figure 4.13: Same as Figure 4.11, but for the 95th percentage of daily precipitation

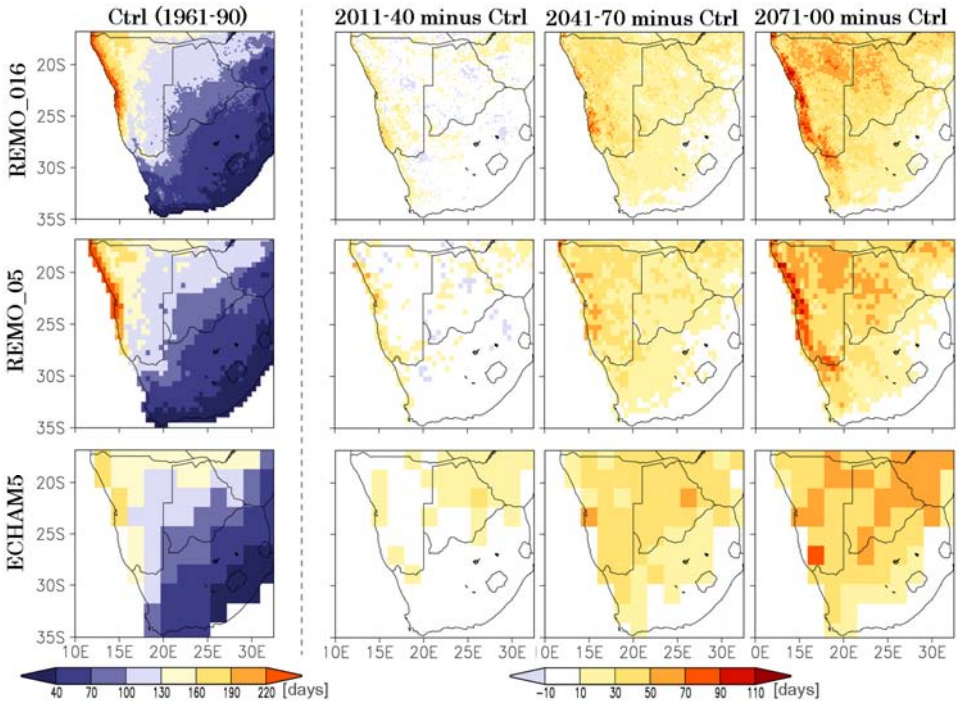

Figure 4.14: Same as Figure 4.11, but for the length of the dry period.

As the focus region of this study lies on the western part of the southern African region, Figure 4.15 provides a more explicit description of future changes along BNST. According to the three simulations, the BNST region is projected to undergo significant changes in both the summer and the winter season. The tendencies of the simulated changes of the global and regional model are the same, but again more details are provided by the high resolution REMO simulation. The most prominent example for this is the winter rainfall peak around the Cape region which is best captured by the 18 km REMO simulation (see also Figure 4.10). For the southern, winter rainfall dominated part of BNST, which is strongly influenced by the Atlantic Ocean, the models project a smaller temperature increase than for the northern section. Nevertheless a remarkable warming is projected to occur along the whole transect, in the order of about 2 to 6 K. Projected decrease of absolute rainfall along BNST is strongest during the specific rainy season, but also dry season rainfall is affected.

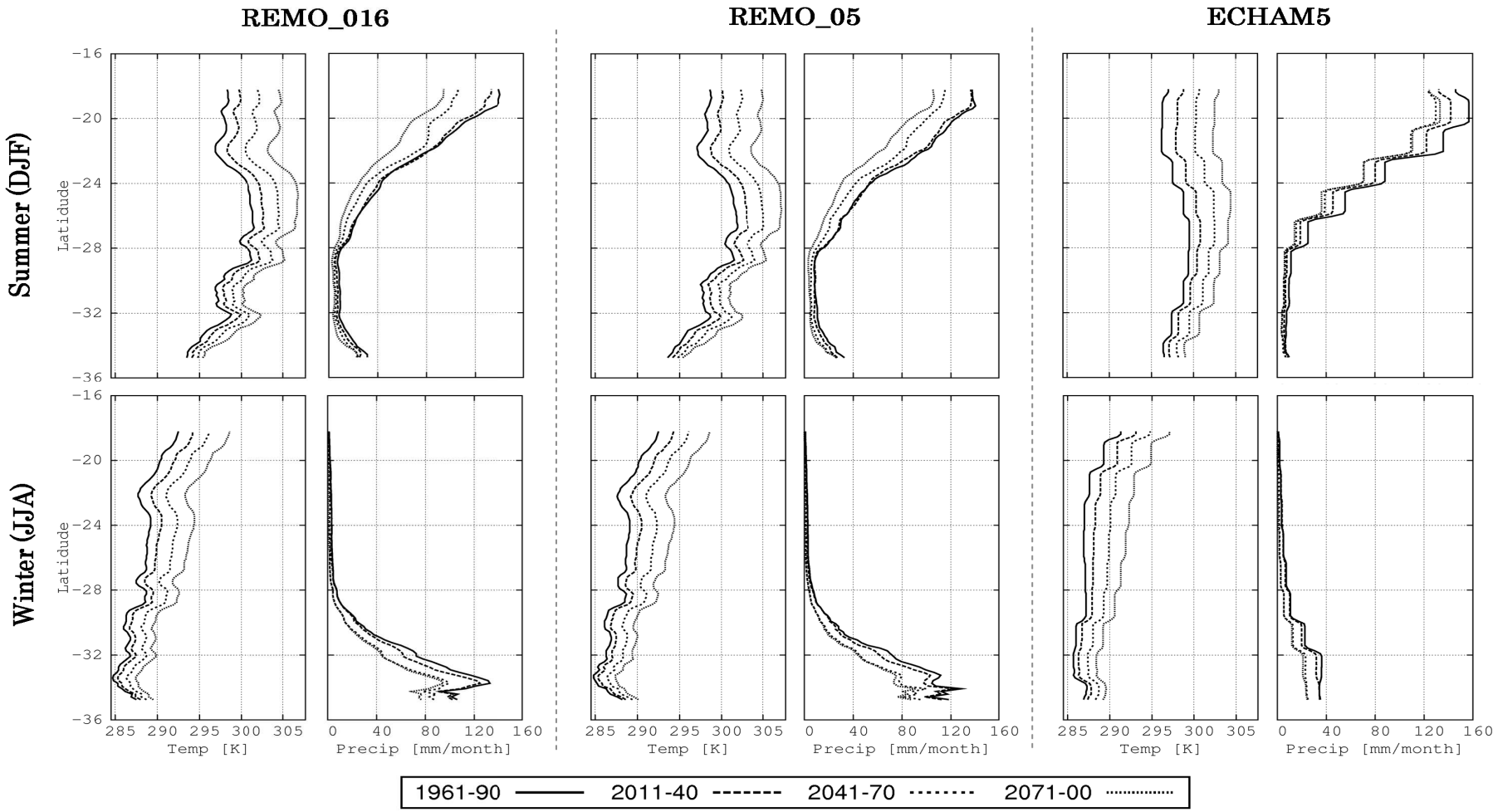

Figure 4.15: Simulated mean seasonal temperature (respective left panels) and precipitation (respective right panels) for the summer (upper panels) and winter (lower panels) over the control period (1961-1990) and three future 30-year periods as zonal mean over the BNST region. The left section of the Figure depicts the high-resolution REMO simulations, the central section the intermediate resolved REMO simulation and the right section the forcing GCM.

In order to investigate the temporal patterns of the projected changes the evolution of the 30-year climatological mean and the respective interannual anomalies were considered for the control as well as for three future periods. For all three regions (as identified in Figure 4.1) the models project a rather linear increase in temperature starting around the year 2010. Maximum warming is smallest for the SWC region with about 3 K at the end of the 21st century compared to the control period. For Namibia and the Orange River however, the temperature increase is more amplified and is supposed to reach up to 5 K (Figure 4.16a). The interannual temperature variation simulated by the models seems to be rather constant throughout the 21st century.

In Figure 4.16b the relative changes of the annual rainfall amounts are shown. For all three regions a severe drying of about 20 to 40% is noticeable in the model simulations towards the end of the 21st century. However the magnitude of the projected drying differs in the different regions and also in the different models. Whereas the models agree for the SWC region REMO projects a slightly larger rainfall reduction than ECHAM5/MPIOM for the Orange catchment and over Namibia. Interannual rainfall variability continues to be rather high over all three regions and for all models and is slightly increased over the SWC region. However, despite the strong drying in the mean state, the projections show that until about the year 2080 it is still very likely to observe annual rainfall amounts higher or at least of the same magnitude as the mean rainfall amount of the control period. This feature can mainly be attributed to the large interannual rainfall variability over the area, which is visible in both, the GCM and RCM simulations. Only during the last 20 years of the simulation, the precipitation amount of the control period is not reached anymore.

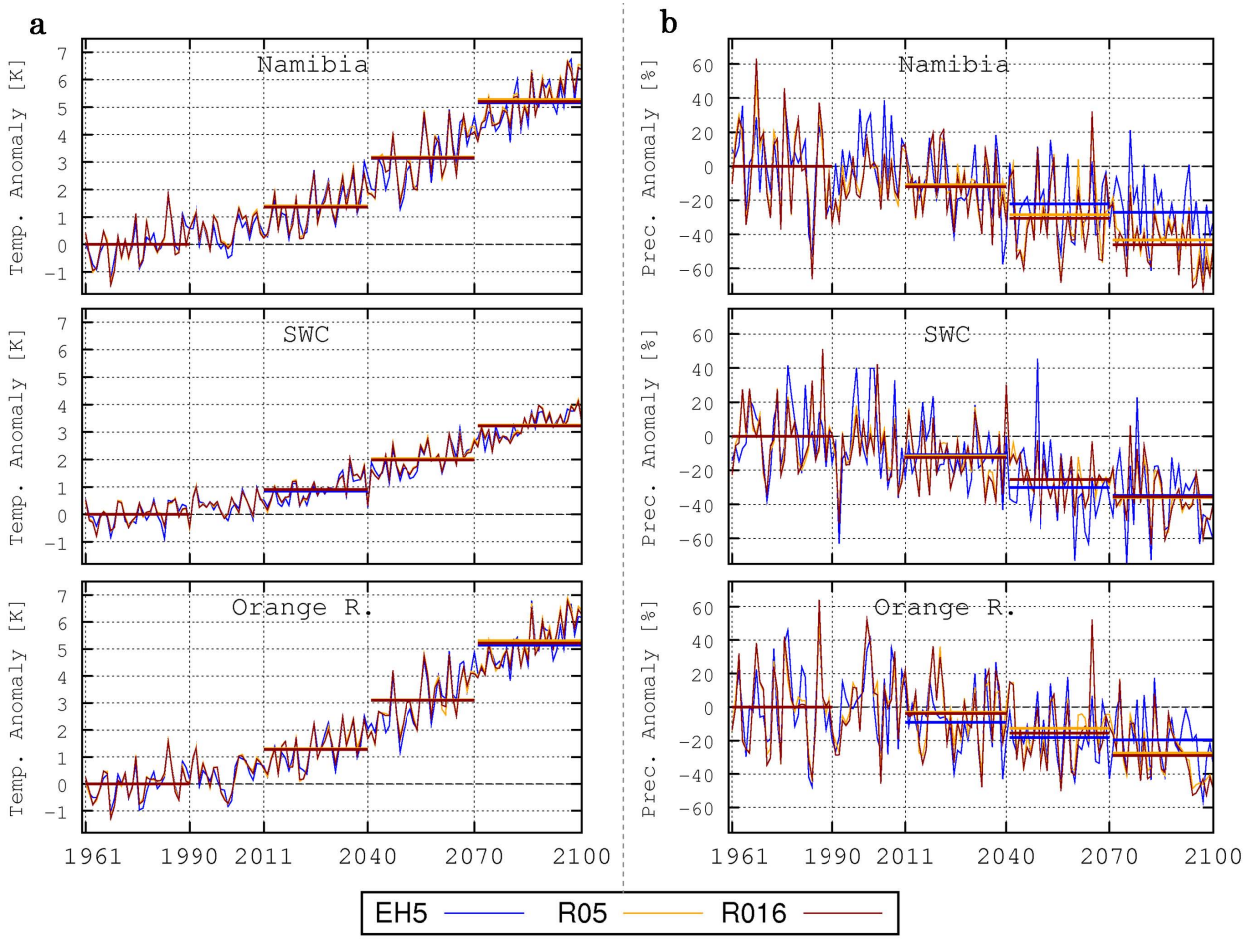

Figure 4.16: Simulated temperature (a) and precipitation (b) anomalies and time mean for the control period (1961-1990) and three future 30-year periods as area average over Namibia, the south-western Cape (SWC) and the Orange River catchment. The anomalies are calculated with respect to the respective 30-year mean values.

4.5 Summary and Discussion

In the first part of the chapter, it was found that if REMO is directly nested into the global ECHAM5/MPIOM forcing fields a large overestimation of simulated rainfall over most parts of the domain occurs. When changing the simulation setup from direct-nesting to double-nesting a significant rainfall reduction is yielded. However, the explanation for this effect can not solely be attributed to the scale transition from the coarse scale GCM at T63 (~180 km) to the high-resolution RCM. In the direct-nested simulation this scale transition is on the order of a factor 10, which is a common scale transition when using dynamical downscaling methods and generally supposed to still lead to reasonable results (Denis et al., 2003). Furthermore, spatial and seasonal rainfall patterns of the single-nested simulation match the observations rather closely. Based on the latter, it can be concluded that the reason for the rainfall overestimation in the direct-nested simulation is not the mismatch in the scale between forcing data and RCM, as this would strongly influence the simulation of the circulation patterns, but the fact that the moisture input provided by the boundary fields is much larger from the GCM fields than from the intermediate resolved RCM fields in the double-nesting case. The increased rainfall formation in the direct-nested RCM simulation, which is also larger than the GCM rainfall over the region (not shown), is therefore just a consequence of a different moisture – rainfall ratio in the RCM compared to the forcing GCM. As the nested 18 km model domain covers only a limited area of the southern Atlantic, the moisture – rainfall equilibrium of the RCM can not be reached before the moisture is transported over land. Applying the double-nesting setup, the coarser resolved RCM, which also spans a much larger domain than the single-nested simulation, therefore acts as a buffer in terms of generating a new moisture equilibrium. This buffering mechanism is expressed in an increased rainfall formation in the outer parts of the domain of the forcing RCM, whereas the interior (where the nested high resolution domain is located) the model is already in an equilibrium state. The role of the atmospheric water vapor advected from the boundary fields on the generation of rainfall in the REMO model has also been discussed earlier by e.g. Jacob (2001b).

The influence of SST on the rainfall formation over the southern African region however is widely known and has already been discussed in several studies (e.g. Reason et al., 2002; Rouault et al., 2003; Muller et al., 2008). It is therefore not surprising that a better representation of the SST leads to an improved rainfall simulation. Nevertheless,

the importance of the SST for the formation of rainfall in the REMO model might also be seen as a quality feature of the RCM. However, as the warm bias in South Atlantic SST seems to be a common feature of current GCMs, the chosen double-nesting setup using the anomaly approach to correct the GCM SST forcing is highly recommended for dynamical downscaling simulations of GCM data over the southern African region. This argument is also supported by the improvement of the rainfall simulation along the BIOTA North-South Transect (BNST; Figure 4.10) and over the Orange catchment (not shown) which was obtained by REMO in comparison to ECHAM5/MPIOM.

In the second part of the chapter, the projected temperature and precipitation changes for the southern African region were presented. These changes were obtained from the longest transient high-resolution climate change projection that has ever been conducted for the region and also from the forcing global and regional model simulations. The added value of a high-resolution climate simulation with respect to a better representation of the rainfall characteristics along BNST, but also due to spatially more detailed projections, has been shown. This finding is consistent with previous studies (e.g. Hagemann et al., 2009), which pointed out that the better description of the surface patterns and surface processes leads to an added value in the representation of the climate characteristics by an RCM. The resulting benefit of long-term RCM simulations as climate input for impact studies on a regional scale has been recognized (e.g. Fowler et al., 2007). Nevertheless, due to the immense computational effort only today's high performance computation systems allow for such long simulations on such fine grid spacing.

The magnitude of the simulated future changes in temperature and precipitation of REMO generally do not differ from the projections of the forcing GCM ECHAM5/MPIOM, which was one of the models described in the IPCC AR4 for the region (Table 4.1). This finding is an indication that the applied SST correction does not have a large impact on the climate change signal. All projections yield a strong warming connected with a substantial drying for the region. This drying seems to be slightly stronger in the RCM projections than in the GCM projections towards the end of the current century. However this larger decrease can partly be explained by the larger wet bias of ECHAM5/MPIOM over the respective regions, which influences the relative

Table 4.1: Comparison between REMO and ECHAM5/MPIOM (EH5) for temperature (upper part of table) and precipitation (lower part of table) regarding the simulation of the control period (left part) as well as projected changes for the future for Namibia, the South-Western Cape (SWC) and the Orange River catchment. The numbers represent area averaged mean values of the respective 30-year period.

	Temperature (in K)	**Namibia**	**SWC**	**Orange R.**
	REMO_016	295.4	290.7	293.3
1960-1990	*REMO_05*	295.5	291.0	293.2
	ECHAM5/MPIOM	294.5	291.4	291.9
	REMO_016	1.3	1.0	1.3
2011-2040	*REMO_05*	1.4	0.9	1.3
	ECHAM5/MPIOM	1.3	0.8	1.3
	REMO_016	3.1	2.0	3.1
2041-2070	*REMO_05*	3.2	2.0	3.1
	ECHAM5/MPIOM	3.0	2.0	3.1
	REMO_016	5.2	3.3	5.2
2071-2100	*REMO_05*	5.3	3.3	5.3
	ECHAM5/MPIOM	5.0	3.2	5.1

	Precipitation (in mm/month and %)	**Namibia**	**SWC**	**Orange R.**
	REMO_016	28.0	39.7	33.1
1960-1990	*REMO_05*	30.2	39.7	37.9
	ECHAM5/MPIOM	39.5	22.9	42.7
	REMO_016	-12.0	-12.6	-4.0
2011-2040	*REMO_05*	-11.0	-11.5	-3.1
	ECHAM5/MPIOM	-11.9	-10.9	-9.0
	REMO_016	-30.6	-25.6	-15.5
2041-2070	*REMO_05*	-28.4	-25.6	-12.6
	ECHAM5/MPIOM	-22.5	-30.0	-18.1
	REMO_016	-46.2	-35.6	-29.0
2071-2100	*REMO_05*	-43.4	-36.1	-27.6
	ECHAM5/MPIOM	-27.5	-34.7	-19.7

changes. Generally it can be stated, that the projected climate change signal of the presented models for the region, is much stronger than the projections presented in AR4. Here the maximum warming towards the end of the 21st century over the region was projected to be about 4 K and the projected drying was less than 20% compared to the base period (Christensen et al., 2007). In particular the stronger decrease in rainfall, which is also connected to a decrease in soil moisture and therefore directly influences the water supply of the region would result in a severe impact on the region (e.g. on its unique biodiversity, as assessed within the BIOTA project). However, the current projection is only one realization of a long-term high-resolution climate change projection and also suffers from a particular degree of uncertainty. It is therefore essential to increase the number of available long-term high-resolution climate change simulations to come up with an ensemble of detailed projections over the southern

African region as it previously was done for other parts of the world (e.g. for Europe; Jacob et al., 2007). This would then allow to classify, if the very strong climate change signal seen in the current projection is a robust signal of future changes on a regional scale. Keeping in mind the above shown added value of the high-resolution climate projections, this effort seems to be well worthy.

4.6 Concluding remarks

In this chapter an adapted simulation setup for dynamical downscaling studies over the southern African region was presented, which accounts for the underrepresentation of the cold upwelling region in the South Atlantic in the GCMs accounted in the IPCC AR4. The changed simulation setup substantially improved the simulation of rainfall over the southern African region and should therefore be considered to be used for dynamical downscaling studies over the region. Furthermore, the first long-term high-resolution climate change projection for the southern African region was conducted. It was found, that the RCM projects a strong climate change signal, with a warming of up to 6 K in the interior and a drying in the range of about 30 to 50 % towards the end of the 21st century compared to the 1961 to 1990 control period. This signal is in the range of the forcing GCM but noticeable stronger than the climate change signal presented in IPCC AR4. As it was shown, that the REMO model better represents the rainfall characteristics of the focus region of this study, it is recommended to use downscaled climate information for impact studies.

Chapter 5

Will the southern African west coast fog be affected by future climate change? Results of an initial fog projection using a regional climate model.

5.1 Introduction

In the present study, a first attempt for a long-term projection of future changes in the occurrence of fog along the southern African west coast is described. In this region advected sea fog is a rather frequent feature (e.g. Schulze, 1969; Lancaster et al., 1984) and provides a major source of moisture for several local species (e.g. Hachfeld, 2000; Hamilton et al., 2003; Henschel and Seely, 2008). Maximum monthly precipitation from fog can reach up to about 50 mm while annual mean rainfall amounts for the region are between ~20 to 40 mm per year (Lancaster et al., 1984). The formation of sea fog in this region is linked to the relatively cold surface waters of the Benguela upwelling system. Warm air passing over these upwelling regions is cooled and reaches saturation. However, not only the occurrence of the upwelling cell matters, but also its spatial extent, which is defined by the regional wind patterns (Shannon, 1985). Olivier and Stockton (1989) postulated that a too large upwelling cell blocks the formation of fog at Lüderitz, whereas an intermediate sized upwelling cell (~200km) is favorable for fog formation. This finding is linked to the fact that in 75% of all fog events at Lüderitz a costal low was present. Coastal lows are mesoscale disturbances that are blocked in their vertical extend by a strong subsidence, generally causing a stable inversion layer

(Reason and Jury, 1990). The costal lows mainly occur during the summer season and are responsible for the transport of dry air masses from south-easterly areas over warm waters, where they take up moisture. These moist air masses are then transported in north-easterly direction over cold waters closer to the coast. There the air masses cool to dewpoint and fog forms, which is then further transported to the land area. If the upwelling cell is too large, however, dry air can not be transported over warm waters causing a reduced water uptake and therefore no saturation of the air masses (Olivier and Stockton, 1989). A schematic of the major upwelling cells as well as of the coastal low and the related flow scheme is also included in Figure 5.1a. It has to be noted, that the upwelling is not a constant feature but occurs in pulses (Shannon, 1985), which might not be represented in the model data (see Section 5.2).

Fog has been regularly observed along the southern African west coast for many years, due to its ecological importance. Based on observations it was shown that fog regularly extends more than 100 km inland (e.g. Lancaster et al., 1984; Hachfeld and Jürgens, 2000) but the number of fog days shows a remarkable gradual decrease from the coast to inland regions. Also, a distinct seasonality in the number of fog days is observed. Directly at the coast, fog is most common in the winter (April to September) season, whereas further inland the main fog season is shifted to early summer (October to December). However, the number of available stations is limited. Therefore, Olivier (1995) established a visual analysis of satellite imagery for the detection of spatial fog extent for the year 1984. It was shown that during the observation period more than 100 fog days occurred along the coast and more than 50 fog days a year were recorded for a band reaching about 50 to 80 km inland. However, as the visual fog identification is quite cumbersome, a method to automatically detect fog is necessary when extending the observed time period. Cermak (2010) therefore recently applied an automated fog/low cloud detection algorithm to Meteosat imagery data for this region for the period 2004 to 2009. This dataset will be used in the present study for the validation of the simulated fog patterns and is described in Section 5.3 in more detail.

Due to its frequent occurrence in a desert region otherwise very poor in precipitation, several studies have suggested the use of fog as a source of drinking water (e.g. Shanyengana et al, 2002; Olivier and de Rautenbach, 2002; Olivier 2004). In the future the potential of fog for drinking water supply can become even more important, as

many studies report a decrease of projected future rainfall precipitation for south-western Africa (e.g. Christensen et al., 2007; MacKellar et al., 2007; Haensler et al, 2010c). However, the long-term development of fog occurrence has not been studied so far. Under this aspect, projections of long-term future developments of fog frequency would be of great value. So far, fog modeling has only been conducted for short timescales, mainly with respect to aviation and road traffic safety using one-dimensional fog forecast models (e.g. Bott and Trautmann, 2002; Haeffelin et al., 2010) or numerical weather prediction systems (e.g. Mueller et al., 2010). A comprehensive review of past achievements in fog research and fog modeling was provided by Gultepe et al. (2007).

The aim of the present study is to test the potential of the regional climate model (RCM) REMO (Jacob, 2001a) to project future changes in fog frequency over the region. Therefore a fog diagnostic scheme was implemented into the model. REMO has already been applied for hindcast (see Chapter 3) as well as transient climate change (see Chapter 4) simulations over the southern African region. In these studies it has been shown that the model is well suited to simulate the region's climate characteristics. Especially due to the very high horizontal resolution of the simulations, region-specific climate features have been shown to be better simulated by REMO than by reanalysis data (Chapter 3, Section 3.4.1).

In Section 5.2 the model and the fog diagnostics are described. In Section 5.3 the available fog datasets are presented and the validation of the model is shown. Section 5.4 deals with the results of the future fog projections. Finally, Section 5.5 provides a discussion of the findings of the validation and climate change sections. The chapter ends with a short conclusions section.

5.2 Model description and simulation setup

The simulations are conducted with the three-dimensional hydrostatic atmospheric circulation model REMO (REgional MOdel) (Jacob and Podzun, 1997; Jacob, 2001a) in its 2008 version. This version was already tested and used over the southern African region in a previous study (see Chapter 4). The model is based on the "Europamodell", the former numerical weather prediction model of the German Weather Service (DWD,

Majewski, 1991). In its original version the physical parameterizations of REMO were based on those of the global climate model ECHAM4 (Roeckner et al., 1996). The prognostic variables of REMO are surface pressure, horizontal wind components, temperature, specific humidity and cloud water. With respect to the fog simulation especially the calculation of the cloud water of large-scale (stratiform) clouds in REMO is of interest. For the stratiform clouds this calculation is based on the approach following Sundqvist (1978), and was taken from the ECHAM4 global climate model (Roeckner et al., 1996). The budget equation for cloud water is calculated including the processes of evaporation of cloud water as well as condensation of water vapor. Also the advective and sub-grid scale transports of cloud water are incorporated in the equation.

The horizontal resolution for the simulations described here was 18x18 km. In the vertical direction the model was run with 20 levels, with the lowest model level approximately 30 m high. The model was integrated for a hindcast simulation for the period from 2001 to 2007 and for two 20-year simulations (Control: 1981-2000; Scenario: 2081-2100) as an initial study to assess potential changes in fog occurrence. The lateral boundary conditions for the simulations are taken from ERA40 reanalysis (Uppala et al., 2005) and operational analysis data of the European Centre for Medium-Range Weather Forecasts (ECMWF) for the hindcast and from the coupled atmosphere ocean general circulation model ECHAM5/MPIOM (Roeckner et al., 2003; Jungclaus et al., 2006) IPCC A1B projections for the climate change simulations. For the latter, however, a SST-correction based on the anomaly approach (see Chapter 4, Section 4.2.3) had to be applied, due to the inability of the global model to resolve the Benguela upwelling. To reach the final 18x18 km resolution the so-called double-nesting setup was applied. In this setup the original boundary forcing is first downscaled to an intermediate resolution REMO simulation (50x50km) and the output of this simulation is then used to force the high-resolution simulation. An overview of the simulation setup including the double-nesting setup is given in Figure 5.1b.

It generally can be claimed that the high temporal variability of the Benguela upwelling system can not captured by the global coupled general circulation models (GCMs), which provide the sea surface temperature (SST) data for the future projections. In Figure 5.2 the simulated SST is compared to satellite observations (NOAA AVHRR

Pathfinder Version 5 data) and ERA40 reanalysis data (SST data of validation simulation). While the upwelling in the annual mean SST seems to be fairly well represented in the ERA40 and also in the corrected GCM data (Figure 5.2, upper panels), the seasonal variability of the GCM (which is not affected by the applied SST correction) is substantially lower than the one of the observations and reanalysis data (Figure 5.2, centre panels). With respect to variations occurring on a daily time scale, the deseasonalized daily SST- variability has been calculated (Figure 5.2, lower panels). Generally the daily variability in the SST is lower in the reanalysis and model data compared to the satellite observations, which also can have an impact on the fog simulation. However, one has to keep in mind that the available daily satellite observations are affected by a large number of missing values due to cloud effects, which might reduces the credibility of this dataset.

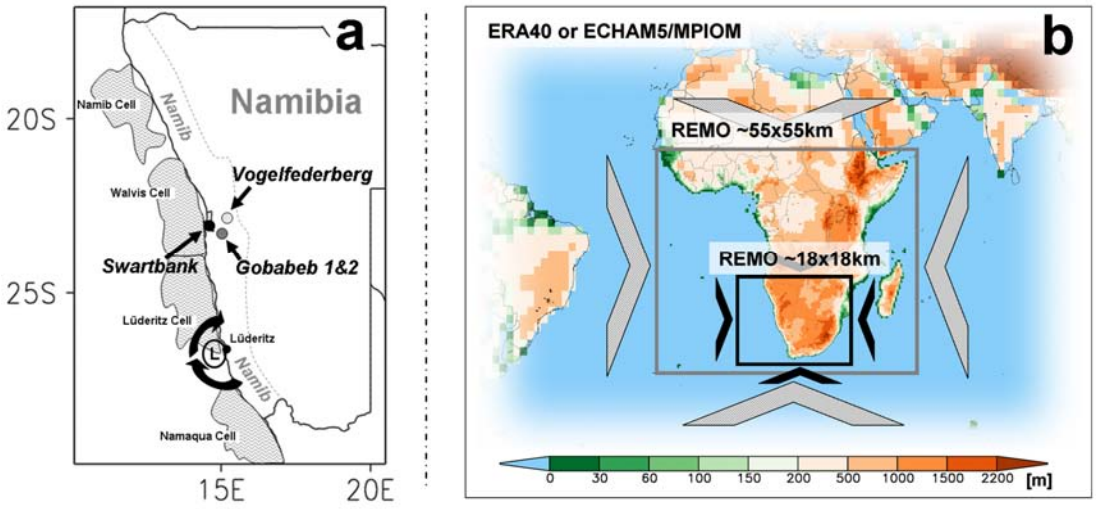

Figure 5.1: (a) Location of the four available stations with fog observations The panel also depicts the main Benguela upwelling cells after Pickford and Senut (1999) and a schematic of the coastal low and its related flow fields after Olivier and Stockton (1989). (b) Sketch of the double nesting setup and extent of the respective REMO domains indicated as grey (~55 x 55 km) and black (~18 x 18 km) boxes

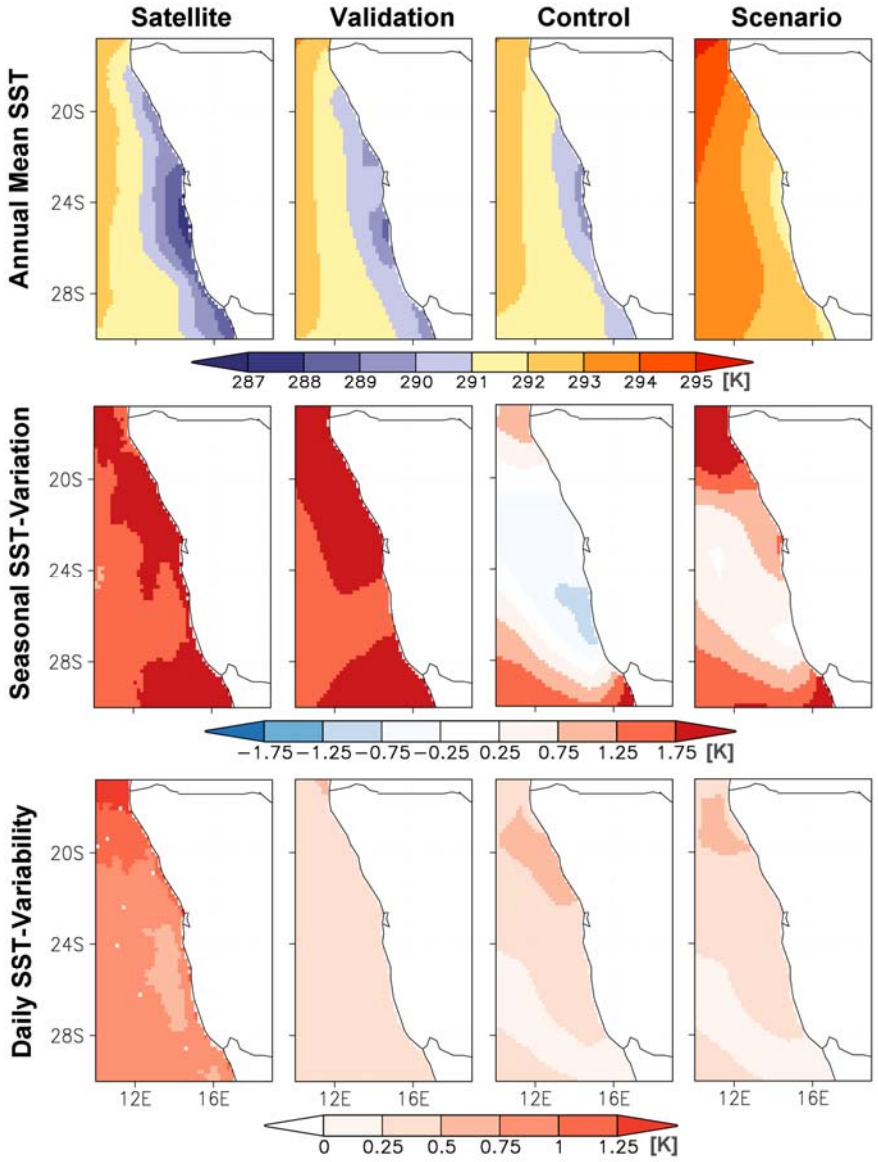

Figure 5.2: Annual mean SST (upper panels), seasonal SST anomaly (summer minus winter; centre panels) and standard deviation of deseasonalized daily mean SST data. The NOAA pathfinder dataset (Satellite) represents the time period from 1990 to 2007. The reanalysis (Validation) and GCM (Control and Scenario) represent the respective simulation periods (Validation: 2001 to 2007; Control: 1981 to 2000; Scenario 2081 to 2100).

5.2.1 Fog diagnostics

Fog is generally defined via the visibility (VIS) and occurs if VIS is lower than 1000 m (WMO, 1992). In REMO, VIS is not an output variable. To identify fog events therefore the empirical visibility relation after Kunkel (1984) was implemented into REMO. The diagnostics is a function of the liquid water content (LWC) and follows

$$VIS = -\frac{\ln(0.02)}{144.7(LWC \times \rho)^{0.88}} \qquad (1)$$

with ρ representing air density. The unit for VIS is km; LWC and ρ have units of kg/kg and g/m^3, respectively. Fog is diagnosed only in the lowermost model level (vertical extent ~30 m) but at each model time step (90 seconds). This diagnostic is frequently used in modeling studies (e.g. Teixeira, 1999) but due to its simplicity it seems to have some disadvantages. Gultelpe et al. (2006) showed that the simulation results can be significantly improved if the droplet number concentration Nd is taken into consideration. However, as Nd is still a preset parameter in the current REMO version the proposed relation could not be used in the present study.

The output interval of the fog simulation was set to one hour, even though fog was diagnosed on a 90 seconds time step. Hence the resulting model output is the fraction of an hour, on which the model simulates fog. In order to compare the simulated fog data to observations on a daily basis (and to not include fog events only occurring on a single model timestep into the analysis) a threshold had to be defined, to distinguish between fog and fog-free days. This threshold for a fog day was defined in a way that at least for 75% of a single hour a day the model has to simulate fog conditions. This definition translates to a minimum of 45 minutes of fog a day in order to be counted as a fog day, which allows identifying both short-term fog events (less than one hour) and long-term fog events.

5.3 Observations and validation of the fog scheme

For the validation of the simulated fog occurrence a fog/low cloud product derived from Meteosat satellite imagery at a horizontal resolution of 3 km is used (Cermak, 2010). In contrast to previous geostationary satellite systems, the Spinning-Enhanced Visible and Infrared Imager (SEVIRI) aboard the newest Meteosat satellites features high spatial, temporal and spectral resolutions, which makes it suitable to be used for cloud type discrimination (Cermak et al., 2008). Areas covered by fog and low cloud are identified on the basis of spectral tests in the visible and infrared regions, informed by radiative transfer computations incorporating the principles discussed in Cermak and Bendix (2008). Originally, this product was only available for Europe, where it could be tested against stations observations. Recently Cermak (2010) transferred the procedure to the southern African region to develop a new product for the identification of fog and low cloud for the Namib region for the period from 2004 to 2009. As no station data was available for this period, the validation of the fog/cloud product had to be based on Cloud-Aerosol Lidar with Orthogonal Polarisation (CALIOP) data. Generally good reliability of the new product could be identified (hit rate above 95%). However, fog and low clouds hidden underneath higher cloud layers can not be identified. Also the dataset used for validation purposes suffers from a particular degree of uncertainty, but was the only reference dataset available. For the south-western African region a data set indicating fog/low cloud presence and absence was compiled covering two time steps per day (0700 and 1400 UTC). A full description of the technique and its validation, as well as climatological interpretation of the product is given in Cermak (2010).

In addition to the satellite data, daily station data were available for four stations. At one of these stations also hourly data was available for a limited time period. All stations are located in the central Namib (see Figure 5.1a). However, apart from the hourly time series, these datasets have significant gaps and are therefore regarded as an additional data source rather than a real validation set. Moreover, they do not cover the same period, but can still serve as an additional data source to assess the quality of the satellite and model data. Table 5.1 summarizes the locations and sampling periods of the station data.

Table 5.1: Locations and sampling periods of the four stations in the central Namib with fog observations.

	Latitude	Longitude	Sampling Period
Swartbank	23.2 S	14.5 E	1970 to 1982 *
Gobabeb 1	23.4 S	15.0E	1966 to 1995 *
			2000 to 2002 **
Gobabeb 2	23.5 S	15.0E	1981 to 1995 *
Vogelfederberg	23.0 S	15.3 E	1979 to 1992 *
Satellite	-	-	2004 to 2009 *

(** hourly readings)

In order to validate the implemented fog diagnostics, the REMO model was applied for the period from January 2001 to August 2008 using ERA40 and operational analysis data as lateral boundaries. This time period and boundary data were chosen because the REMO model had already been validated for this setup (see Chapter 3). However, to assure the same time period for model and satellite date only the period from 2004 to 2007 was regarded for the validation. For this period the mean number of simulated fog days is compared to the satellite observations on an annual as well as on a seasonal (Summer: October to March; Winter: April to September) basis (Figure 5.3). Generally, the satellite data show a strong negative gradient in fog occurrence from the coast to locations further inland. At the coast the maximum number of fog days is around 160 days per year. According to the satellite product, up to about 200 km inland an average of at least five fog days per year is observed around the central Namib. Seasonally, the satellite shows more fog days for the summer season. A comparison with the model reveals that REMO is able to simulate the general seasonal and spatial patterns of fog, with more fog at the coast and less fog further inland. However, the model seems to overestimate the fog occurrence at the coast and over the ocean and underestimate the number of fog days further inland. This seems to be the case for both, the summer and winter seasons. Differences between satellite and model may be related to the different horizontal resolution of the datasets. A major source of uncertainty is also the threshold set to define a fog day in the REMO model. While it has no influence on the simulated fog seasonality, it definitely has an impact on the absolute number of fog days. In addition to this, also the previously discussed weakness in the SST data has to be considered. Further it has to be noted that in the model fog is diagnosed for the whole lowest level (~30m) whereas the satellite does not take into account the vertical

extension of the fog layer. Thus, the general agreement of patterns between model and satellite is taken as an indication of satisfactory representation of fog conditions be the model.

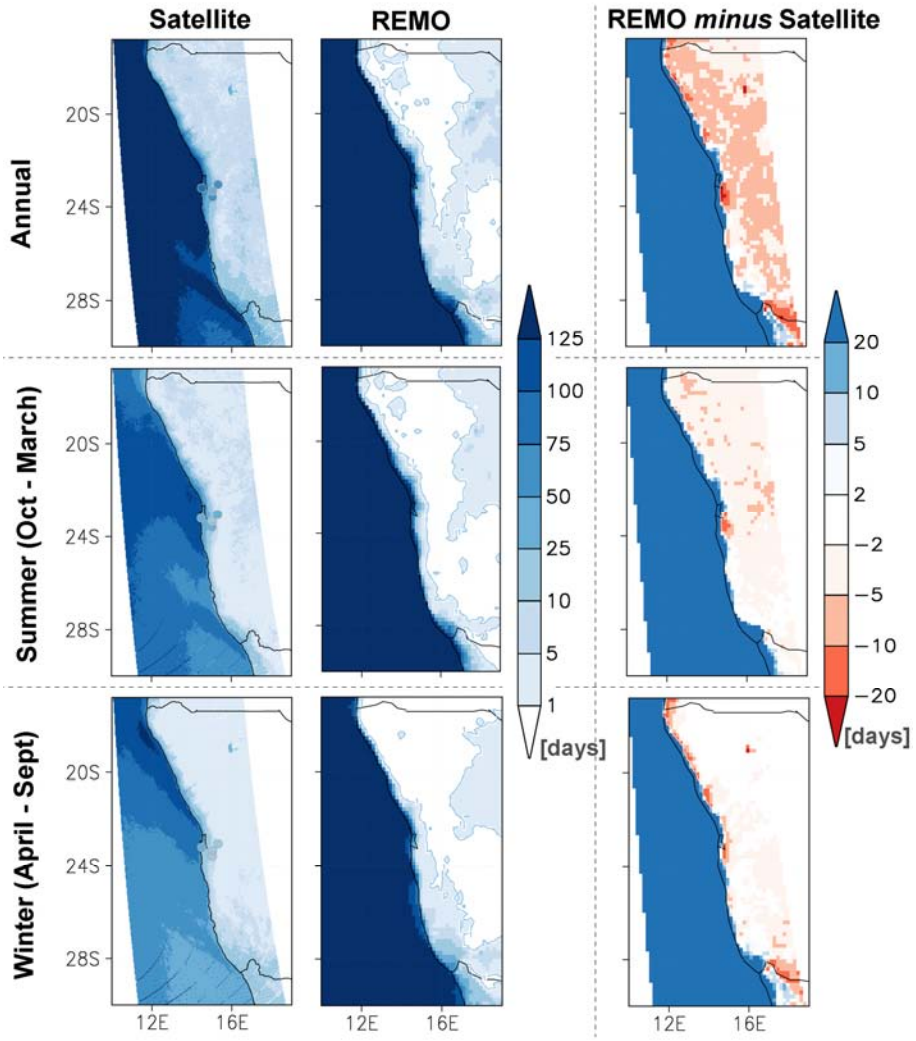

Figure 5.3: Mean number of fog days per year (upper row) and for the summer (central row) and winter (bottom row) seasons as observed (left column) and simulated by REMO (central column) for the period from 2004 to 2007. Additionally the observed fog days at each station, represented by coloured circles, are included in the left panels. However the time period of the data differs from the satellite and model (see Table 5.1). The absolute differences between simulated and observed fog occurrence for the respective seasons is displayed in the right-hand panel. Note that the 3 km satellite data was remapped to the 18 km REMO grid for direct comparison.

To compare satellite data and model output directly to the station observations an inverse distance-weighted method was used to compute a value for the gridded satellite and model data at each station location. In comparison to the stations, both, the satellite data as well as the model show a stronger gradient in the mean number of fog days per year from the station closest to the coast (Swartbank) to the inland stations (Gobabeb and Vogelfedersberg) than those recorded at the station (Table 5.2). Especially the

Table 5.2: Summary of the annual fog statistics for the four stations as observed and simulated by REMO. Note that the station data represent different time periods than the satellite and model data (see Table 5.1 and Figure 5.3).

	Station				Satellite				Model			
[days]	Mean	Min	Max	SDev	Mean	Min	Max	SDev	Mean	Min	Max	SDev
Swartbank	80	62	104	13	100	82	120	14	163	152	180	10
Gobabeb 1	41	14	64	12	22	19	27	3	15	14	16	1
Gobabeb 2	55	20	73	12	28	20	33	5	11	9	15	2
Vogelfederberg	57	15	80	18	7	4	12	3	4	3	5	1

pronounced difference of the satellite and station data has to be noted. This difference can partly be assigned to the interpolation of the gridbox average to the point location. But the remaining discrepancies still show that also the observations suffer from a particular degree of uncertainty, which has to be kept in mind while evaluating the model results. The observed and simulated mean annual cycles for all stations are depicted in Figure 5.4. To better compare the simulated and observed seasonalities, the data have been normalized to the respective maximum climatological fog occurrence. The satellite and model data generally show a more pronounced seasonality than the stations. This is most probably related to the fact that the station data suffer from large data gaps. However, the position of the peak is comparable to the one of the satellite data. For the Swartbank and Vogelfederberg the mean seasonal cycle as observed by the satellite and simulated by REMO agree rather well, but REMO shows the peak fog occurrence one month earlier at Vogelfederberg and slightly later at Swartbank than observed. For the two Gobabeb Stations, the model seems to miss the secondary fog maximum in early summer which is visible in the satellite data.

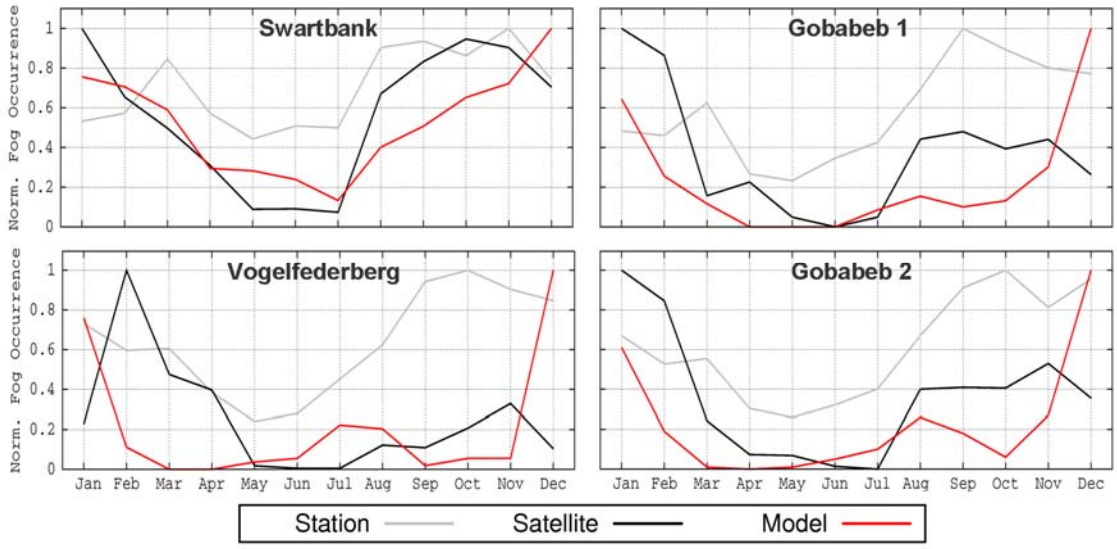

Figure 5.4: Observed and simulated mean seasonal fog distribution for the four stations in the central Namib. Note that each data series was normalized to its respective maximum value. Furthermore, the station data represent different time periods than the satellite and model data (see Table 5.1 and Figure 5.3).

At the Gobabeb 1 station also automatically sampled hourly data are available for the period 2000 to 2002. This dataset is not affected by large data gaps as it has data at more than 95% of all potential recordings. Therefore, the diurnal cycle of fog occurrence can be analyzed as well. According to the station data the maximum of fog occurrence is near 0600 UTC (Figure 5.5), which also matches rather well the timing discussed in the literature (e.g. Schulze, 1969). REMO reproduces the observed diurnal cycle almost perfectly showing only a delay of about one hour in the fog maximum. Also the satellite seems to have the maximum in the morning. However, with only two available samples per day a robust analysis cannot be performed.

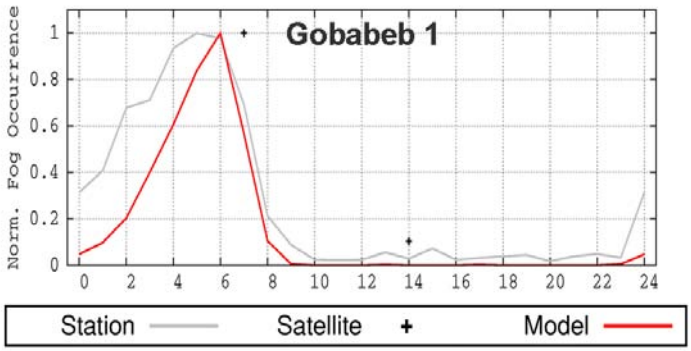

Figure 5.5: Observed and simulated mean diurnal fog distribution for the Gobabeb 1 station. Note that each data series was normalized to its respective maximum value. Furthermore, the station data represent different time periods than the satellite and model data (see Table 5.1 and Figure 5.3).

5.4 Scenario of future fog extent

For the assessment of future changes in the fog occurrence along the southern African west coast the output of the coupled global atmosphere-ocean model ECHAM5/MPIOM was used to force the regional model. Two 20-year time-slices for the periods 1981-2000 (control) and for 2081-2100 (scenario) were simulated for this initial study. The SRES A1B (Nakicenovic et al., 2000) emission path as an intermediate scenario was used to drive the simulation. In Figure 5.6, the simulated mean number of fog days per year and for the two seasons are presented for the control and scenario simulations. Generally REMO projects a slight increase of the number of fog days over the ocean and along the coastal land areas. Further inland however, a decrease in the number of fog days is projected, leading to a stronger negative gradient

Table 5.3: Summary of the annual fog statistics for the four stations as simulated by REMO for the control (1981-2000) and scenario (2081-2100) periods.

	Ctrl (1981-2000)				Scen (2081-2100)				% Change	
[days] and [%]	Mean	Min	Max	SDev	Mean	Min	Max	SDev	Mean	SDev
Swartbank	153	129	171	11	167	148	206	13	10	16
Gobabeb 1	21	10	40	7	17	6	32	7	-23	-4
Gobabeb 2	20	9	35	6	14	5	29	7	-30	6
Vogelfederberg	11	5	25	5	7	2	20	4	-39	-12

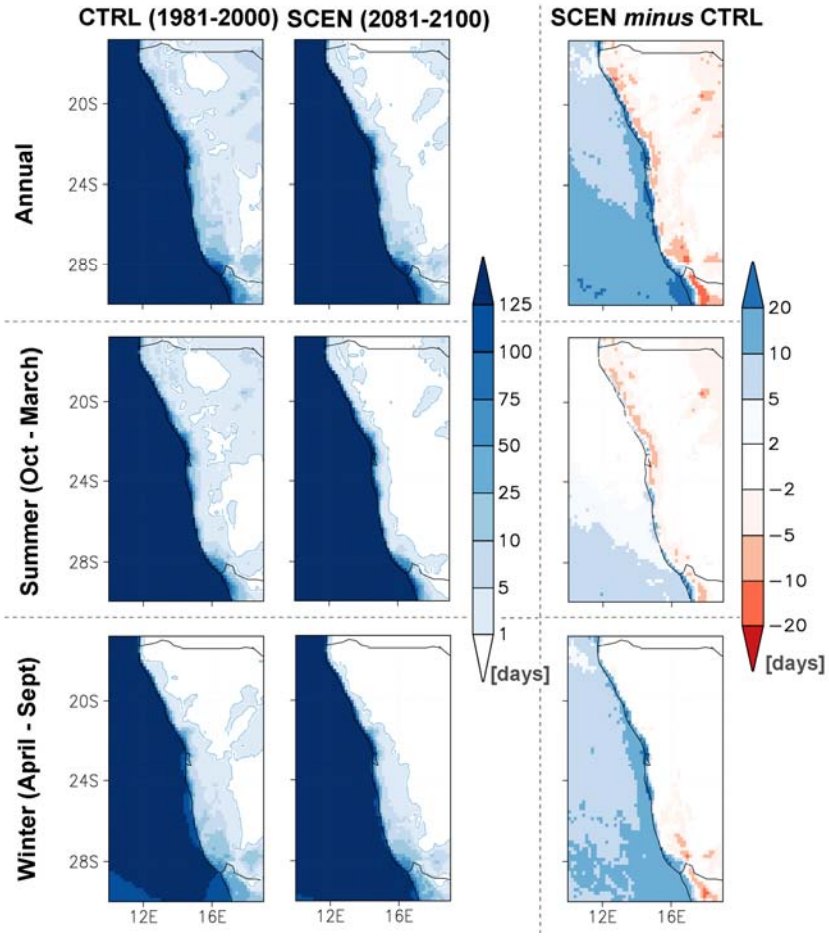

Figure 5.6: Mean number of fog days per year (upper row) and the summer (central row) and winter (bottom row) seasons as simulated by REMO for the control (1981-2000; left column, 'CTRL') and the scenario (2081-2100; central column, 'SCEN') periods. The absolute differences between control and scenario fog occurrence for the respective seasons are displayed in the right-hand panel.

from the coast inland. This change pattern seems to be consistent throughout the year, as there is not much difference between the summer and winter situations. As there seems not to be a general change in the regional-scale circulation (see Chapter 6) a possible explanation for the reverse change in the fog occurrence might be related to changes in the thermal characteristics. While the general warming over the ocean would favor an increased moisture load at the coastal areas, the strong warming of over land might lead to stronger fog dissipation.

At the four station locations, the situation seen in Figure 5.6 is also represented (Table 5.3). Whereas close to the coast (Swartbank) fog occurrence is projected to slightly increase (~10%), the model results at the location of the inland stations show a decrease from about 25 % (Gobabeb) to almost 40% (Vogelfederberg). The calculated decrease

in the number of fog days at these three stations is limited to the main fog season during late summer, whereas the simulated secondary maximum during the winter season is slightly shifted towards early winter. The calculated increase at Swartbank station is projected to solely occur during winter time (Figure 5.7). Both change patterns lead to a reduced seasonality in the projected future fog patterns. As expected, no change is visible for the diurnal cycle at all four stations (not shown), since the dissipation of fog in the early morning is mainly linked to thermal processes connected to the diurnal temperature cycle. Even if the absolute temperature is projected to increase in the future (see Section 4.4) the diurnal temperature range is simulated to only slightly increase (~0.5K) in the future for this region. Therefore, the cooling during night time still maintains the presence of advected fog.

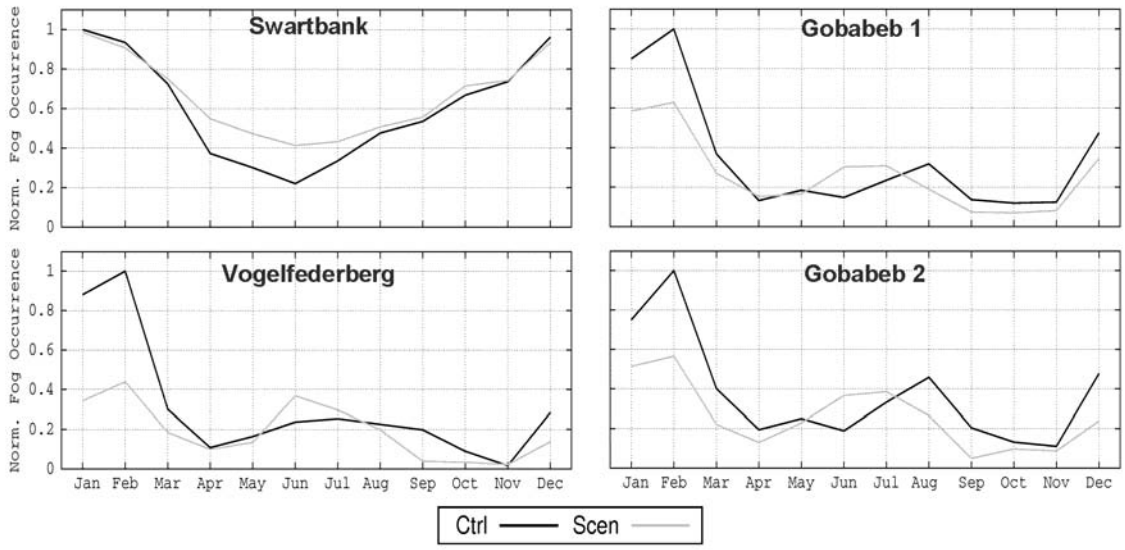

Figure 5.7: Simulated mean seasonal fog distribution for the four stations in the central Namib for the control (1981-2000) and scenario (2081-2100) periods. Note that the data series are normalized to the climatological maximum value of the control period.

5.5 Discussion

In this chapter a first attempt of a long-term fog projection using a regional climate model was presented. The simulated fog occurrence shows patterns similar to those observed, with much higher fog occurrence along the coast compared to locations further inland. But still, there are some remarkable deviations between model and satellite observations. Especially the inland penetration of fog seems to be underestimated by the model. However, a lack in inland moisture transport simulated by the model does not seem to be the cause for this deficit, as the regional circulation characteristics (see Chapter 3, Figure 3.3) as well as the local, thermally induced wind fields (see Chapter 6) are well reproduced by REMO. Also the seasonality and the diurnal cycle of the fog occurrence agree rather well with observations giving a further indication that the circulation patterns are captured by REMO. Hence, the deficit in inland fog simulation can more likely be assigned to the coarse model resolution and the very simple fog diagnostics – including the chosen threshold to define a fog day – that were implemented. Especially the vertical extent of the lowest model level has to be assessed critically (Masbou, personal communication; Tardif, 2007) and should be reduced remarkably in future applications. However as a change in the vertical resolution requires a comprehensive validation of the model itself, it was decided to use the already validated model for this initial study. Other reasons for disagreements could be errors in the satellite data set mainly connected to the inability to identify fog, if high-level clouds are present. Also the internal variability of the model could be a reason for the disagreement as the time period for which satellite data are available is rather short.

Further, the simple fog diagnostic based only on the LWC has to be critically reexamined. Previous work by Gultepe et al. (2006) shows that the error can be as high as 50%. However this number refers to fog forecasting studies, where the timing and extent of individual fog events are relevant. In this approach however, the main interest is in the long-term changes rather than the simulation of fog events. Therefore the error is likely to be smaller. Another worthwhile approach for fog simulations with a horizontal resolution in the range of about 20km could be to use a multivariable-based fog diagnostics as proposed in a recent paper by Zhou and Du (2010). They defined fog based on a decision cascade considering first the LWC, then the vertical cloud extent

and finally 10m wind speed and relative humidity. The application of these four criteria significantly improved fog forecasting, especially wind speed and relative humidity proved to be important factors to consider. However, one has to keep in mind that the event-based verification of the decision chain, as usually performed for numerical weather forecast models, cannot be applied to an RCM. Therefore, a multivariable approach might also enhance the uncertainty involved in the diagnostic process.

The presented scenario simulation gives a first indication of how reliable fog occurrence will be in the future. Generally, a decrease in the number of fog days is projected for inland fog. This even leads to the disappearance of fog in many locations. Less fog days per year will most likely lead to an overall decrease in fog water input. In connection with the projected rainfall decrease mentioned before (e.g. Section 4.4; MacKellar et al., 2007), the regional water availability is likely to be substantially reduced in the future. However it has to be kept in mind that for the assessment of future fog extent only a 20 year time slice experiment was conducted. Therefore, the projected changes serve rather as an indication for what the future could be, than as absolute number. For a more robust projection, a longer time period needs to be assessed and more scenario simulations (also including more models) should be conducted.
It also has to be noted that due to the change of the forcing from the ERA40 re-analysis data (used on the validation simulation) to the ECHAM5/MPIOM data (used for the control and scenario simulations) a difference in the simulated fog days for present-day climate conditions appears. However, due to the fact that the deficits in the validation simulation (Section 5.3) are reduced in the control simulation (see Table 5.2 and 5.3), the application of the model for a scenario simulation seems to be justified.

Finally, the role of the sea surface temperature (SST) should be critically reassessed. The feedback of future changes in the circulation characteristics onto the region’s ocean circulation should also be considered in future projections (e.g. Haensler et al., 2010c and Haensler et al., 2010d). The importance of the Benguela Upwelling system for fog formation along the southern African west coast was shown by Olivier and Stockton (1989). In the current simulation, ocean characteristics are taken from the coupled ECHAM5/MPIOM model. However, due to the coarse horizontal resolution of a GCM the individual upwelling cells cannot be resolved in the required degree of detail (see Figure 5.2). Therefore, a fully coupled regional atmosphere-ocean model, such as

already in place for the Mediterranean region (Elizalde et al., in prep), could provide very valuable information.

5.6 Concluding remarks

In this chapter a first study to assess whether future climate change might influence the occurrence of fog along the southern African west coast was presented. It was found that the regional climate model REMO with a basic fog diagnostics scheme can represent the major fog patterns over the region, even though a discrepancy in the number of fog days exists. For the future, this initial study projects an increase of fog along the coast and a decrease further inland. Keeping in mind the uncertainty of the projections it is still reasonable to conclude that along the coast fog could act as a supplementary drinking water source for local communities in the future. However, to provide a more robust data base for regional stakeholders and decision makers more scenarios (including multi-model ensemble simulations) have to be conducted for the region covering a much longer time period.

Chapter 6

Assessment of the simulation of thermo-topographically induced local wind systems over the central Namib Desert using a high-resolution regional climate model.

6.1 Introduction

This chapter provides a detailed investigation of the simulation of the circulation patterns of the southern African region. This includes both the regional scale circulation of the entire region, as well as the local, thermo-topographically induced circulation patterns over the central Namib Desert. While the regional scale circulation is mainly determined by seasonal changes in the large scale flow, the local circulation shows a pronounced diurnal cycle. Hence, the analysis of these features can be used to identify the potential of the regional climate model REMO to simulate processes on different spatial and temporal scales.

The general circulation over the southern African region has already been shortly described in Chapters 2 and 3. Also a Figure depicting the mean sea level pressure and the near surface flow fields for the summer and winter season is given in Chapter 3 (Figure 3.3). To recall the main features a short summary of the major circulation patterns is given at this point. The southern African region is generally influenced by the southern hemisphere high pressure belt, whose position varies seasonally. It extends furthest to the south in late summer (February) and the furthest north during winter (June to August). Due to the different surface heating of ocean and land masses the high

pressure belt is separated into two cells, the Atlantic and the Indian Ocean high (e.g. Schulze, 1969). During the summer season a shallow low pressure system – sometimes also referred to as heat low (e.g. Mason and Jury, 1997) – develops over the central region and shifts the Indian Ocean cell further to the east. In the winter season the position of this cell is located further west. Therefore the situation mainly shifts to a predominant anticyclonic circulation caused by this large single high pressure cell (Schulze, 1969). In Chapter 3 it was shown that REMO ably represents the major seasonal surface circulation characteristics. However, the simulation of middle and upper tropospheric patterns, e.g. the position and strength of the subtropical jet stream has not been assessed in the validation study and will therefore be included in the present study.

Regarding the simulation of the surface patterns other RCMs have also proven to reasonably simulate the regional scale circulation patterns over the southern African region (e.g. Hudson and Jones, 2002; Joubert et al., 1999). However, the ability of RCMs to simulate small-scale circulation features so far has not been studied in detail for this region. This is likely related to the limited number of high-resolution climate simulations available for the southern African region (see Chapter 3 and 4). Local scale air flow can substantially deviate from the regional circulation characteristics and is mostly determined by topographically as well as thermally induced diurnal oscillations of the near surface wind fields (e.g. Simpson, 1994). The Namib Desert is unique in that it constitutes a well studied region with a largely decoupled local wind system. Goldreich and Tyson (1988) defined the ratio of diurnal to inter-diurnal variability of hourly wind records as an indicator of the importance of local in contrast to regional scale winds. They showed that over the central Namib this ratio is one of the highest for the whole south-equatorial Africa. The reason for this can on the one hand be found in the large land-sea temperature contrast along the west coast (Lengoasa et al., 1993), which is mainly induced by the cold sea-surface temperatures (SSTs) of the Benguela upwelling system as well as by the hot surface of the Namib Desert further inland. On the other hand the region is also defined by a steep orographic gradient called the “Great Escarpment” at the eastern boundary of the Namib Desert (e.g. Watson and Lemon, 1985). Due to these rather unique preconditions, three major local wind systems (see Figure 6.1 for schematic) could be identified for this region. Based on station observations Lindesay and Tyson (1990) described these systems as follows:

i.) Sea-breezes (SBs):

South-westerly winds that occur regularly throughout the year. The onset of the SB conditions shows a gradient from the coast towards the slope of the escarpment. On the Namib coast they develop shortly after sunrise and decay again shortly after sunset. During summer they are displaced by north-westerly plain-mountain winds while during winter nocturnal north-easterly land breeze (LB) takes over at the coast. Further inland, SB development is shifted to the early (central Namib) and late afternoon (foothills of the escarpment), respectively. Also at these locations SBs decay rapidly after sunset. The maximum vertical extend of SBs during the summer season is about 1000m and is also reached earlier at the coast than further inland. During wintertime SB conditions still occur rather frequently, but are generally less developed.

ii.) Plain-Mountain Winds (PMWs)

North-westerly winds that occur mainly during the summer season. The winds result from a thermal gradient between the gravel plains to the north and the escarpment to the east. As during summer the surface heating effects are at a maximum the PMW is a rather constant feature throughout the day with only little disturbances. Their vertical extent is at maximum during the late afternoon and reaches up to about 1000 to 1600 m. Disruptions at the surface can occur during times when SB conditions develop and also around sunrise, when the reverse mountain plain wind might occur. During wintertime PMWs are a daytime phenomenon only and do not reach as deep into the boundary layer as during the summer season.

iii.) Mountain-Plain Winds (MPWs)

Night-time east south-easterly winds that predominantly occur during the winter season. During this time of the year the nocturnal cooling effects are strongest. Hence an inverse thermal gradient between the coastal plains and the escarpment is established, which prefers the development of a seaward air flow. MPWs develop at around 2200h and decay shortly after sunrise. Their maximum depth is about 1000m. MPWs are mainly predominant in the central and eastern part of the Namib. Directly at the coast rather the night-time north-easterly LB is developing during the winter season. During summer MPWs occur only very infrequently for a short time close to sunrise, but do not reach very deep into the PBL.

Under special synoptic conditions, however, the daily sequence of the thermo-topographically induced boundary layer airflow over the Namib Desert can be completely interrupted (Lengoasa et al., 1993). Here, mainly two systems have to be considered. The first are coastal lows, which are mainly restricted to the summer season and are supposed to play an important role for the fog formation over the region (see Chapter 5). They are characterised by an abrupt change in the prevailing wind direction and usually propagate along the whole coast of southern Africa (Reason and Jury, 1990). The second and more common system over the central Namib are so-called berg wind events with predominant north north-easterly flow, which mainly occur during the winter season. Favourable conditions for the development of berg winds are relatively high pressure systems over the interior and low pressures over seaward regions (van Rooy, 1936), hence resulting in a strong pressure gradient parallel to the escarpment from the coast to further inland regions (Tyson, 1964). This prerequisite explains why berg winds are mainly limited to the winter season, when the southern African region is under the influence of anticyclonic conditions. On average berg winds occur with a rate of about 50 days a year at the coast (e.g. van Roy, 1936; Tyson, 1964); and rather infrequent at a rate of about 15 days further inland (Gobabeb; Schulze, 1969). Due to the involved regional scale subsidence berg winds show föhn-like behaviour and cause a remarkable increase in surface temperature (van Roy, 1936). This leads to the unique conditions that observed air temperatures are highest during the winter season (Tyson, 1964). On a diurnal scale, the main berg wind occurrence is during morning hours, whereas in the afternoon sea breeze conditions usually take over. Regarding their magnitude berg wind events sometimes can be connected with high wind speed (Lancaster et al, 1984). Due to this and also because of the fact that berg winds blow from the direction of the dry interior a substantial dust load is often connected to these events (Soderberg and Compton, 2007).

Even though the local wind systems at the west coast of southern Africa are well documented, so far only few studies are available for the region that try to simulate the specific patterns. Mesoscale models with horizontal resolution between 25 km and 1 km have been applied over the Cape region at specific occasions to investigate the inland sea-breeze penetration during the wine-growing season (Bonnardot et al., 2001; Bonnardot et al., 2005). The analysis of the simulation of thermally and topographically induced wind systems in climate models however has so far not been conducted for the

region. This is most probably due to the computational expensive high horizontal grid resolution, which is required to simulate these processes. Hence this study, which is based on high-resolution simulations of the regional climate model REMO, provides an initial analysis of the ability of an RCM to simulate these processes. Due to the fact that REMO also has been applied for a transient high-resolution climate change projection over the southern African region, the further scope of this study is to investigate, if future climate change might influence the regional or local circulation patterns over the region. As already summarized in Chapter 4, various studies (including Haensler et al., 2010c) projected a substantial increase in near surface air-temperature as well as a strong reduction in the water availability over the southern African region for the future. Therefore, one of the key issues is to estimate, if this change in the surface energy balance will lead to an altered circulation on the regional or even local scale.

This chapter is organized as follows. The subsequent section describes the RCM simulations, the available observational data as well as the method applied to identify the local circulation patterns. In Section 6.3 the validation of the simulated wind fields is conducted on regional and local scales. Section 6.4 focuses on the analyses of the transient climate projection, thereby comparing current and future circulation characteristics. Section 6.5 is dedicated to the ability of REMO to simulate the synoptic scale disturbances. Finally a discussion and a conclusion section are provided.

6.2 REMO simulations, available observations and applied method

For this study two simulations of the regional climate model REMO (Jacob & Podzun, 1997) were analysed. The model version and the respective simulation setup are described in the respective Chapters 3 and 4. To measure the ability of the model to reproduce the regional as well as the local scale circulation patterns the ERA40 forced hindcast simulation described in Chapter 3 was used. The potential future change in the circulation characteristics was analysed on the basis of the climate change projection described in Chapter 4. Forcing for this simulation was provided by an ECHAM5/MPIOM simulation following the A1B SRES emission pathway. However a manual SST-correction had to be applied to the data (see Chapter 4 for details). Out of this projection two 30 year time slices (control: 1961 to 1990; scenario: 2071 to 2100)

were extracted to quantify the climate change signal. Both, the hindcast simulation as well as the climate change projection were conducted at a horizontal resolution of 18x18 km using the double nesting setup (for details see Chapter 3 and 4, respectively).

As area-wide observations of wind direction and wind speed are sparse for the region, the ERA40 reanalysis dataset was considered for the validation of the regional scale circulation characteristics. Near surface as well as data on several vertical atmospheric levels were averaged on a seasonal mean basis for the period from 1961 to 1990 and compared to the respective REMO data. However, one has to keep in mind that the ERA40 data is only available on T159 (~125km) resolution. Therefore it is not expected that the data yields all details that are important for the local climate.

To investigate the simulation of the local circulation patterns over the central Namib Desert, hourly wind data – available for three stations representing a west-east transect through the study area – were analyzed. The data were partly collected within the BIOTA South project (Jürgens et al., 2010) and partly by the Gobabeb Desert Research Station. Due to the fact that the station at the slope of the escarpment seemed to have some bias in the wind direction (most probably due to a channeling effect, as the station is already located on the slopes of the escarpment), also data published in the literature (mainly by Lindesay and Tyson, 1990; and Lancaster et al., 1984) were included in the analysis. A summary of the location of the available stations as well as the covered time period is given in Table 1, their positions are shown in Figure 6.1. Owing to the different time periods covered by the station records, a 10 year period from 1998 to 2007, which covers almost the whole time period of all stations, was considered for the REMO simulations.

Table 6.1: Overview of the location and duration of available station data

	Name	Period	Lat	Lon
Coast	Wlotkasbakken	2001 to 2007	22.32S	14.46E
Central Namib	Gobabeb	2000 to 2002	23.53S	15.07E
Slope	Roisand*	2006 to 2009	23.23S	16.10E

* The recorded wind direction is biased due to topographic channeling effects

In addition to the validation of surface wind fields at the station level, a vertical transect of the lower atmosphere (> 500hPa) wind direction and wind speed along a cross-section through the central Namib (12E to 17E) was evaluated (see Figure 6.1). As no station data on the vertical expansion of the different local wind systems were available, the model results were compared to ERA40 data instead.

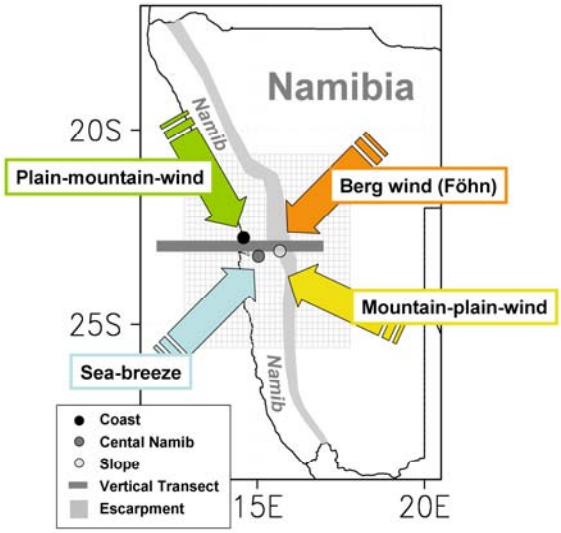

Figure 6.1: Schematic of the flow direction of the four components of the local wind systems over the central Namib. Additionally the location of the available stations and the location of the cross-section are included. Also the main topographic features of the region as well as a part of the REMO grid at a horizontal resolution of 18x18 km are shown. The latter is used to demonstrate the number of grid boxes between the coast and the escarpment.

The analysis of the wind patterns at the station level as well as along the transect is mainly based on the frequency analysis of the different wind systems. As the wind direction of a specific component is not constant, but varies in a certain range, a wind direction interval of 50 degree was assigned to each of the four major wind systems introduced above (Table 6.2). For the purpose of better illustration, a representative colour code was assigned to each component, which is also listed in Table 6.2.

Table 6.2: Overview of the predominant local wind systems of the central Namib Desert. Note that the land breezes and berg wind events can only be distinguished via the temperature signal, but not through their wind characteristics.

Name	Shortname	Winddirection			Colorcode	Prozess
		Pred.	Pred. [degree]	Assigned Range [degree]		
Sea-Breeze	SB	SW	225	200 to 250	light-blue	thermal
Land-Breeze	LB	NE	45	20 to 70	brown	thermal
Plain-Mountain Winds	PMW	NNW	330	305 to 355	light-green	thermal
Mountain-Plain-Winds	MPW	ESE	115	90 to 140	khaki	thermal
Bergwinds	BW	NE	45	20 to 70	brown	synoptic

As a regional model is not intended to represent the climatic features at each single gridbox, the standard procedure when comparing model data to station data is to average the model output over a larger number of model grid boxes centred around the station. This procedure might work for cumulative records (e.g. precipitation) but cannot be applied for impulse data, as during the averaging process the signal might get blurred. To avoid this effect a representative gridbox for the greater region around the station was identified and analysed. For this purpose a multiple regression analysis was performed for the closest nine model grid boxes around the three stations. Finally the gridbox with the highest correlation coefficient was selected and further analysed.

For the frequency analysis of the wind direction a bin size of two degrees was assigned. In order to assess the diurnal as well as the seasonal cycle of the circulation activity, the frequency analysis was conducted on an hourly basis for the summer (December to January) as well as for the winter (June to August) season. For the analysis of the vertical structure of the lower atmosphere only six hourly data were available. Here only the mean wind system at a given time of the day and season was included in the analysis.

6.3 Evaluation of the simulated wind fields on different scales

6.3.1 Regional scale

A first validation of the simulated surface wind fields compared to ERA40 reanalysis data has already been provided in Chapter 3 (see Figure 3.3). There it has been shown, that REMO satisfactorily represents the near surface characteristics for both, the summer and the winter season. However, during the summer season REMO slightly overestimates the surface heat low and also simulates an increased inflow of moist maritime air into the domain. For the middle and upper troposphere the simulation quality of the model however has not been assessed. Figure 6.2 depicts the zonally averaged (20°E to 25°E) seasonal mean vertical cross-section of the zonal wind component. Compared to ERA40 data REMO simulates the position of the subtropical jet stream in both seasons very satisfactorily. Regarding the magnitude of the jet, a slightly too strong (up to about 5 m/s in the centre) jet is simulated by the model for both seasons. Furthermore, the distinctive north-south gradient in the mid-tropospheric (500hPa) geopotential height is ably captured by the model (Figure 6.3). Only over the heat-low and adjacent ocean regions the 500hPa layer is simulated slightly too high. Over mountainous regions however, the high-resolution REMO simulation shows notably more details in the 500hPa height than the coarse ERA40 data.

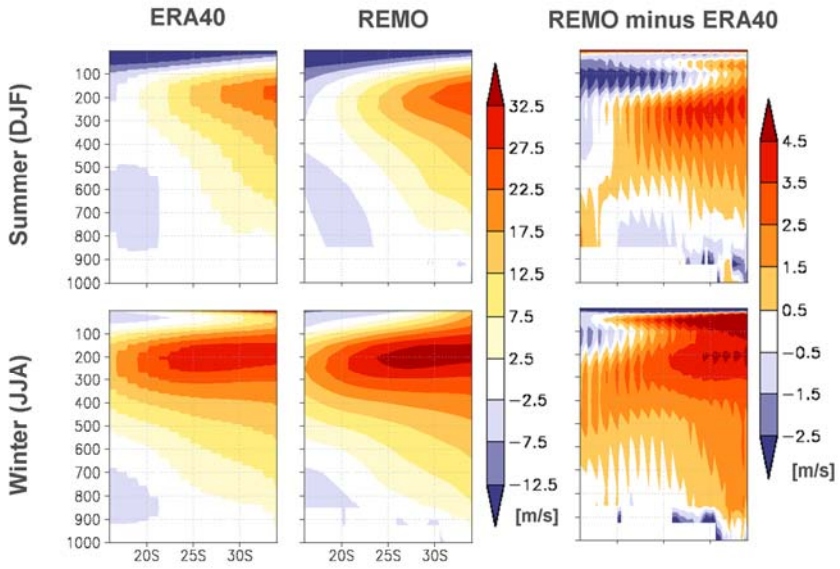

Figure 6.2: 30 year (1961-90) mean observed (ERA40; left) and simulated (right) vertical profile of the seasonal mean zonally averaged u wind component for summer (upper panels) and winter (lower panels). The respective differences between ERA40 and REMO are depicted in the right panels.

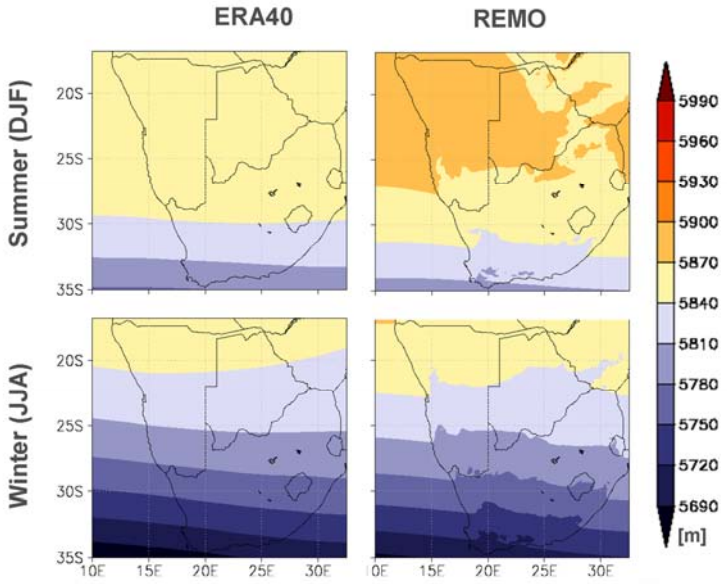

Figure 6.3: 30 year (1961-90) mean observed (ERA40; left) and simulated (right) the seasonal mean 500hPa geopotential height for summer (upper panels) and winter (lower panels).

6.3.2 Local scale

Based on hourly timeseries of observed and simulated wind data at each station a frequency distribution of the wind direction was generated for each season and each hour of the day. As a first step it was assessed whether the model was able to simulate the predominant local wind patterns. Hence the wind direction showing the highest frequency was selected at each hour. To not include outliers in the analysis a 10 degree running mean was applied to the frequency distribution previous to the selection process. Figure 6.4 shows the diurnal cycle of the predominant observed (black squares) and simulated (red circles) wind fields at each of the three stations. Also data taken from the literature (blue circles: Lindesay and Tyson, 1990; Lancaster et al., 1984) were included in the figure to account for local channelling effects. The coloured segments of the figure indicate the range of the respective wind systems as previously defined in Table 6.2. Sunrise and sunset are indicated with the orange lines. The observed seasonal and diurnal cycles are well captured by the model for the coastal and central Namib station. At the biased slope station the model does not agree with

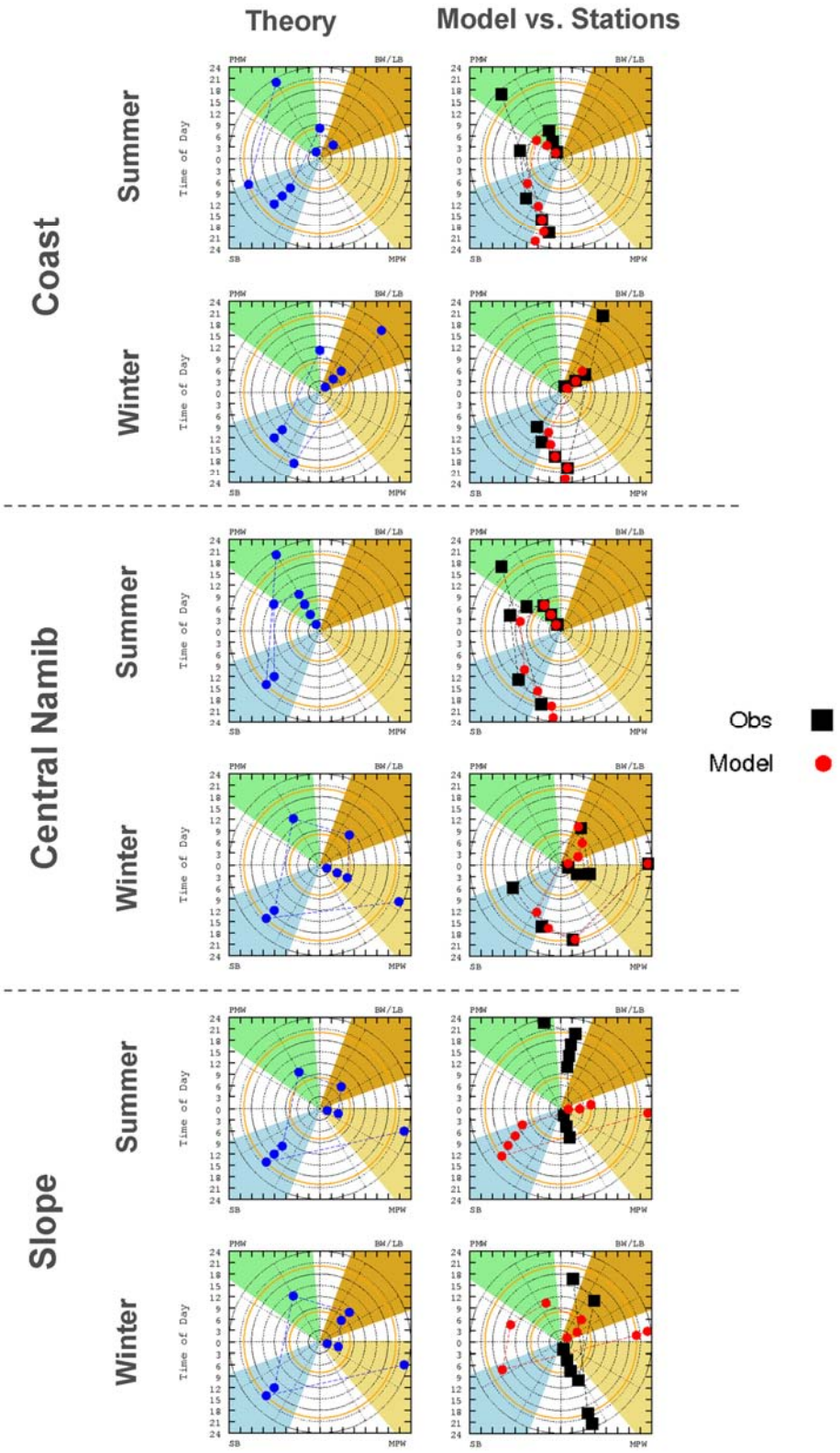

Figure 6.4: Diurnal cycle of predominant wind system for the summer and winter season at three different stations as derived from literature (left panels; blue), observed at the stations (right panels, black squares) and simulated with REMO (right panels; red circles). The orange circles represent the sunrise and sunset, respectively. The coloured areas in the polar diagrams represent the flow direction of the respective wind component (see Table 6.2).

observations. However, considering the diurnal and seasonal variations described in the literature the model is in good agreement for this station. Directly at the coast, the shift to the SB conditions during daytime is captured by the model. However, the night-time turn to PMW during summer and to LB during winter (indicated by the position of the outermost square and circle, respectively) seems to be delayed by the model, indicating a slower cooling of the land areas. Also further inland (central Namib) a delay in the summer season night-time turn from SBs to PMWs is visible in the model. Conversely, during the winter season, the night-time turn to MPWs is well captured by REMO, but a too strong north-easterly component develops during the second half of the night. At the slope of the escarpment, the model follows the idealized data taken from literature (Figure 6.4, lower left panels) rather closely.

In order to not only consider the position of the maximum frequency of the wind direction also the relative fraction of each wind component at a given hour of the day was included into the analysis. Even though the position of the maximum fits rather nicely to the observations, the fractional distributions of simulated and observed wind patterns slightly differ (Figure 6.5). One noteworthy feature seems to be that at all stations the SB component is simulated too intensively during summer. Also some deficiencies in the timing of the different features (e.g. the switch from SB to PMW during summer at the central Namib) can be identified (see above). For the coastal station it further can be noted that REMO does not simulate the clear SB/PMW wind pattern as observed during the summer season. Here the model shows a higher frequency of winds during the night time, which can not be assigned to one of the four schemes.

Additionally, the diurnal cycle of the wind magnitude is shown in Figure 6.5. REMO simulates the mean wind speed in surprisingly good agreement with the stations. This also includes the position of the diurnal peak magnitude, which apart from the coastal station, slightly shifts over the course of a year from around late afternoon (summer) to around midday (winter). When analysing the wind magnitudes of the different wind components REMO seems to have some slight deficiencies compared to the observations. However, the general tendencies like the intensification of SB winds in the afternoon and the higher magnitude of north north-westerly winds during the winter season (see also Section 6.5) are captured by the model.

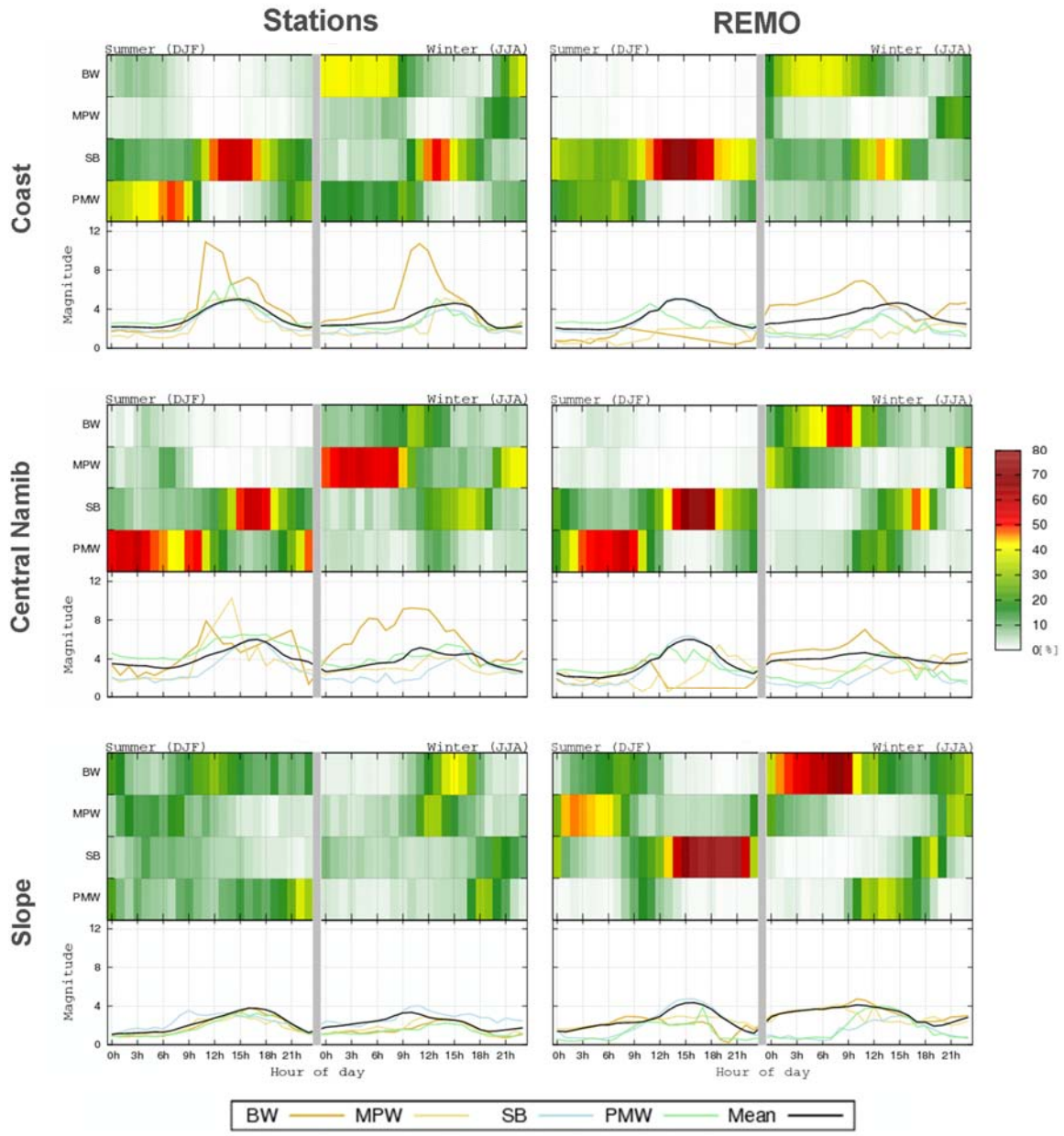

Figure 6.5: Diurnal cycle of the frequency of the respective wind components for the summer and winter season at three different stations as observed (left panels) and simulated with REMO (right panels).

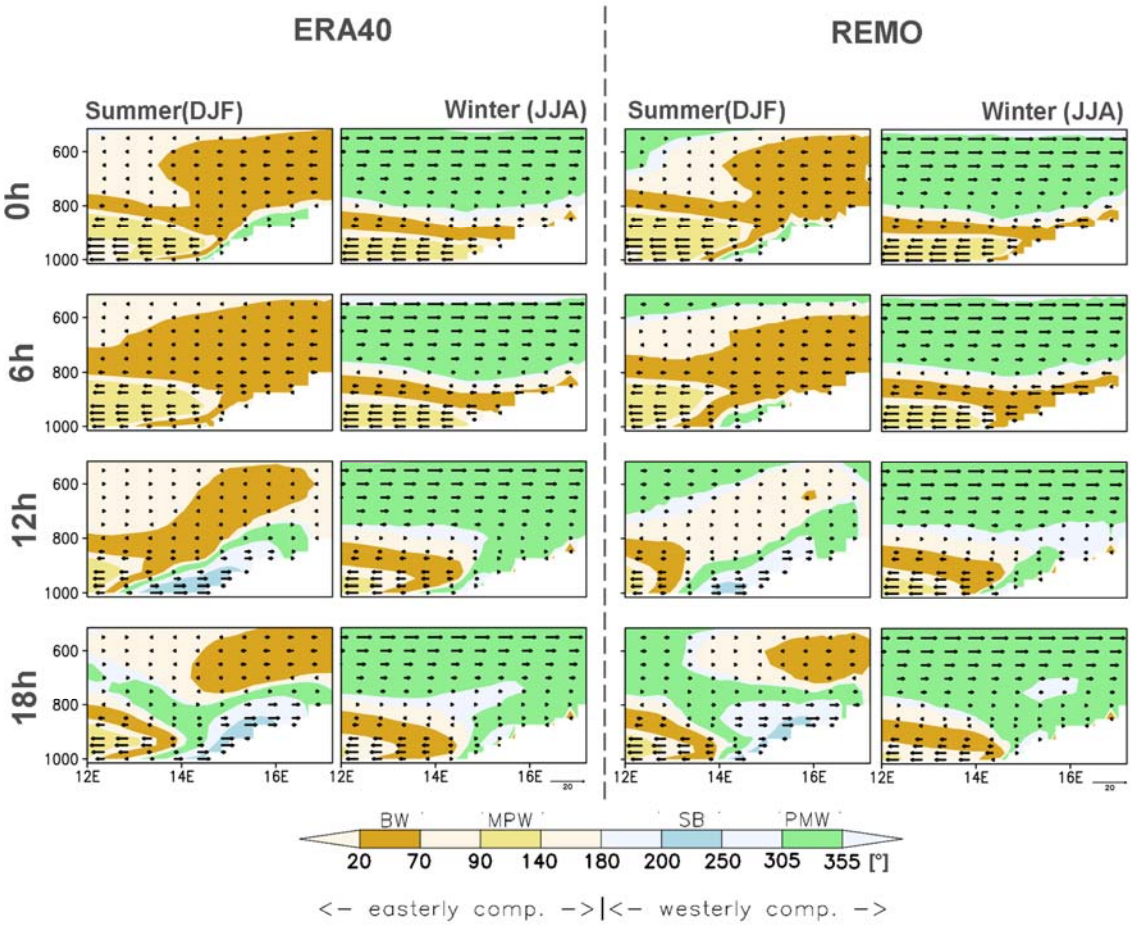

Figure 6.6: Diurnal cycle of a vertical profile of the mean flow direction (colours, direction of arrows) and magnitude (length of arrows) for the summer and winter season as observed (left panels; ERA40) and simulated with REMO (right panels).

Not only the horizontal but also the vertical extent of the different local wind systems undergo a notable diurnal and seasonal variation. These variations in the lower atmosphere as observed (ERA40) and simulated are shown in Figure 6.6 for a west-east transect through the central Namib. According to Lindesay and Tyson (1990), the summer condition close to the surface is defined mainly by westerly PMWs (indicated with the green coloured areas) and afternoon SB (blue colour) events. This westerly flow is overlain by easterly directed gradient flow. The vertical extent of the PMWs and SBs increases during the course of the day and reaches its maximum extent at about 1000 to 1500 m with the maximum SB activity in the late afternoon. These features can be seen in the ERA40 data as well as in the REMO hindcast simulation. Especially the inland movement of the SBs during the afternoon can convincingly be identified. In the REMO simulation however, the SB seems to be slightly shallower than in ERA40.

Additionally it can be seen that during the summer season the PMWs are interrupted in ERA40 in the early morning, which is in contrast to observations (Lindesay and Tyson, 1990). Even the PMWs at the surface can be infrequently disrupted by shallow MPWs (brown colour), they still should be persistent in the upper part of the PBL (Lindesay and Tyson, 1990). During winter the lower troposphere up to about 2000m is dominated by easterly and north-easterly wind components. On top of this westerly gradient winds predominate. During late afternoon the prevailing easterly flow is interrupted by the development of a shallow SB component, therefore the wind turns to westerly conditions. The major flows during the winter season are well represented by REMO. However, the surface winds over land seem to have a too strong north-easterly component, which can be also seen in the Figures 6.4 and 6.5.

6.4 Projection of future regional and local circulation characteristics

In Chapter 4 it was shown that REMO projects a strong warming over the whole southern African region with a maximum warming in the interior, therefore enhancing the land sea temperature contrast. This non-uniform heating of air masses might involve the potential for an increased circulation activity (especially when thermally induced) over the region in the future. On the other hand moisture availability over the region is substantially reduced, which potentially reduces the availability of kinetic energy and therefore rather dampens the circulation activity. To estimate which of the two effects dominate in the REMO projection a detailed analysis of projected future circulation activities on a regional as well as on a local scale will be provided.

6.4.1 Regional scale

Regarding the mean sea level pressure, the major patterns are projected to persist into the future. Overall, the mean sea level pressure (MSLP) is slightly reduced over the central parts of the southern African land areas in both seasons. This leads to a small intensification of the summer heat low and a slight weakening of the winter high pressure cell. Over the ocean a moderate amplification of the high pressure systems is visible. In terms of near surface wind fields the change in MSLP translates into almost unchanged patterns over land. For the summer season however, REMO projects an

amplification of the northward flow offshore the Namibian coastline (Figure 6.7; upper panels). During winter a southward shift of the westerly flow offshore the cape region can be noted. This shift is a common feature of most models assessed within the IPCC AR4 (Christensen et al., 2007) and causes a decrease in simulated rainfall in the models over the south-western part of the southern African region during that time of the year.

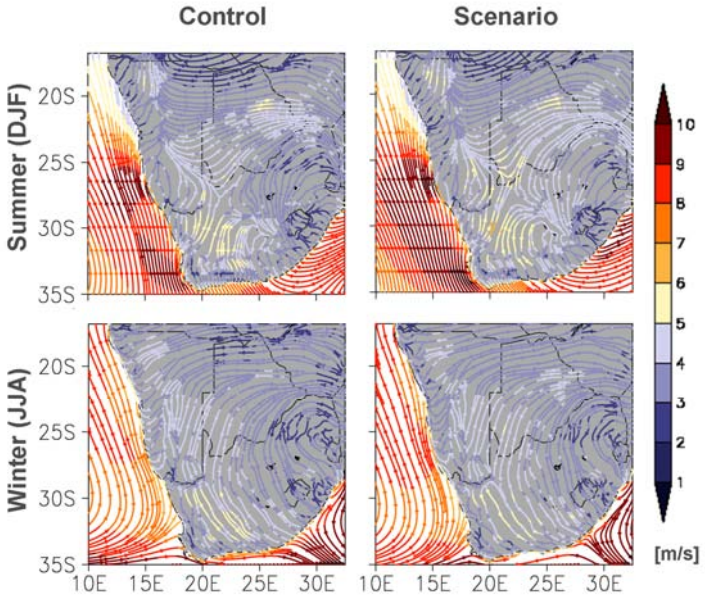

Figure 6.7: Simulated seasonal mean 10m wind fields (streamlines) and wind speed (colours) for summer (upper panels) and winter (lower panels) as mean over the control (1961 - 1990, left panels) and the scenario (2071 - 2100; right panels) period.

Connected to the projected increase in the air temperature is a general increase in the 500 hPa geopotential height (not shown) which is inline with the general expansion of the lower atmosphere as reported in the IPCC AR4 (Meehl et al., 2007) for regions that substantially heat up. Upper troposphere circulation patterns remain rather unchanged. Westerly flow in the range of the subtropical jet-stream is projected to be slightly increased in its centre. Also an expansion towards the south and towards higher altitudes can be seen in the REMO simulations (Figure 6.8).

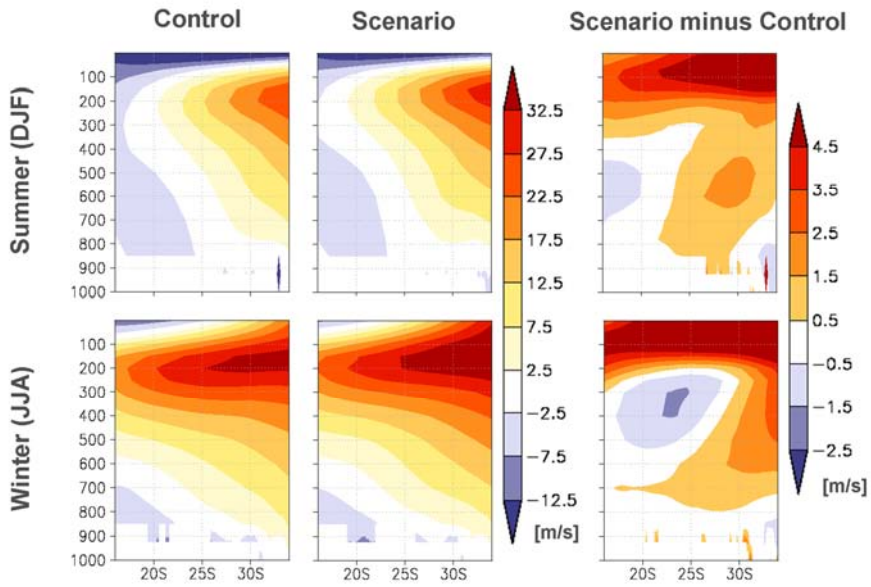

Figure 6.8: Simulated vertical profile of the seasonal mean zonally averaged zonal wind component for summer (upper panels) and winter (lower panels) as mean over the (1961 - 1990; left panels) and the scenario (2071 - 2100; right panels) period.

6.4.2 Local scale

The analysis of the diurnal cycle of the peak wind direction for the control and the scenario period revealed for all three stations that the predominant circulation is projected to be constant under future climate change conditions. This finding includes both, the diurnal cycle of the wind fields as well as the characteristic wind direction that was assigned to each component. However considering the fractional distribution of the different components some systematic changes can be identified (Figure 6.9). For the summer season a general increase in the SB occurrence is projected for all times of the day. Especially at the coastal station a noticeable shift from PMWs to SB conditions is projected, connected to a longer duration of SB events. For the winter season a moderate increase in SB conditions is also visible during the afternoon. Especially at the coast and also in the central Namib a bipolar SB change is projected, indicating a slight shift of the SB to an earlier time of the day.

Mean wind speed is projected to stay rather constant. Looking at the wind speed of the different systems some pronounced changes are projected for the easterly winds (MPWs, berg winds) during summer. However as they occur only at a few occasions, these changes do not influence the mean wind speed.

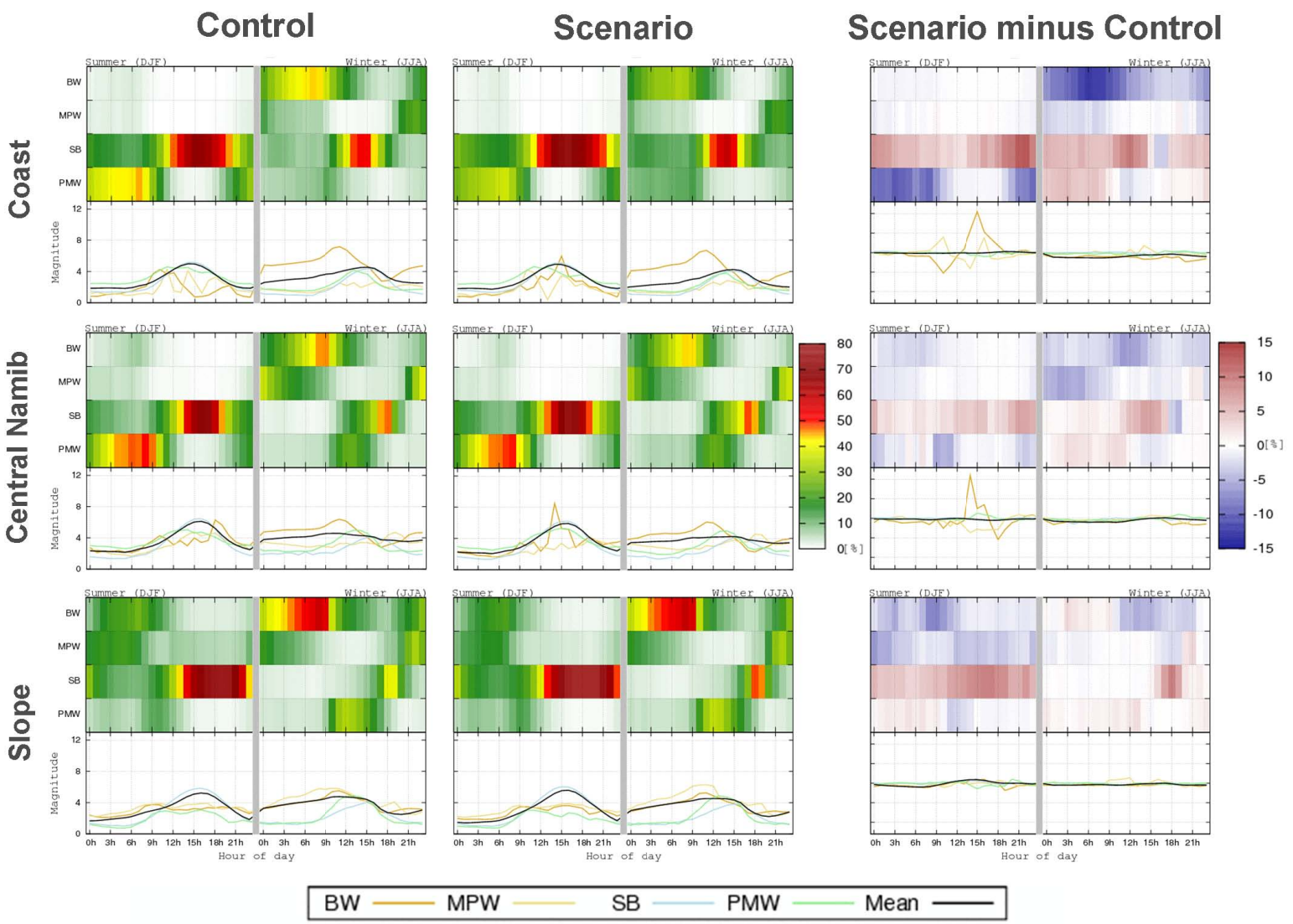

Figure 6.9: Diurnal cycle of the frequency of the respective wind component for the summer and winter season at three different stations as simulated with REMO for the control (1961 to 1990; left panels) and scenario (2071 to 2100; central panels) period. The respective differences between the scenario and the control period are depicted in the right panels.

Figure 6.10 depicts the simulated mean winds for the west - east cross section for the control and scenario period. Even though a warming of the lower atmosphere may be expected to lead to an increased vertical extend of the SB flow only a minor change is projected towards the 21st century. With respect to changes in the horizontal extent, westerly PMWs and SB flows are expected to slightly penetrate further inland during the summer season. Mean summer flows in the middle troposphere are projected to slightly turn towards westerly direction. The situation during the winter season remains unchanged.

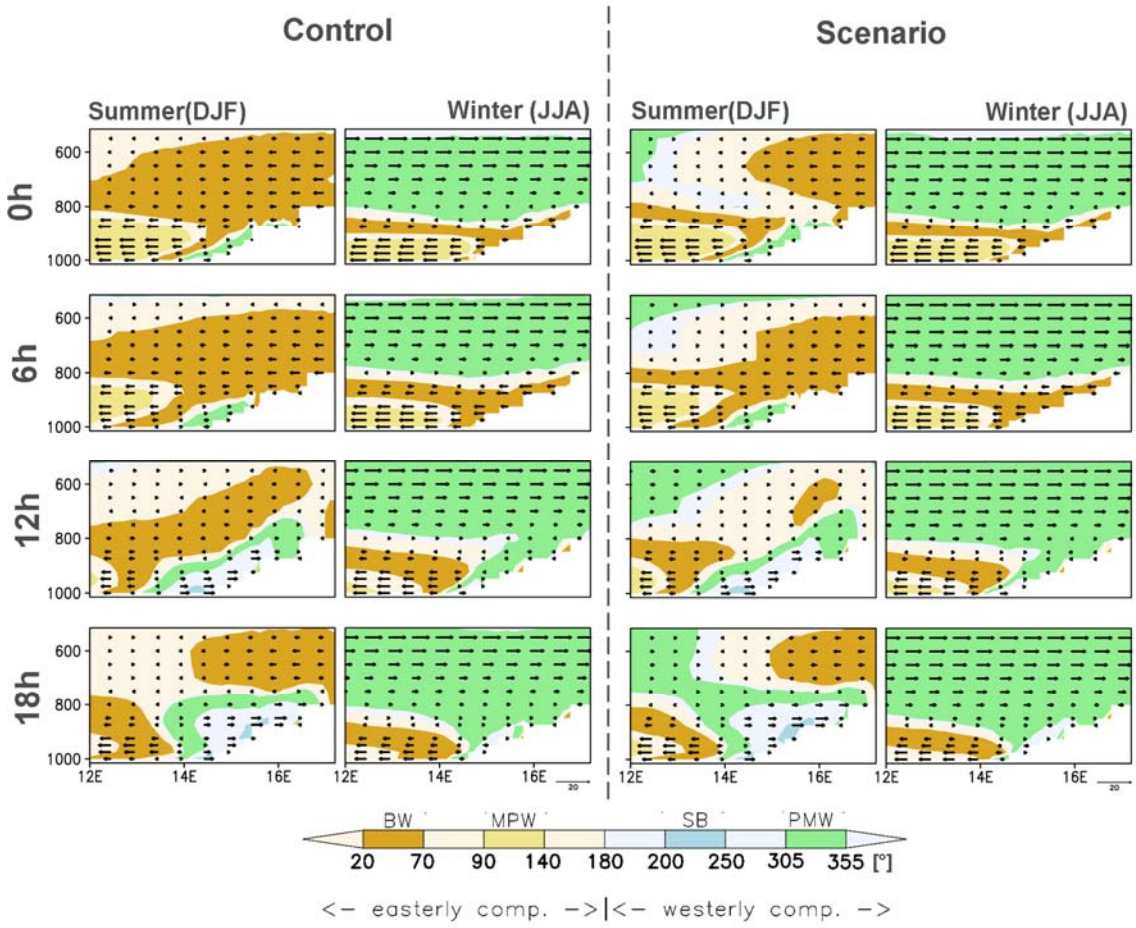

Figure 6.10: Diurnal cycle of a vertical profile of the mean flow direction (colours, direction of arrows) and magnitude (length of arrows) for the summer and winter season for the control (1961 - 1990; left panels) and the scenario (2071 - 2100; right panels) period.

6.5 Simulation of synoptic scale disturbances – berg winds

This section provides an analysis of the simulation of synoptically induced berg wind-events, which predominantly occur during the winter season. Both, the hindcast simulation as well as the transient climate projection were included in the analysis. In an initial step - to assess the quality of the simulation of berg winds - the frequency analysis was applied to the strongest one percent of hourly wind records (Figure 6.11). This procedure was motivated by the fact that high magnitude winds over the region are usually connected to north north-easterly flow (see Figure 6.5). As expected, the observations reveal that the strongest winds occurring in the region are mainly restricted to wintertime north north-easterly winds, which correspond to the berg wind characteristics. For the coastal station, the distribution of heavy winds is well captured by the model. Regarding the central Namib station, the high-magnitude winds are not solely restricted to the winter season but also occur during spring and early summer and can partly also be assigned to SB conditions. Also the simulated 99th percentile of hourly wind speed is substantially lower at the central Namib station compared to the one observed (see Figure 6.11) whereas at the other stations the simulated 99th percentile of wind speeds matches rather closely. For the station on the slope of the escarpment the model differs substantially from the station as expected. Also at this station strong winds can not solely be assigned to north north-easterly flow during wintertime, but also occur during spring and early summer from the easterly direction.

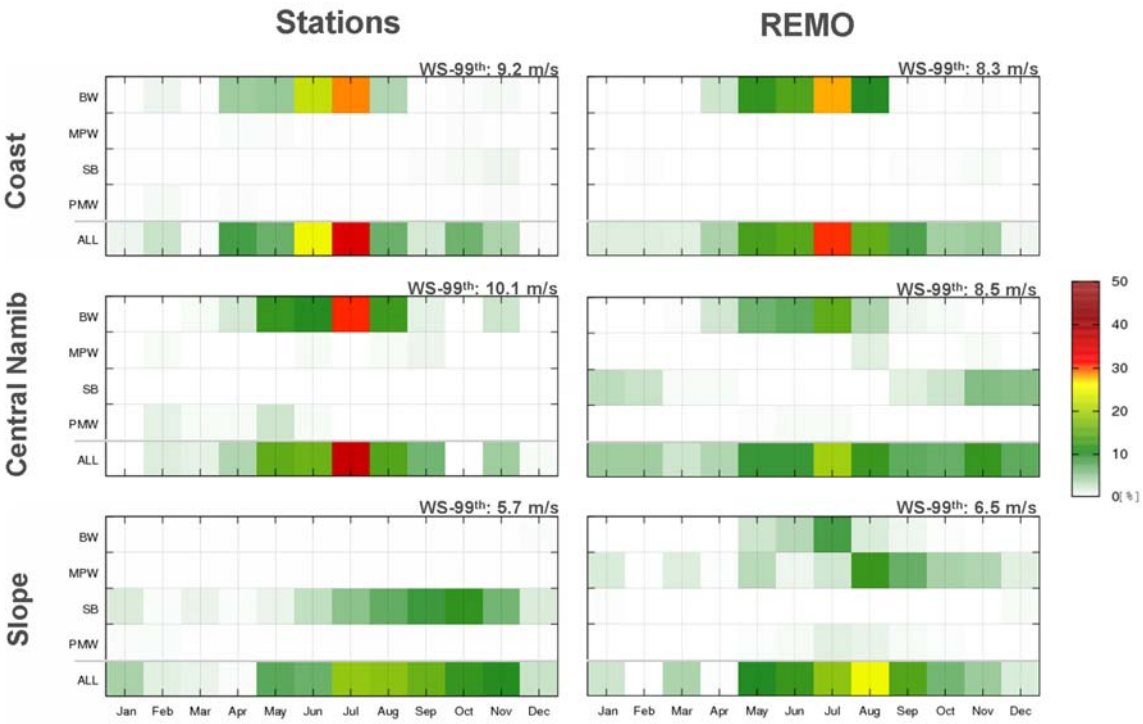

Figure 6.11: Diurnal cycle of the frequency of the strongest one percent of respective wind component for the summer and winter season at three different stations as observed (left panels) and simulated with REMO (right panels). The respective wind speed at the 99th percentile is given for each station at the top right corner of the panel.

To quantify the mean number of berg wind events per year not only the high-magnitude winds can be considered, as this is not a prerequisite of berg winds. A unique characteristic of berg wind events however is a dramatic increase in air temperature (e.g. Tyson, 1964) caused by regional scale subsidence of dry air. Therefore the change in the daily maximum temperature was included in the analysis. For the coastal station the temperature observations reveal an above average winter temperature of about 12K under the north north-easterly high-magnitude winds (as shown above). Even though the temperature increase connected to high-magnitude berg winds is slightly lower in the model (about 7K), the deviation from the mean is statistically significant (on a 99.9 confidence interval using t-statistics). To prove that this strong temperature increase in the model is due to the subsidence of air originating from the plateau region in the interior, the regional scale berg wind temperature anomaly is shown in Figure 6.12. While in the interior the daily maximum temperature is unchanged or slightly lower, a significant increase in coastal daily maximum temperature is visible for high-magnitude coastal berg wind events.

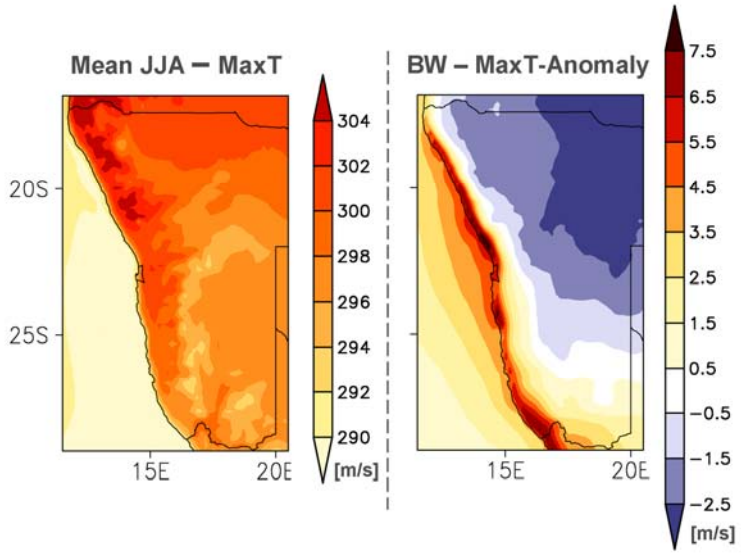

Figure 6.12: Simulated mean daily maximum temperature for the winter season (left) and the anomaly of daily maximum temperature during berg wind events.

Based on the finding that REMO can reproduce the extreme temperatures involved in the berg wind process several criteria to quantify the simulated mean number of days with berg wind events have been defined. Only days that show the following criteria have been included in the analyses. These criteria are as follows:

i.) Winds during the morning hours have to be predominantly from north north-westerly direction (between 20° and 70° – see Table 6.2).

ii.) A substantial rise in maximum temperature compared to the previous day has to occur. As a threshold for this increase two times the standard deviation of the fluctuations of daily maximum temperature was chosen.

iii.) If the berg wind already occurred on the previous day and present wind characteristics follow the requirements defined above, maximum temperature has not to rise drastically, but should not be substantially cooler than the one of the previous day. Therefore the possible cooling rate was set to be no more than half of the standard deviation of the fluctuations of daily maximum temperature.

As the available observational datasets are affected by several data gaps, a quantitative analysis was only possible for the REMO simulations which, however, can be at least compared to available literature data. Following these definitions the model simulates on average 22 berg wind events per year when forced with ERA40 data for the coastal station, at which berg winds events are supposed to be most prominent. In the ECHAM5/MPIOM forced control simulation about 15 days a year with berg wind conditions are simulated. Approximately the same number is projected for the future period (Table 6.3). Even though the absolute number of berg wind events deviates significantly from the literature records (~50 events per year), REMO captures the seasonality of the berg wind occurrence, which shows a peak of events during the winter season. Also noteworthy is the substantial interannual variability in simulated berg wind-events which is also listed in Table 6.3. This variability is well simulated in the hindcast simulation. However, it has to be noted that the ECHAM5/MPIOM forced climate change simulation seems to produce a too large interannual variability. With respect to the air temperature during berg wind events a significant increase on the order of about 4 K is projected for the future period. This increase is larger than the projected mean temperature increase for the coast, but corresponds to the warming further inland (~ 2.5 K, see Chapter 4; Figure 4.11). This finding indicates that during berg wind events air is transported from inland areas towards the coastal plains. Mean wind speed is projected to stay rather constant at ~5m/s. Compared to the mean wind speed for the coastal station (Figures 6.5 and 6.9) berg winds have, as expected, notably stronger wind speeds than the thermally induced wind systems.

Table 6.3: Overview of the mean number of berg wind events per year at the coastal region as simulated with REMO in the hindcast (1998 - 2007) as well as for the control (1961 - 1990) and scenario (2071 - 2100) simulation. Additional the interannual and the seasonal variations are included.

	Annual			Seasonal				Mean berg wind		Nr. of BW-events solely based on wind direction
	Mean	Max	Min	DJF	MAM	JJA	SON	Temperature [K]	Wind Speed [m/s]	
Hindcast	22	28	12	0	5	15	1	305.7	4.9	45
Control	15	33	2	0	3	10	2	307.7	5.0	50
Scenario	13	30	1	0	2	10	1	311.8	5.2	30

6.6 Discussion

In Chapter 3 it was speculated that the overestimation of the summer heat low in the REMO simulation in comparison to ERA40 data could be an explanation for the observed wet bias of the model, as this overestimation is might connected to a larger inflow from moist maritime air masses. The increased inflow of moisture into the south-eastern part of the domain when compared to the forcing model is a feature, which was already been observed before when applying a RCM over the region (Hudson & Jones, 2002). The overestimation of the heat low could also lead to an increased convective activity in the model over this region. An indication for this can be the difference in 500 hPa height, which REMO tends to simulate at a higher altitude than observed over that region. Overall, however, the model shows a rather good performance in representing the regional scale circulation activity.

On the local scale the model satisfactorily represents the circulation patterns. Especially the SB onset and frequency is well captured by REMO. A slightly lower simulation skill is connected to the PMW and MPW systems, which can have two reasons. On the one hand the forcing for these systems lies partly in the topography of the region. Hence, a deficit could arise from the simplified topography in the model. As the model assumes a constant topography for each of the 18x18 km gridboxes the details can not be represented. To assess if this effect is important, a model simulation at a higher horizontal resolution could be conducted for the region. One the other hand, the PMW – MPW system strongly depends on temperature contrast between the plains and the adjacent hinterland (Lindesay and Tyson, 1990). However, as REMO simulates a too warm temperature for the plain area (see Chapter 3), this gradient is reduced in the model.

The analysis of the berg wind events further revealed that on the synoptic scale the model is strongly determined by the large scale forcing provided through the lateral boundary conditions. While on the local scale almost no change between the hindcast and the control runs is visible, indicating a large degree of independence of the regional model from the large scale forcing, a substantial deviation in the mean and especially in the interannual variability of synoptically induced berg wind events is notable. To relate this difference of simulated berg winds to the large scale forcing events can be justified,

even though the seasonal mean circulation patterns of the hindcast and control simulation agree rather well, with a slightly increased high pressure system in the control simulation (Figure 6.13; upper panels). As the berg wind events are mainly linked to the infrequent occurrence of a strong pressure gradient between the coast and the interior (Tyson, 1964) the short-term position or extent of the winter time high pressure system can deviate substantially in the hindcast and control simulation without being present in the mean circulation pattern. An indication for this can be found when analysing the standard deviation of daily wintertime mean sea level pressure which is - especially over the central parts of the domain - notably larger in the control simulation (Figure 6.13; central panels). This argumentation is supported by the anomaly of the mean sea level pressure of berg wind events, which shows a generally increased pressure over land for both the hindcast as well as the control simulation (Figure 6.13; lower panels).

Additionally it has to be mentioned that the absolute number of berg wind events simulated by the model also depends on the previously defined criteria. Especially the temperature criteria seem to have quite a strong impact on the mean number of berg wind events. If one would only consider the wind direction, berg wind conditions would be simulated to occur much more frequently at a rate of ~50 events per year (Table 6.3). This frequency would exactly correspond to the published number of events (e.g. Tyson, 1964). Also the projected changes would be substantially larger, when only the wind direction would be considered. This feature can also be seen in Figure 6.9. However, the temperature criterion is an important prerequisite of berg wind events and has to be considered in the analysis. Nevertheless, the predefined temperature threshold used to identify berg wind events is not fixed and therefore could have a notable impact on the quantification of berg wind events. If for example the temperature threshold would only be set to one standard deviation of the daily temperature variations the number of berg wind events would increase by about 20% for both the hindcast and the transient climate change simulations. However, as no clear definition for the magnitude of the sharp increase in temperature is given in the literature the two standard deviation threshold was kept, as this can be used as an approximation for a significant deviation at the 95^{th} confidence interval.

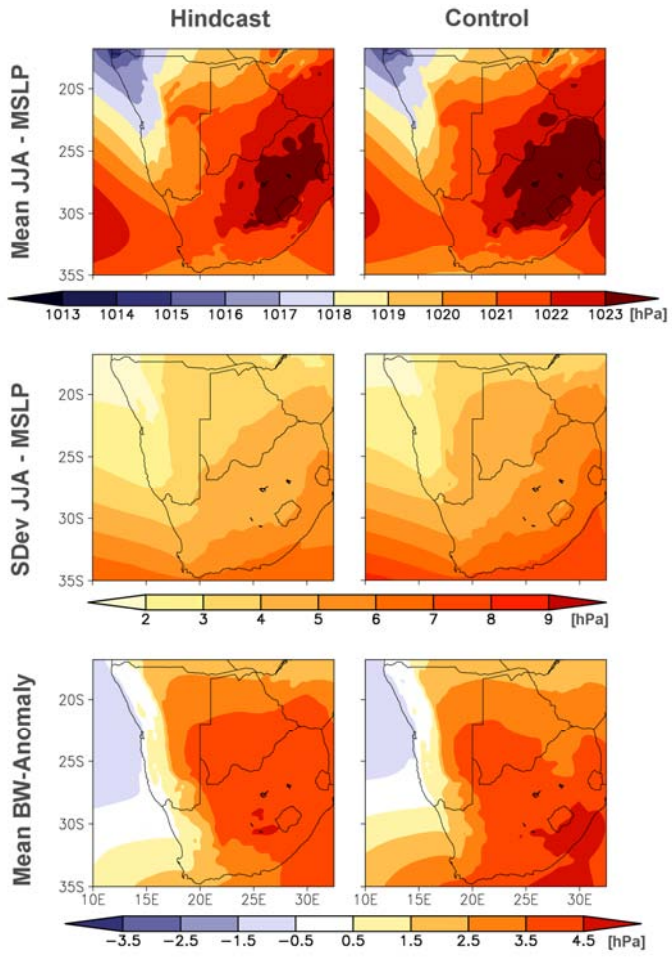

Figure 6.13: Simulated mean sea level pressure (upper panels), standard deviation of daily records of mean sea level pressure (central panels) as well as the anomaly of mean seas level pressure during berg wind events (lower panels) during the winter season. The hindcast simulation (1998 – 2007) is depicted in the left panels, the control (1961 – 1990) simulation in the right panels.

Concerning the projected changes of the middle and upper troposphere, REMO is inline with changes already reported in previous studies. An example for this can be the projected positive anomalies in upper troposphere zonal winds (Figure 6.8) that have already been shown before (e.g. Kushner et al., 2001). This increase can mainly be associated to different warming patterns for the tropics and the southern ocean, which results in large scale changes in pressure gradients. However due to the position of the simulation domain, which tackles the jet only at its southernmost border, the study can not deliver a comprehensive analyses of the possible future development of subtropical jet streams.

The fact that REMO projects a persistent circulation pattern during the 21st century at the local scale may seem surprising at first glance. Especially when recalling the projected increase in near surface temperature which is substantially larger over land than over ocean (Chapter 4), the weak response in the thermally induced winds seems to be contradictory. However, having a closer look at the simulated mean surface temperature along the west – east transect for the control and the scenario period reveals that even though the overall temperature level is projected to be higher in the future, the gradient between ocean and land temperature remains constant in the coastal areas (Figure 6.14). Only further inland an increased ocean land temperature gradient is visible. The same also holds for the temperature gradient between the coastal plains and the adjacent regions further inland.

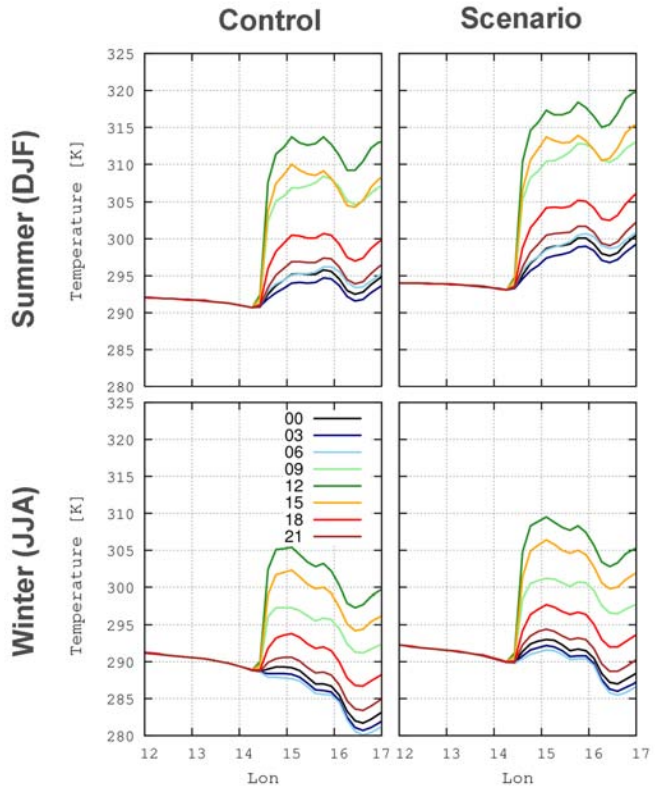

Figure 6.14: Simulated mean diurnal cycle of the surface temperature along the west east transect depicted in Figure 6.1 for the summer (DJF; upper panels) and the winter (JJA, lower panels) season over the control (1961 – 1990; left panels) and the scenario (2071 – 2100; right panels) period.

Regarding future changes of the regional to local scale near surface circulation activity one clearly has to keep in mind that in the conducted projection the ocean is not directly

coupled to REMO (see Chapters 4 and 5 and Haensler et al., 2010d). A change in the SST initiated by changed near surface flows would certainly initiate a feedback onto the circulation itself. The response in the circulation characteristics would especially occur over regions, which are strongly determined by large ocean – land temperature contrasts like the central Namib region. The current study of future changes along this region therefore might be seen as an initial analysis of the response of the circulation to a strong (but regionally diverse) climate change signal, but more work has to be dedicated to this topic in the future. However, even here some shortcomings in the setup of this regional climate change projection remain; the findings of this study clearly indicate that REMO is suitable to capture both the regional as well as the local scale circulation features over the south-western African region.

6.7 Summary and Conclusions

In this chapter a comprehensive analysis of the simulation of thermo-topographically induced wind systems over the central Namib was provided. It was shown, that the regional climate model REMO captures the diurnal as well as the seasonal wind characteristics along a west-east transect through the central Namib Desert. Also the vertical extent of the different systems is ably simulated by the model. Deficits however remain in the simulation of berg wind events which are defined as infrequent but noteworthy synoptic scale disturbances. Here REMO tends to simulate a too low frequency for the central Namib station.

With respect to the future development of the local wind systems along the coastal regions of south-western Africa, REMO projected the circulation to remain rather constant throughout the 21st century. This finding can mainly be linked to the local scale temperature gradient between the ocean and the adjacent hinterland area, which is projected to stay unchanged, even though the overall temperature level is increased. However, it has to be noted that the ocean is not fully coupled to the atmosphere in the current simulations. Therefore the projected absence of a clear shift in the local circulation has to be carefully interpreted – especially when considering the projected increase of the regional scale flow off the coast line, which drives the Benguela upwelling system.

Chapter 7

Concluding remarks

7.1 Summary

In this thesis the regional climate model REMO was applied to assess the impact of climate change on the coastal climate of south-western Africa. Within this work, several regional climate simulations have been conducted at roughly 50 and 18 km grid spacing. While analyzing the simulations a focus was given to the high-resolution 18 km simulations. These simulations comprise a hindcast simulation to validate the model over the region, a 150 year transient climate change projection as well as three time-slice simulations with a REMO version that includes fog diagnostics. The conducted transient climate change projection was the first regional climate projection ever conducted at such a high horizontal resolution.

On the basis of this suite of simulations it was possible to analyze the impact of climate change on the predominant climatic features of the southern African region that occur on different spatial scales. Apart from a regional scale assessment of future climate change also mesoscale features like the west coast fog and even local scale processes as the thermo-topographically induced wind system over the central Namib could be studied for the first time with a regional climate model. Related to these processes on different spatial scales is also a change in the temporal scale. Whereas the regional scale climate change analysis was based on seasonal and interannual time scales, changes of the diurnal cycle had to be included into the assessment of the local scale wind systems.

In the introductory chapter of this thesis several key research questions have been outlined. Based on the analyses conducted within this work the major findings with respect to these focal points can be concluded as follows:

i) In Chapter 3 it was shown that REMO well reproduces the main climatic features of the southern African region. The model captures the specific rainfall patterns with the strong seasonality as well as the large interannual variability. Therefore it can be concluded that the model is suitable for climate studies over the region, even though some coastal warm bias remains.

ii) In Chapter 3 it could further be shown that the rainfall in the winter rainfall region around the Cape region is substantially better captured by REMO than by the forcing ERA40 reanalysis data. As rain formation over this region mainly depends on the advection of moisture and uplifting along the escarpment, the added value in the rain simulation could be attributed to a better representation of orographic rain due to the higher model resolution.

iii) A method to account for the mismatch of the simulated SST of coupled global atmosphere ocean models over the Benguela upwelling system was presented in Chapter 4. Based on a combination of SST - correction using the anomaly approach and the application of the double nesting method, the previously existing wet bias could be substantially reduced without drastically changing the large scale forcing. As the warm bias over the upwelling region seems to be a general feature of coupled atmosphere ocean GCMs, this method was proposed to be used as the standard method for the setup of regional climate models over the region.

iv) The climate change signal projected by the REMO model was also presented in Chapter 4. Compared to the forcing global model, REMO simulates a stronger warming especially towards the end of this century. Also the projected drying is more pronounced in the RCM than in the GCM.

v) The simulation of west coast fog was presented in Chapter 5. Even though it was only possible to implement a very basic fog diagnostic scheme into the model, the comparison to satellite data led to reasonable results. Especially the temporal patterns could be adequately simulated by the model. Regarding the future fog occurrence REMO projected a general decrease in inland fog but a slight increase in coastal wintertime fog.

vi) A detailed study on the simulation of the thermo-topographically induced local wind systems of the central Namib region was presented in Chapter 6. It could be shown that the major local scale wind characteristics are well represented by model. This finding comprises both, the seasonal as well as the diurnal cycle of the wind characteristics.

In summary this thesis showed that the REMO model ably represented the regions climate features and therefore proved to be used for regional climate modeling studies over the southern African region. Especially the high horizontal resolution of the conducted simulations allowed studying some regional scale important features that can not be resolved in coarse scale global models. Also a clear added value in the simulation of seasonal rainfall could be assigned. The latter is especially important when climate model data is used as input for impact assessment studies.

7.2 Outlook

This study comprises a first analysis of high-resolution climate simulations over the southern African region, however, much work still needs to be done in the future in this field. The main aspect to be mentioned here is that the number of available regional scale high-resolution climate simulations has to be significantly increased. Only with an ensemble of high-resolution climate change projections a robust analysis of the magnitude of future climate change can be established. A first attempt leading in this

direction is the currently ongoing CORDEX (COordinated Regional climate Downscaling EXperiment) activity. Here a multi-model ensemble of high-resolution climate change projections will be established for the entire African continent. On the basis of this multi-model ensemble an identification of the uncertainty involved in the projected climate change signal will be possible.

The CORDEX activity can further be used to identify common model errors. An example of this can be the warm bias of REMO over some parts of the region, which was identified in Chapter 3. A first analysis of the CORDEX Africa hindcast simulations (Nikuli and Jones, 2010) showed that all applied RCMs, as well as the ERAinterím reanalysis dataset, suffer from this warm bias along the southern African upwelling region. A recent study by Jacob et al. (in preparation) showed that a coastal warm bias in REMO is also visible for all major coastal upwelling regions of the globe. Currently it can only be speculated on the origin of the bias in the models. As an initial step it is however recommended to carefully reassess the simulation of stratiform clouds in the models but also include the uncertainty of the observational datasets into the analysis.

To improve regional scale projections over the southern African region not only weaknesses in the regional models have to be removed, but also methods have to be developed to cope with shortcomings of the forcing global models. A good example for this is the Benguela upwelling which can not be simulated by the available coupled atmosphere ocean GCMs. In the current work a static method for the SST correction was applied. However, a fully coupled regional scale atmosphere ocean model should be employed to also include feedbacks between the atmosphere and the ocean into the system. The focus thereby should be on the realistic simulation of the mesoscale upwelling regions. As they are mainly induced through near surface wind fields along the coast line the horizontal resolution of the model has to be chosen in a way that the coastal topography is sufficiently represented.

A better simulation of the upwelling regions would also have a positive impact on the simulation of the west coast fog. In the initial study on fog modeling presented in Chapter 5, it was shown that REMO can capture the major fog patterns along the coastal regions. However for further studies a more comprehensive fog diagnostic scheme

should be considered. This scheme should include the droplet number concentration (Nd) as several studies have shown (e.g. Gultepe et al., 2007) that this improves the fog simulation. To include such a scheme into REMO, the model's Nd however has to be changed from a static field to a prognostic variable. This effort is currently undertaken by an ongoing PhD work.

For the simulation of climatic features occurring on a scale of tens to a few hundred kilometers (as it was done within this work) a very high horizontal and vertical model resolution is needed. Especially the simulation of the fog patterns and the simulation of the local thermo-topographically induced wind systems require a sufficient representation of the boundary layer processes in the model. To assess if the simulation quality of these systems improves when using a better resolved boundary layer, a model simulation with a very high resolution in the lower atmosphere should be initiated.

Most of the above mentioned steps to improve regional scale simulations over the southern African region do require a vast amount of computational resources. In view of the rapid technological development during the past few years – especially with respect to massive parallel processing – it should be possible to tackle all of the listed shortcomings within the coming years.

Acknowledgements

First of all, I would like to thank Stefan Hagemann and Daniela Jacob for the supervision of this PhD thesis. Throughout the whole time of my thesis they were available for discussing striking problems and helped a lot to keep on track. They also provided the money for this project, as well as for many informative and helpful meetings and conferences that I could attend throughout the PhD.

I am further thankful to Martin Claußen, as my panel chair, who provided some very clear and fruitful comments during the panel meetings.

I also would like to thank the International Max Planck Research School on Earth System Modelling. It has been a great pleasure to meet so many fellow students from all over the world. Many thanks go to Antje Weitz and Cornelia Kampmann for their support throughout the PhD.

I appreciate the support of Jan Cermak and the Gobabeb Training and Research Centre, for providing me with satellite and station based fog observations, respectively. I further thank my colleagues from the BIOTA South project (especially Norbert Jürgens and Ute Schmiedel) for providing the BIOTA station observations.

A very big thank you goes to my colleagues from the Terrestrial Hydrology Group and the Regional Modelling Group at the Max Planck Institute for Meteorology. At all times, I greatly enjoyed the friendly, cooperative and inspiring atmosphere in the two groups.

My office mates during the last years: Tanja Blome, Fahad Saeed and Tobias Stacke. I would like to thank you for the lively and excellent working atmosphere with a lot of discussions, which not always were about climate modelling.

My former colleague Jan Härter not only shared his knowledge in statistics with me, but also reviewed most parts of this thesis. Thank you very much for your help.

Last but not least I would like to thank my family and friends for their support. My deepest and warmest gratitude I would like to address to Theresa - thank you for being with me.

Bibliography

Arnell, N. W., Hudson, D. A. and Jones, R. G. (2003): Climate change scenarios from a regional climate model: Estimating change in runoff in southern Africa, *Journal Of Geophysical Research-Atmospheres* **108**(D16), 4519.

Ashfaq, M., Skinner, C. and Diffenbaugh, N. (2010): Influence of SST biases on future climate change projections, *Climate Dynamics* , Springer Berlin / Heidelberg, 1--17.

Bonnardot V., (2002): Diurnal Wind, Relative Humidity and Temperature in the Stellenbosch-Groot Drakenstein Wine-growing Area, *S. Afr. J. Enol. Vitic.* **23**, 62--71.

Bonnardot, V., Planchon, O. and Cautenet, S. (2005): Sea breeze development under an offshore synoptic wind in the South-Western Cape and implications for the Stellenbosch wine-producing area, *Theoretical and Applied Climatology* **81**(3), 203--218.

Bott, A. and Trautmann, T. (2002): PAFOG - a new efficient forecast model of radiation fog and low-level stratiform clouds, *Atmospheric Research* **64**(1-4), 191--203.

Cermak, J. (2010): Low clouds and fog along the south-western African coast - satellite based retrival and spatial patterns, *Atmospheric Reseach.* **Submitted**.

Cermak, J. and Bendix, J. (2008): A novel approach to fog/low stratus detection using Meteosat 8 data, *Atmospheric Research* **87**(3-4), 279--292.

Cermak J., Bendix J. and Dobbermann M. (2008): FMet - An Integrated Framework for Meteosat Data Processing for Operational Scientific Applications, *Computers and Geosciences* **34**(11): 1638--1644.

Christensen, J. and Christensen, O. (2007): A summary of the PRUDENCE model projections of changes in European climate by the end of this century, *Climatic Change* **81**, 7--30.

Christensen, J., Hewitson, B., Busuioc, A., Chen, A., Gao, X., Held, I., Jones, R., Kolli, R., Kwon, W., Laprise, V., Mearns, L., Menéndez, C., Räisänen, J., Rinke, A., Sarr, A. and Whetton, P. (2007): Regional Climate Projections. In: *Climate Change 2007: The Physical Science Basis. Contribution of Working Group I to the Fourth Assessment Report of the Intergovernmental Panel on Climate Change [Solomon, S., Qin, D., Manning, M., Chen, Z., Marquis, M., Averyt, K.B., Tignor, M. and Miller, H.L. (eds.)]*. *Cambridge University Press, Cambridge, United Kingdom and New York, NY, USA,*.

Cowling, R., Pressey, R., Rouget, M. and Lombard, A. (2003): A conservation plan for a global biodiversity hotspot – the Cape Floristic Region, South Africa, *Biological Conservation* **112**(1-2), 191--216.

Davies, H. C. (1976): Lateral Boundary Formulation For Multilevel Prediction Models, *Quarterly Journal Of The Royal Meteorological Society* **102**(432), 405--418.

de Castro, M., Gallardo, C., Jylha, K. and Tuomenvirta, H. (2007): The use of a climate-type classification for assessing climate change effects in Europe from an ensemble of nine regional climate models, *Climatic Change* **81**, 329--341.

Denis, B., Laprise, R. and Caya, D. (2003): Sensitivity of a regional climate model to the resolution of the lateral boundary conditions, *Climate Dynamics* **20**, 107--126.

Elizalde, A., Jacob, D. and Mikolajewicz, U. (in preparation): An Atmosphere-Ocean Coupled Model for the Mediterranean Climate Simulation.

Engelbrecht, F. A., McGregor, J. L. and Engelbrecht, C. J. (2009): Dynamics of the Conformal-Cubic Atmospheric Model projected climate-change signal over southern Africa, *International Journal of Climatology* **29**(7), 1013--1033.

Fauchereau, N., Trazaska, S., Rouault, M. and Richard, Y. (2003): Rainfall Variability and Changes in Southern Africa during the 20th Century in the Global Warming Context, *Natural Hazards* **29**, 139--154.

Fowler, H. J., Blenkinsop, S. and Tebaldi, C. (2007): Linking climate change modelling to impacts studies: recent advances in downscaling techniques for hydrological modelling, *International Journal of Climatology* **27**(12), 1547--1578.

Giorgi, F. (2006): Regional climate modeling: Status and perspectives, *Journal de Physique IV* **139**, 101--118.

Giorgi, F. (1990): Simulation of Regional Climate Using a Limited Area Model Nested in a General Circulation Model, *Journal of Climate* **3**(9), 941--963.

Goldreich, Y. and Tyson, P. D. (1988): Diurnal and inter-diurnal variations in large-scale atmospheric turbulence over southern Africa, *The South African Geographical Journal* **70**, 48--56.

Gultepe, I., Mueller, M. D. and Boybeyi, Z. (2006): A new visibility parameterization for warm-fog applications in numerical weather prediction models, *Journal Of Applied Meteorology And Climatology* **45**(11), 1469--1480.

Gultepe, I., Tardif, R., Michaelides, S. C., Cermak, J., Bott, A., Bendix, J., Mueller, M. D., Pagowski, M., Hansen, B., Ellrod, G., Jacobs, W., Toth, G. and Cober, S. G. (2007): Fog research: A review of past achievements and future perspectives, *Pure And Applied Geophysics* **164**(6-7), 1121--1159.

Hachfeld, B. (2000): Rain, fog and species richness in the Central Namib Desert in the exceptional rainy season of 1999/2000, *Dinteria* **26**, 113--146.

Hachfeld, B. and Jürgens, N. (2000): Climate patterns and their impact on the vegetation in a fog driven desert: The Central Namib Desert in Namibia, *Phytocoenologia* **30**(3-4), 567--589.

Haeffelin, M., Bergot, T., Elias, T., Tardif, R., Carrer, D., Chazette, P., Colomb, M., Drobinski, P., Dupont, E., Dupont, J-C., Gomes, L., Musson-Genon, L., Pietras, C., Plana-Fattori, A., Protat, A., Rangognio, J., Raut, J-C., Rémy,S., Richard, D., Sciare, J., and Zhang, X. (2010): PARISFOG: Shedding New Light on Fog Physical Processes, *Bulletin of the American Meteorological Society*, **91**(6), 767--783.

Haensler, A., Hagemann, S. and Jacob, D. (2010a): Climate history of Namibia and western South Africa. In: *Biodiversity in southern Africa. Volume 2: Patterns and processes at regional scale [Schmiedel, U., Jürgens, N. (eds.)]*. *Klaus Hess Publishers, Göttingen and Windhoek.*

Haensler, A., Hagemann, S. and Jacob, D. (2010b): Dynamical downscaling of ERA40 reanalysis data over southern Africa: added value in the representation of seasonal rainfall characteristics, *International Journal of Climatology*. DOI:10.1002/joc.2242.

Haensler, A., Hagemann, S. and Jacob, D. (2010c), Regional climatological patterns and their simulated change. In: *Biodiversity in southern Africa. Volume 2: Patterns and processes at regional scale [Schmiedel, U., Jürgens, N. (eds.)]*. *Klaus Hess Publishers, Göttingen and Windhoek.*

Haensler, A., Hagemann, S. and Jacob, D. (2010d): How the future climate of the southern African region might look like: Results of a high-resolution regional climate change projection, *Nova Acta Leopoldina* **112**(384), 183--193.

Haensler, A., Hagemann, S. and Jacob, D. (2011a): The role of the simulation setup in a long-term high-resolution climate change projection for the southern African region. *Theoretical and Applied Climatology*. DOI: 10.1007/s00704-011-0420-1.

Haensler, A., Hagemann, S. and Jacob, D. (2011b): Will the southern African west coast fog be affected by future climate change? Results of an initial fog projection using a regional climate model. *ERDKUNDE* (accepted June 2011).

Hagemann, S. (2002): An improved land surface parameter dataset for global and regional climate models, *Max Planck Institute for Meteorology*, **Rep 336**, 21 pp.

Hagemann, S. and Dümenil Gates, L. (2003): Improving a subgrid runoff parameterization scheme for climate models by the use of high resolution data derived from satellite observations, *Climate Dynamics* **21**(3), 349--359.

Hagemann, S., Goettel, H., Jacob, D., Lorenz, P. and Roeckner, E. (2009): Improved regional scale processes reflected in projected hydrological changes over large European catchments, *Climate Dynamics* **32**(6), 767--781.

Hamilton, W. J., Henschel, J. R. and Seely, M. K. (2003): Fog collection by Namib Desert Beetles, *South African Journal Of Science* **99**(3-4), 181--181.

Henschel, J. R. and Seely, M. K. (2008): Ecophysiology of atmospheric moisture in the Namib Desert, *Atmospheric Research* **87**(3-4), 362--368.

Hewitson, B. C. and Crane, R. G. (2005): Gridded area-averaged daily precipitation via conditional interpolation, *Journal Of Climate* **18**(1), 41--57.

Hewitson, B. C. and Crane, R. G. (2006): Consensus between GCM climate change projections with empirical downscaling: Precipitation downscaling over South Africa, *International Journal Of Climatology* **26**(10), 1315--1337.

Hudson, D. and Jones, R. (2002): Regional climate model simulations of present-day and future climates of southern Africa, *Hadley Centre technical note* **39**.

Jacob, D. (2001a): A note to the simulation of the annual and inter-annual variability of the water budget over the Baltic Sea drainage basin, *Meteorology and Atmospheric Physics* **77**, 61--73.

Jacob, D. (2001b): The role of water vapour in the atmosphere. A short overview from a climate modeller's point of view, *Physics and Chemistry of the Earth, Part A: Solid Earth and Geodesy* **26**(6-8), 523--527.

Jacob, D., Elizalde, A., Haensler, A., Hagemann, S., Kumar, P., Podzun, R., Rechid, D., Remedio, A., Saeed, F., Sieck, K., Teichmann, C. and Wilhelm, C. (in preparation): Evaluation of regional climate characteristics over several CORDEX regions simulated by REMO using the Koeppen-Trewartha climate classification.

Jacob, D., Barring, L., Christensen, O. B., Christensen, J. H., de Castro, M., Deque, M., Giorgi, F., Hagemann, S., Lenderink, G., Rockel, B., Sanchez, E., Schar, C., Seneviratne, S. I., Somot, S., van Ulden, A. and van den Hurk, B. (2007): An inter-comparison of regional climate models for Europe: model performance in present-day climate, *Climatic Change* **81**, 31--52.

Jacob, D., Goettel, H., Lorenz, P., Kotlarski, S. and Sieck, K. (2008): Klimaauswirkungen und Anpassung in Deutschland - Phase 1: Erstellung regionaler Klimaszenarien fuer Deutschland, *Umweltbundesamt, http://www.umweltbundesamt.de*.

Jacob, D. and Podzun, R. (1997): Sensitivity studies with the regional climate model REMO, *Meteorology And Atmospheric Physics* **63**(1-2), 119--129.

Joubert, A. M., Katzfey, J. J., McGregor, J. L. and Nguyen, K. C. (1999): Simulating midsummer climate over southern Africa using a nested regional climate model, *J. Geophys. Res.* **104**(D16), 19015--19025.

Jürgens, N., Schmiedel, U. and Hoffman, M. (2010): BIOTA Southern Africa. In: *Biodiversity in southern Africa. Volume 1: Patterns at a local scale - the BIOTA Observatories [Schmiedel, U., Jürgens, N. (eds.)]*. *Klaus Hess Publishers, Göttingen and Windhoek.*

Jungclaus, J., Keenlyside, N., Botzet, M., Haak, H., Luo, J., Latif, M., Marotzke, J., Mikolajewicz, U. and Roeckner, E. (2006): Ocean circulation and tropical variability in the coupled model ECHAM5/MPI-OM, *Journal of Climate* **19**(16), 3952--3972.

Kgatuke, M. M., Landman, W. A., Beraki, A. and Mbedzi, M. P. (2008): The internal variability of the RegCM3 over South Africa, *International Journal Of Climatology* **28**(4), 505--520.

Krug, C., Esler, K., Hoffman, M., Henschel, J., Schmiedel, U. and Jürgens, N. (2006): North-South cooperation through BIOTA: an interdisciplinary monitoring programme in arid and semi-arid southern Africa, *South African journal of science* **102**(5-6), 187--190.

Kruger, A. C. and Shongwe, S. (2004): Temperature trends in South Africa: 1960-2003, *International Journal Of Climatology* **24**(15), 1929--1945.

Kunkel, B. A. (1984): Parameterization Of Droplet Terminal Velocity And Extinction Coefficient In Fog Models, *Journal Of Climate And Applied Meteorology* **23**(1), 34--41.

Kushner, P. J., Held, I. M. and Delworth, T. L. (2001): Southern Hemisphere atmospheric circulation response to global warming, *Journal Of Climate* **14**(10), 2238--2249.

Lancaster, J., Lancaster, N. and Seely, M. (1984): Climate of the central Namib Desert, *MADOQUA.* **14**(1), 5--61.

Laprise, R. (2008): Regional climate modelling, *Journal of Computational Physics* **227**(7), 3641--3666.

Large, W. G. and Danabasoglu, G. (2006): Attribution and Impacts of Upper-Ocean Biases in CCSM3, *Journal of Climate* **19**(11), 2325--2346.

Lengoasa, J. R., Lindesay, J. A. and van Nierop, A. M. (1993): The influence of a synoptic-scale disturbance on topographically induced boundary layer circulations over the central Namib Desert, *Madoqua* **18**(2), 71--78.

Lindesay, J. A. and Tyson, P. D. (1990): Thermo-topographically induced boundary layer oscillations over the central Namib, southern Africa, *International Journal of Climatology* **10**(1), 63--77.

MacKellar, N., Hewitson, B. and Tadross, M. (2007): Namaqualand's climate: Recent historical changes and future scenarios, *Journal of Arid Environments* **70**(4), 604--614.

MacKellar, N. C., Tadross, M. A. and Hewitson, B. C. (2009): Effects of vegetation map change in MM5 simulations of southern Africa's summer climate, *International Journal Of Climatology* **29**(6), 885--898.

Majewski, D. (1991): The Europa-Modell of the Deutscher Wetterdienst, *ECMWF Seminar on Numerical Methods in Atmospheric Models* **2**, 147--191.

Masbou, M. (2010): pers. communication.

Mason, S. J. and Jury, M. R. (1997): Climatic variability and change over southern Africa: A reflection on underlying processes, *Progress In Physical Geography* **21**(1), 23--50.

Meehl, G. A., Stocker, T., Collins, W., Friedlingstein, P., Gaye, A., Gregory, J., Kitoh, A., Knutti, R., Murphy, J., Noda, A., Raper, S., Watterson, I., Weaver, A. and Zhao, Z. (2007): Global Climate Projections. In: *Climate Change 2007: The Physical Science Basis. Contribution of Working Group I to the Fourth Assessment Report of the Intergovernmental Panel on Climate Change [Solomon, S., Qin, D., Manning, M., Chen, Z., Marquis, M., Averyt, K.B., Tignor, M. and Miller, H.L. (eds.)]. Cambridge University Press, Cambridge, United Kingdom and New York, NY, USA.*

Midgley, G. F., Hannah, L., Millar, D., Thuiller, W. and Booth, A. (2003): Developing regional and species-level assessments of climate change impacts on biodiversity in the Cape Floristic Region, *Biological Conservation* **112**(1-2), 87--97.

Mueller, M.D., Masbou, M. and Bott, A. (2010): Three dimensional fog forecasting in complex terrain, *Quarterly Journal of the Royal Meteorological Society*, **136**(653), 2189--2202.

Muller, A., Reason, C. J. C. and Fauchereau, N. (2008): Extreme rainfall in the Namib Desert during late summer 2006 and influences of regional ocean variability, *International Journal Of Climatology* **28**(8), 1061--1070.

Nakicenovic, N., Alcamo, J., Davis, G., de Vries, B., Fenhann, J., Gaffin, S., Gregory, K., Grubler, A., Jung, T., Kram, T. and others (2000): Special report on emissions scenarios: a special report of Working Group III of the Intergovernmental Panel on Climate Change, Technical report, Pacific Northwest National Laboratory, Richland, WA (US), Environmental Molecular Sciences Laboratory (US).

New, M., Lister, D., Hulme, M. and Makin, I. (2002): A high-resolution data set of surface climate over global land areas, *Climate Research* **21**(1), 1--25.

New, M., Hewitson, B., Stephenson, D. B., Tsiga, A., Kruger, A., Manhique, A., Gomez, B., Coelho, C. A. S., Masisi, D. N., Kululanga, E., Mbambalala, E., Adesina, F., Saleh, H., Kanyanga, J., Adosi, J., Bulane, L., Fortunata, L., Mdoka, M. L. and Lajoie, R. (2006): Evidence of trends in daily climate extremes over southern and west Africa, *Journal Of Geophysical Research-Atmospheres* **111**(D14), D14102.

Nikulin, G. and Jones, C. (2010): Evaluating the first CORDEX simulations over Africa. Available online under: http://www.smhi.se (December 2010)

Olivier, J. (1995): Spatial-Distribution Of Fog In The Namib, *Journal Of Arid Environments* **29**(2), 129--138.

Olivier, J. (2004): Fog harvesting: An alternative source of water supply on the West Coast of South Africa, *GeoJournal* **61**(2), 203--214.

Olivier, J. and de Rautenbach, C. J. (2002): The implementation of fog water collection systems in South Africa, *Atmospheric Research* **64**(1-4), 227--238.

Olivier, J. and Stockton, P. L. (1989): The Influence Of Upwelling Extent Upon Fog Incidence At Luderitz, Southern-Africa, *International Journal Of Climatology* **9**(1), 69--75.

Paeth, H., Born, K., Girmes, R., Podzun, R. and Jacob, D. (2009): Regional Climate Change in Tropical and Northern Africa due to Greenhouse Forcing and Land Use Changes, *Journal Of Climate* **22**(1), 114--132.

Paeth, H. and Thamm, H. P. (2007): Regional modelling of future African climate north of 15 degrees S including greenhouse warming and land degradation, *Climatic Change* **83**(3), 401--427.

Peixoto, J. and Oort, A. (1992): *Physics of Climate*, American Institute of Physics.

Pickford, M. and Senut, B. (1999): Geology and palaeobiology of the Namib Desert, southwestern Africa., *Geological Survey of Namibia* **Memoir 18**.

Reason, C. J. C. and Jury, M. R. (1990): On the generation and propagation of the southern African coastal low, *Quarterly Journal of the Royal Meteorological Society* **116**(495), 1133--1151.

Reason, C. J. C., Rouault, M., Melice, J. L. and Jagadheesha, D. (2002): Interannual winter rainfall variability in SW South Africa and large scale ocean-atmosphere interactions, *Meteorology And Atmospheric Physics* **80**(1-4), 19--29.

Rechid, D., Raddatz, T. and Jacob, D. (2009): Parameterization of snow-free land surface albedo as a function of vegetation phenology based on MODIS data and applied in climate modelling, *Theoretical and Applied Climatology* **95**(3), 245--255.

Roeckner, E., Arpe, K., Bengtsson, M., Christoph, M., Claussen, M., Duemenil, L., Esch, M., Giorgetta, M., Schlese, U. and Schulzweida, U. (1996): The atmospheric general circulation model ECHAM-4: Model description and simulation of present-day climate, *Max Planck Institute for Meteorology*, **Rep 218**, 90 pp.

Roeckner, E., Bäuml, G., Bonaventura, L., Brokopf, R., Esch, M., Giorgetta, M., Hagemann, S., Kirchner, I., Kornblueh, L., Manzini, E., Rhodin, A., Schlese, U., Schulzweida, U. and Tompkins, A. (2003): The atmospheric general circulation model ECHAM5. Part I: Model description, *Max Planck Institute for Meteorology*, **Rep 349**, 127 pp.

Rouault, M., Florenchie, P., Fauchereau, N. and Reason, C. J. C. (2003): South East tropical Atlantic warm events and southern African rainfall, *Geophysical Research Letters* **30**(5), 8009.

Saeed, F., Hagemann, S. and Jacob, D. (2009): Impact of irrigation on the South Asian summer monsoon, *Geophysical Research Letters* **36**, L20711.

Schneider, U., Fuchs, T., Meyer-Christoffer, A. and Rudolf, B. (2008): Global precipitation analysis products of GPCC, GPCC, Technical report, German Weather Service, http://gpcc.dwd.de.

Schulze, B. R. (1965): South Africa, *In Thompson, B.W. (ed.): The Climate of Africa. Oxford University Press, Nairobi*.

Schulze, B. R. (1969): The climate of Gobabeb, *Scientific Papers of the Namib Desert Research Station* **38**, 5--12.

Schulze, R. and Maharaj, M. (2003): Development of a Database of Gridded Daily Temperatures for Southern Africa, Technical report, University of Natal, Pietermaritzburg, RSA, School of Bioresources Engineering and Environmental Hydrology. ACRUcons Report, 41, pp 81.

Shannon, L. (1985): The Benguela Ecosystem: 1. Evolution of the Benguela, physical features and processes, *Oceanography and marine biology: an annual review* **23**.

Shanyengana, E. S., Henschel, J. R., Seely, M. K. and Sanderson, R. D. (2002): Exploring fog as a supplementary water source in Namibia, *Atmospheric Research* **64**(1-4), 251--259.

Silvestri, G., Vera, C., Jacob, D., Pfeifer, S. and Teichmann, C. (2009): A high-resolution 43-year atmospheric hindcast for South America generated with the MPI regional model, *Climate Dynamics* **32**(5), 693--709.

Simpson, J. E. (1994): *Sea breeze and local winds*, Cambridge Univ. Press.

Soderberg, K. and Compton, J. (2007): Dust as a Nutrient Source for Fynbos Ecosystems, South Africa, *Ecosystems* **10**(4), 550--561.

Sundqvist, H. (1978): A parameterization scheme for non-convective condensation including prediction of cloud water content, *Quarterly Journal Of The Royal Meteorological Society* **104**(441), 677--690.

Tadross, M. A., Gutowski, W. J., Hewitson, B. C., Jack, C. and New, M. (2006): MM5 simulations of interannual change and the diurnal cycle of southern African regional climate, *Theoretical And Applied Climatology* **86**(1-4), 63--80.

Tadross, M., Jack, C. and Hewitson, B. (2005): On RCM-based projections of change in southern African summer climate, *Geophysical Research Letters* **32**(23), L23713.

Tardif, R. (2007): The impact of vertical resolution in the explicit numerical forecasting of radiation fog: A case study, *Pure And Applied Geophysics* **164**(6-7), 1221--1240.

Teixeira, J. (1999): Simulation of fog with the ECMWF prognostic cloud scheme, *Quarterly Journal Of The Royal Meteorological Society* **125**(554), 529--552.

Trenberth, K., Jones, P., Ambenje, P., Bojariu, R., Easterling, D., Klein Tank, A., Parker, F., Renwick, J., Rusticucci, M., Soden, B. and Zhai, P. (2007): Observations: Surface and Atmospheric Climate Change. In: *Climate Change 2007: The Physical Science Basis. Contribution of Working Group I to the Fourth Assessment Report of the Intergovernmental Panel on Climate Change [Solomon, S., Qin, D., Manning, M., Chen, Z., Marquis, M., Averyt, K.B., Tignor, M. and Miller, H.L. (eds.)]. Cambridge University Press, Cambridge, United Kingdom and New York, NY, USA*.

Tyson, P. D., Dyer, T. and Mametse, M. (1975): Secular changes in South African rainfall: 1880 to 1972, *Quarterly Journal of the Royal Meteorological Society* **101(430)**, 817--833.

Tyson, P. D. (1964): Berg Winds of South Africa, *Weather* **19**, 7--11.

Uppala, S. M., Kållberg, P. W., Simmons, A. J., Andrae, U., da Costa Bechtold, V., Fiorino, M., Gibson, J. K., Haseler, J., Hernandez, A., Kelly, G. A., Li, X., Onogi, K., Saarinen, S., Sokka, N., Allan, R. P., Andersson, E., Arpe, K., Balmaseda, M. A., Beljaars, A. C. M., van de Berg, L., Bidlot, J., Bormann, N., Caires, S., Chevallier, F., Dethof, A., Dragosavac, M., Fisher, M., Fuentes, M., Hagemann, S., Hólm, E., Hoskins, B. J., Isaksen, L., Janssen, P. A. E. M., Jenne, R., McNally, A. P., Mahfouf, J. F., Morcrette, J. J., Rayner, N. A., Saunders, R. W., Simon, P., Sterl, A., Trenberth, K. E., Untch, A., Vasiljevic, D., Viterbo, P. and Woollen, J. (2005): The ERA-40 re-analysis, *Quarterly Journal of the Royal Meteorological Society* **131**(612), 2961--3012.

Van Rooy, M. (1936): Influence of berg winds on the temperatures along the west coast of South Africa, *Quarterly Journal of the Royal Meteorological Society* **62**(267), 528--537.

Von Storch, H., E., Z. and Cubasch, U. (1993): Downscaling Of Global Climate-Change Estimates To Regional Scales - An Application To Iberian Rainfall In Wintertime, *Journal Of Climate* **6**(6), 1161--1171.

Warburton, M. and Schulze, R. (2005): Historical precipitation trends over southern Africa: a hydrology perspective, *In: Climate change and water resources in southern Africa: studies on scenarios, impacts, vulnerabilities and adaptation [Schulze R.E. (ed)]. Water Research Commission, Pretoria, RSA, WRC Report 1430/1/05. Chapter19, 325--338*.

Washington, R. and Preston, A. (2006): Extreme wet years over southern Africa: Role of Indian Ocean sea surface temperatures, *Journal Of Geophysical Research-Atmospheres* **111**(D15), D15104.

Watson, I. and Lemon, R. R. (1985): Geomorphology Of A Coastal Desert - The Namib, South-West-Africa Namibia, *Journal Of Coastal Research* **1**(4), 329--342.

WMO (1992): International Meteorological Vocabulary, *WMO 182*, 782pp.

Zhao, Y., Camberlin, P. and Richard, Y. (2005): Validation of a coupled GCM and projection of summer rainfall change over South Africa, using a statistical downscaling method, *Climate research* **28**(2), 109--122.

Zhou, B. B. and Du, J. (2010): Fog Prediction from a Multimodel Mesoscale Ensemble Prediction System, *Weather And Forecasting* **25**(1), 303--322.



ISSN 1614-1199